

Dipartimento di Scienze della Terra e dell'Ambiente

Direttore: Prof. S. Seno

Corso di Laurea in Geoscienze per lo Sviluppo Sostenibile

Structural and stratigraphic analysis of the upper Val d'Ambria by means of Digital Outcrop Models (DOMs)

Analisi strutturale e stratigrafica dell'alta Val d'Ambria mediante l'uso di Digital Outcrop Models (DOMs)

Relatore:

Prof. Ausonio Ronchi

Correlatori:

Prof. Niccolò Menegoni

Dott. Rudy Scarani

Tesi di Laurea

in Geoscienze per lo Sviluppo Sostenibile

di STEFANO BONIZZONI

Matr. 564276

Anno Accademico 2025/2026

INDEX

RIASSUNTO **5**

ABSTRACT **6**

1. INTRODUCTION AND AIM OF THE WORK **7**

2. GEOGRAPHICAL SETTING **8**

3. GEOLOGICAL SETTING OF THE OROBIC BASIN **11**

3.1 The Orobic Basin 11

3.2 Permian stratigraphy of the Orobic Basin 13

3.2.1 Basal Conglomerate *16*

3.2.2 Cabianca Volcanite *16*

3.2.3 Pizzo del Diavolo Formation *17*

3.2.4 Verrucano Lombardo *26*

4. STRUCTURAL SETTING OF THE OROBIC BASIN **28**

4.1 Tectonic evolution 30

4.1.1 Late-to-post Variscan tectonics *30*

4.1.2 Pre-Alpine extensional phase *30*

4.1.3 Alpine Orogeny *34*

5. MATERIALS AND METHODS **36**

5.1 Cartographic analysis 36

5.2 UAV survey 36

5.3 Digital Outcrop Models (DOMs) development and analysis 37

6. RESULTS **41**

6.1 Critical interpretation of previous maps 41

6.1.1 Southern sector of the upper Val Brembana *41*

6.1.2 Central sector of the upper Val Brembana *41*

6.1.3 Fault trace analysis *46*

6.2 DOM analysis 48

6.2.1 Sector A *49*

6.2.2 Sector B *54*

6.2.3 Sector C *56*

7. DISCUSSION **59**

8. CONCLUSIONS **74**

9. REFERENCES **76**

RINGRAZIAMENTI **83**

RIASSUNTO

Il seguente lavoro analizza l'assetto strutturale e stratigrafico dell'alta Val d'Ambria, un'area del Bacino Orobico situata all'interno del Parco delle Orobie Valtellinesi, compresa tra il Monte Aga, il Pizzo del Diavolo di Tenda e il Pizzo dell'Omo, e si inserisce all'interno di un progetto di ricerca più ampio nato nel 2022 a seguito del ritrovamento di un'associazione molto ricca di impronte di tetrapodi e invertebrati.

A causa di problemi logistici legati al rilievo sul terreno della successione permiana affiorante (pareti molto inclinate e subverticali), in particolare per quanto riguarda le aree più in quota (dai 2000 ai 2914 m s.l.m.), sono stati utilizzati rilievi fotogrammetrici da drone (UAV surveys) e il software *CloudCompare* per generare e interpretare un modello digitale tridimensionale dell'area, ricavando 178 misure di piani di faglie e fratture e 139 di piani di stratificazione.

Dall'analisi strutturale sono emersi tre set di faglie principali, denominati *K1*, *K2* e *K3*, possibilmente associati all'Orogenesi Alpina. *K1* (NE-SW) e *K3* (NW-SE) rappresentano probabilmente un sistema di faglie coniugato, con un campo di stress compatibile con la compressione alpina descritta in letteratura, mentre *K2* (N-S) si sarebbe sviluppato in fasi deformative successive. Alcune strutture, inoltre, ricadono in *K1* e *K3* per giacitura ma sembrano mostrare una cinematica opposta. Suggerendo che i due set possano includere riattivazioni tardive.

Da un punto di vista stratigrafico, l'analisi delle superfici mostra due set (*St1* e *St2*), immersioni generalmente rivolte verso nord-nordovest e inclinazioni comprese tra 60° e 80°. Tali geometrie risultano compatibili con i dati pubblicati da altri studi, confermando l'assetto strutturale della Formazione del Pizzo del Diavolo, tiltato dalla tettonica alpina.

L'utilizzo del modello digitale ha inoltre permesso di mettere in dubbio la presenza di un'eventuale piega a medio-grande scala, mostrando invece che gli strati della successione sedimentaria sono sub-paralleli tra loro.

Le caratteristiche strutturali dell'area sono state infine integrate, grazie anche all'esame dettagliato della cartografia geologica esistente, in una carta geologico-strutturale (alla scala 1:20,000) proposta per rappresentare il settore dell'alta Val d'Ambria.

ABSTRACT

This Master's thesis analyzes the structural and stratigraphic context of the upper Val d'Ambria (Orobic Basin), located within the Parco delle Orobie Valtellinesi between Monte Aga, Pizzo del Diavolo di Tenda, and Pizzo dell'Omo. This study is part of a broader research project initiated in 2022 following the discovery of tetrapod and invertebrate footprints. Due to logistical challenges in accessing and taking direct measures in the field, particularly in high-altitude areas, UAV photogrammetric surveys and *CloudCompare* software were used to build and analyze a 3D digital model of the area (DOM), extracting 178 fault surface measurements and 139 bedding planes.

The structural analysis revealed three main fault sets, named *K1*, *K2*, and *K3*, possibly associated with the Alpine Orogeny. *K1* (NE-SW) and *K3* (NW-SE) likely represent a conjugate fault system, whose inferred stress field is compatible with the Alpine shortening described in the literature. whereas *K2* (N-S) developed during subsequent deformation phases. Furthermore, some structures plot within *K1* and *K3* by orientation but show an apparent opposite kinematics, suggesting that the two sets may include later reactivations.

From a stratigraphic point of view, bedding plane analysis identified two sets (*St1* and *St2*), predominant NNW-dipping orientations and dip angles between 60° and 80°. These data appear to be in line with some previous studies, confirming the structural setting of the Pizzo del Diavolo Formation. Furthermore, the 3D digital model ruled out the presence of a medium-to-large-scale fold - previously hypothesized from field observations and panoramic photos -, demonstrating instead that the sedimentary strata appear to be sub-parallel throughout the sequence.

Finally, the structural features of the area were incorporated into an updated geological-structural map proposed for the upper Val d'Ambria sector.

1. INTRODUCTION AND AIM OF THE WORK

This Master's thesis is part of a wider-ranging research project, initiated in 2022 following a report by hikers of the presence of fossil footprints in Val d'Ambria (Sondrio Province, Northern Italy). These tracks were subsequently attributed to lower Permian tetrapods and arthropods, especially temnospondyl amphibians, reptiles and synapsids. The discovery generated considerable scientific interest and led to the development of a multidisciplinary research project carried out in collaboration with Dipartimento di Scienze della Terra e dell'Ambiente of the University of Pavia, the Parco delle Orobie Valtellinesi, Soprintendenza Belle Arti e Paesaggio per le province di Como, Lecco, Sondrio e Varese, the Museo di Storia Naturale of Milan and the Museum für Naturkunde of Berlin.

The aim of this study is to provide a detailed reconstruction of the structural context of the Orobic Basin in the sector bounded by Pizzo del Diavolo di Tenda, Pizzo dell'Omo and Monte Aga. The analysis considered both the northern side, including Val d'Ambria itself, and the southern one of the Upper Val Brembana.

Since the logistic conditions hampered direct measuring of tectonic structures in the field, several three-dimensional digital models were generated through drone-based photogrammetric surveys (UAV photogrammetry). The models were basically used to analyze deformation structures recorded within the sedimentary layers, using *CloudCompare* software. The same models also gave useful and detailed information on the recognition and stacking of stratigraphic units.

A crucial point was to distinguish the post-Variscan structures related to the formation of the Permian Basin from those of the rifting phase (pre-Alpine or "early" Alpine) and from the Alpine orogeny. This task was performed also checking the available geological maps of the area: Carta geologica del bacino di Brembo di Carona (Mengoli, 1993); Cadel et *al.* (1996); Carta geologica della provincia di Bergamo alla scala 50.000 (Forcella and Jadoul, 2000); Sondrio sheet 056 CARG (Boriani et *al.*, 2012; Servizio Geologico d'Italia); carta geologica 1:5,000 in Zanchi et *al.* 2019; Geological map of the Val d'Ambria area (Cattaneo, 2025b).

Ultimately, the main fault system identified through this digital analysis was integrated to produce a high-resolution geological map of the study area, highlighting the key tectonic features that helped shape this portion of the Orobic Basin, to date roughly known.

In the first part of the thesis geographical, geological, stratigraphical and structural settings are described. Methods, interpretations and results are discussed in the second half of the study.

2. GEOGRAPHICAL SETTING

This thesis focuses on an area of the Orobic Alps, namely Val d'Ambria, one of the secondary valleys of Val Venina, together with Valle del Lago di Venina itself, Valle di Scais, Val Vedello and Val Caronno (from west to east). The valley is located within the Parco delle Orobie Valtellinesi, within the municipality of Piateda, in the province of Sondrio (SO), in northern Italy (Fig. 1).

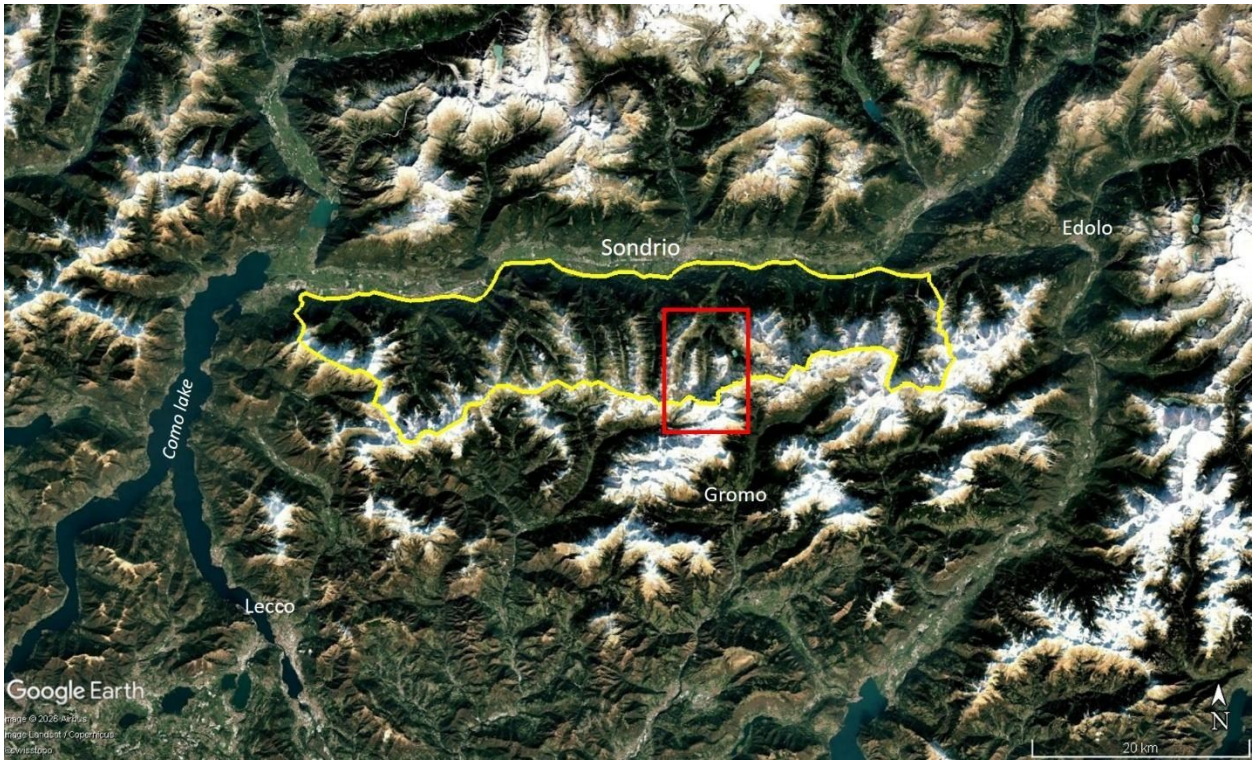


Figure 1. *Perimeter of the Parco delle Orobie Valtellinesi (yellow line) and location of the Val d'Ambria (red shape). Google Earth, modified.*

The Val d'Ambria, which is of fluvial origin and extends mainly along a north-south axis, is bounded to the south by the main peaks of the ridge, namely Pizzo dell'Omo (2773 m), Monte Aga (2720 m) and Pizzo del Diavolo di Tenda (2914 m), which separate it from the Upper Val Brembana (municipality of Carona, BG) (Figs. 2-3).

Gravitational processes such as landslides and *debris flows* at the highest elevations, as well as glacial and fluvioglacial processes in the vicinity of small glaciers, torrential activity, and the formation of relatively small lakes (e.g. Lago Zappello, located in the central part of the valley) are among the main factors currently shaping the morphology of Val d'Ambria (Boriani et *al.*, 2012).

The study area is represented in the 1:10,000 Carta Tecnica Regionale (section C3D4) and in the Foglio 056 – Sondrio, *Carta Geologica d'Italia* alla scala 1:50,000 (Fig. 4).



Figure 2. *Three-dimensional model of the Val d'Ambria. Google Earth, modified.*



Figure 3. *View of the Val d'Ambria from the Lago Zappello.*

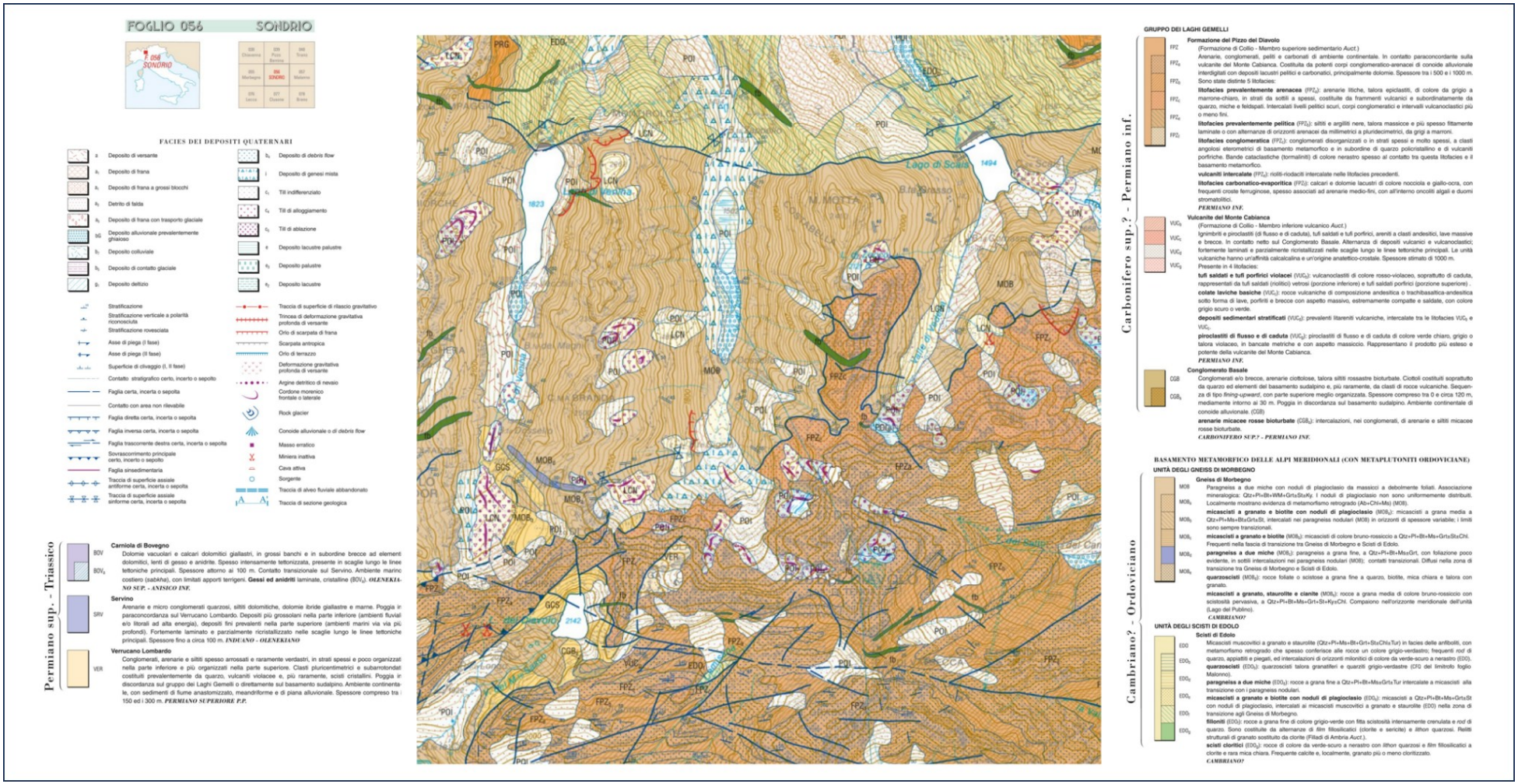


Figure 4. *Area of Val d'Ambria. Modified from Servizio Geologico d'Italia (2012) – Carta Geologica d'Italia alla scala 1:50,000 – F. 056 Sondrio.*

3. GEOLOGICAL SETTING OF THE OROBIC BASIN

3.1 The Orobic Basin

The Orobic Basin, together with the Collio Basin (also known as the Val Trompia or Triumplino Basin) is one of the widest Permian sedimentary basins of the Southern Alpine Domain – Orobic Alps (De Sitter & De Sitter-Koomans, 1949; Casati & Gnaccolini, 1967; Cadel et *al.*, 1996).
It extends for about 45 km in length (E-W) and less than 10 km in width (N-S). The tectonic framework of the basin is characterized, in its northern sector, by the above mentioned Orobic Thrusts, the south-verging thrust system developed during the Eo-Alpine phase of the Alpine Orogeny, in which the crystalline basement overrides the overlying sedimentary cover sequences. The other distinctive feature of this sector of the Southern Alps is the occurrence of large-scale basement culminations overlain by Permian-Triassic volcano-sedimentary successions, the Orobic Anticlines.

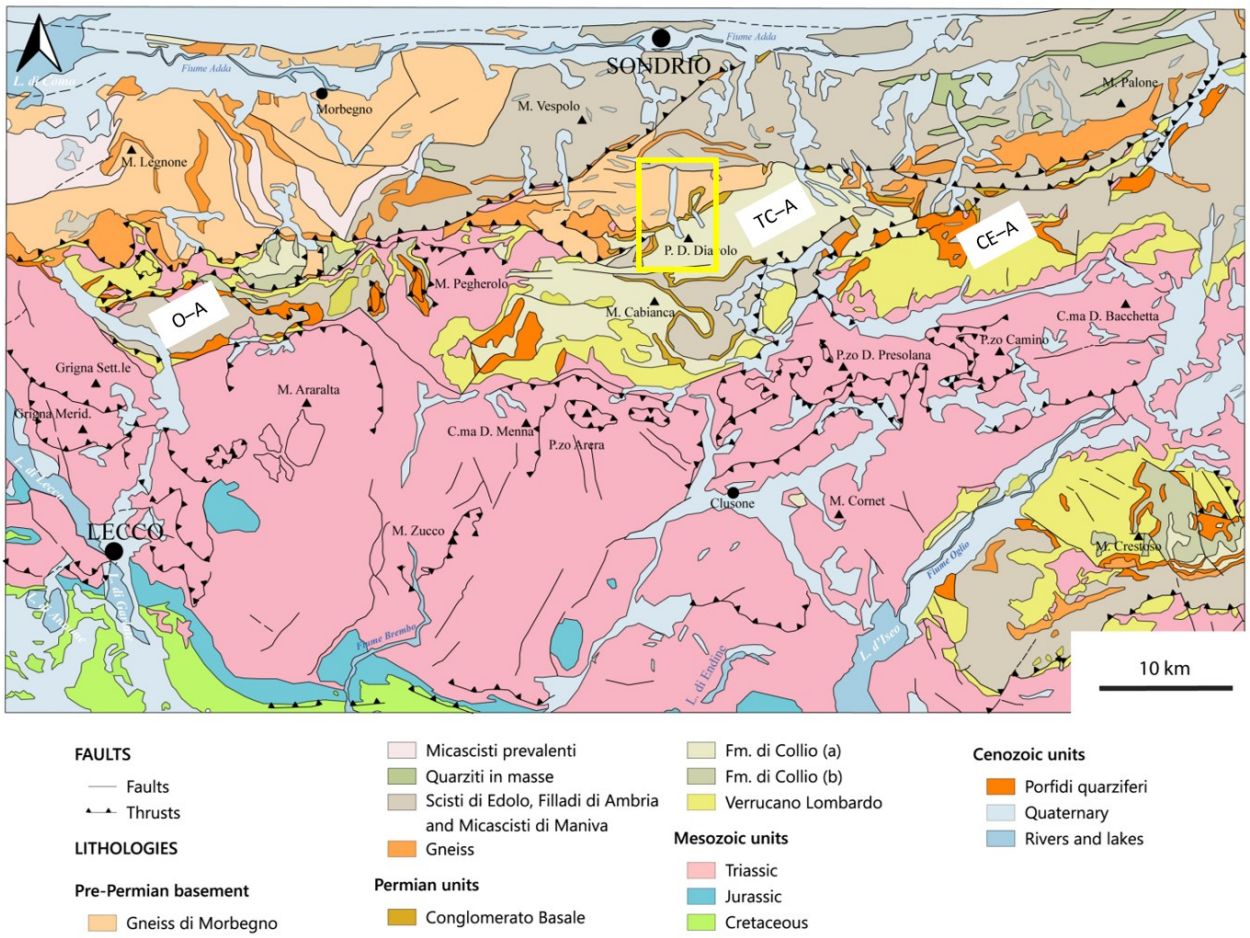


Figure 5. *Main structures of the Orobic Basin. Orobic Anticline s.s. (O-A); Trabuchello-Cabianca Anticline (TC-A); Cedegolo Anticline (C-A). Yellow shape: location of the Val d'Ambria. Redrawn and modified from the Carta Geologica della Lombardia, scala 1:250,000 (Servizio Geologico Nazionale) – Montrasio et al. (1990).*

These structures, with WSW-ENE-trending axes, variably imbricated and verge southward, are subdivided into the Orobic Anticline s.s. (O-A), the Trabuchello-Cabianca Anticline (TC-A), and the Cedegolo Anticline (CE-A), from west to east (Bonizzoni, 2024; Boriani et *al.*, 2012) (Fig. 5).

Traditionally, the opening of the Orobic Basin, as well as the development of the other Permian pull-apart basins of the Southern Alps, has been interpreted as the result of a predominantly transtensional tectonic regime, which controlled both basin subsidence and the distribution of the Lower Permian volcano-sedimentary succession (Cassinis et *al.*, 2012; Berra et *al.*, 2016; Marchetti et *al.*, 2022). Although this interpretation has long represented the reference geodynamic framework for the evolution of the Southern Alpine Permian basins, recent studies have highlighted the importance of a major system composed of the so-called *Low-Angle Normal Faults* (LANFs) and their related *High-Angle Normal Faults* (HANFs) in controlling the basin architecture (Zanchi et *al.*, 2019; Locchi et *al.*, 2022). Two major LANFs, recorded by the sediments of the Pizzo del Diavolo Formation in the northern area of the Orobic Basin, have been recognised: the Aga-Vedello and the Masoni LANFs (Zanchi et *al.*, 2019; Locchi et *al.*, 2022). The geodynamic significance of this model is still debated and will be discussed in the following chapter.

This structural configuration, comparable to that of the Basin-and-Range Province (western USA), as suggested by Locchi et *al.* (2022), helped shaping the asymmetrical semi-graben general structure of the basin, with sedimentary thickness that strongly increases from the south to the north (Boriani e Bini, 2011).

The Permian fault planes are usually decorated with black cryptocrystalline to aphanitic tourmalinites formed along the basement-cover fault contacts, and impregnating cataclasites. Presumably, the origin of these tourmalinites is linked to the circulations of Boron-rich hydrothermal fluids released after the emplacement of the granitic and granodioritic bodies in the upper crust (Locchi et *al.*, 2022; Zanchi et *al.*, 2019) (Fig. 6).

These basins were later filled with terrigenous sediments, volcanic products and volcaniclastic deposits, representing the Lower Permian succession (named *Laghi Gemelli Group*, for the Ororbic Basin). This material formed under semi-arid conditions (Cassinis & Perotti, 2007; Marchetti et *al.*, 2015; Berra et *al.*, 2016) and during fault activity, as indicated by the presence of co-seismic soft-sediments deformation structures and synsedimentary normal fault (Berra et *al.*, 2015; Locchi et *al.*, 2019).



***Figure 6**. Example of a tourmalinite impregnating the cataclasites and the underlying Corno Stella Geniss, marking a fault zone structure in the area of the Masoni Fault. Modified from Zanchi et al. (2019).*

3.2 Permian stratigraphy of the Orobic Basin

Two main tectono-sedimentary cycles can be distinguished within the Late Carboniferous to Permian successions of the Southern Alps. The lower cycle comprises the Variscan basement and the Early Permian units, and is characterized by fluvio-lacustrine sediments and volcanic deposits. The upper cycle, represented by the Verrucano Lombardo, is devoid of volcanic products and consists of alluvial sediments unconformably covering the previous succession. The two cycles are separated by a marked unconformity sealing a Middle Permian time gap, generally estimated at over 10 Ma (Cassinis & Perotti, 2007; Cassinis et *al.*, 2012). Boriani et *al.*, 2012 proposed an inversion of the tectonic regime, from transtensional to transpressional dynamics, possibly coincident with the formation of this discontinuity.

This is the reason why, from a stratigraphic perspective, the Collio and Orobic basins exhibit several shared features (Fig. 7). In both cases, the succession originates from the Variscan metamorphic basement, which is unconformably overlain by the Lower Permian sequence, starting with the Basal Conglomerate. This basal layer is followed by an extensive volcanic complex — Lower Quartz Porphyries in the Collio Basin, and Cabianca Volcanite in the Orobic Basin. The sequence continues with the overlying sedimentary successions: the Pizzo del Diavolo Formation, in the Orobic area, and the Collio Formation (comprising the Pian delle Baste and Val Dorizzo

members) together with the Ponteranica Conglomerate in the former and Dosso dei Galli Conglomerate, in the latter. The entire early Permian 1st cycle is overlain by the upper Permian Verrucano Lombardo, representing the 2nd cycle (Fig. 8).

Sedimentological evidence of the Pizzo del Diavolo Fm. indicates a depositional continuum: from a proximal fan dominated by mass-flow phenomena, to distal fan sandy sheet-flows and a silty floodplain, where sheet-flood events dominate. Laterally, continuous siltstones and dark shales with microbial carbonate intercalations and carbonate nodules indicate alternating conditions of shallow lake and desiccated floodplain environments (Berra et *al.*, 2016; 2019).

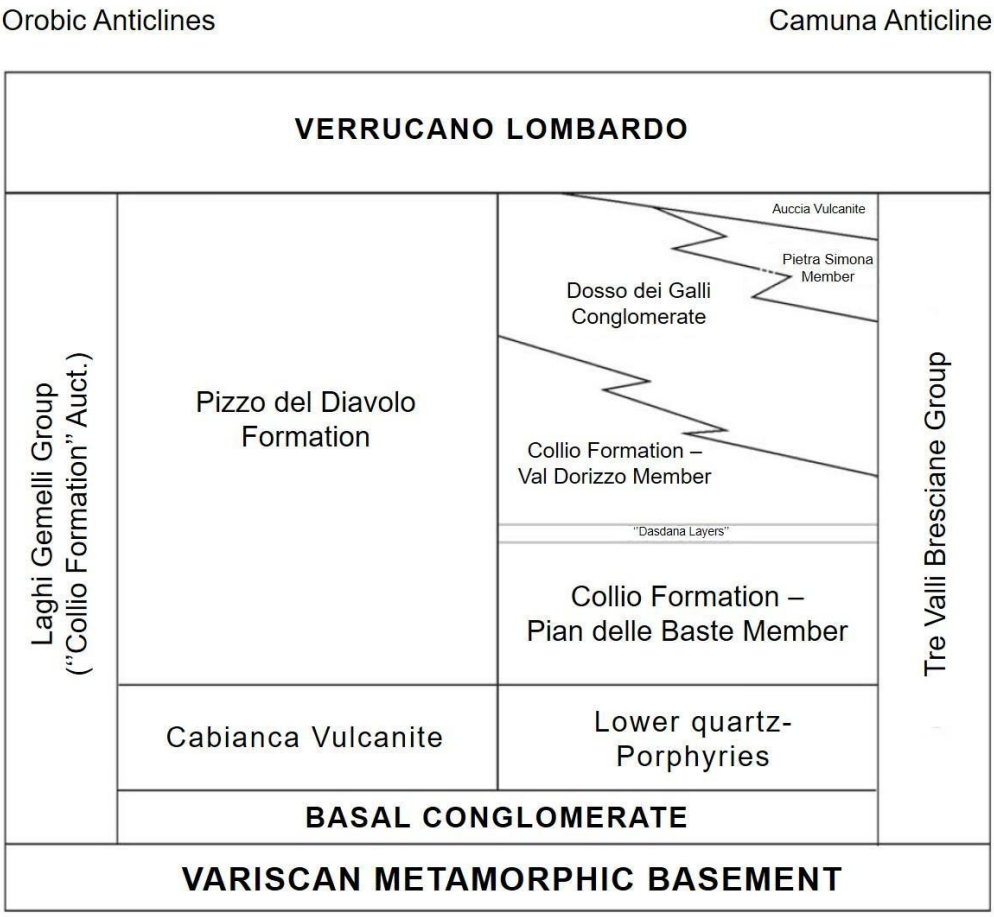


Figure 7. *Comparison between the stratigraphic successions of both Collio and Orobic Basins. Translated and adapted from Cassinis (2007).*

Starting from the Triassic to the Late Jurassic, a major marine transgression occurred, which led to the deposition of marine-marginal sediments – at first, shallow water carbonates (Servino Formation), and dolostones with intercalated evaporites (Carniola di Bovegno), then pelagic limestones and siliciclastic sediments – on top of the Permian alluvial-lacustrine ones (Boriani et *al.*, 2012).

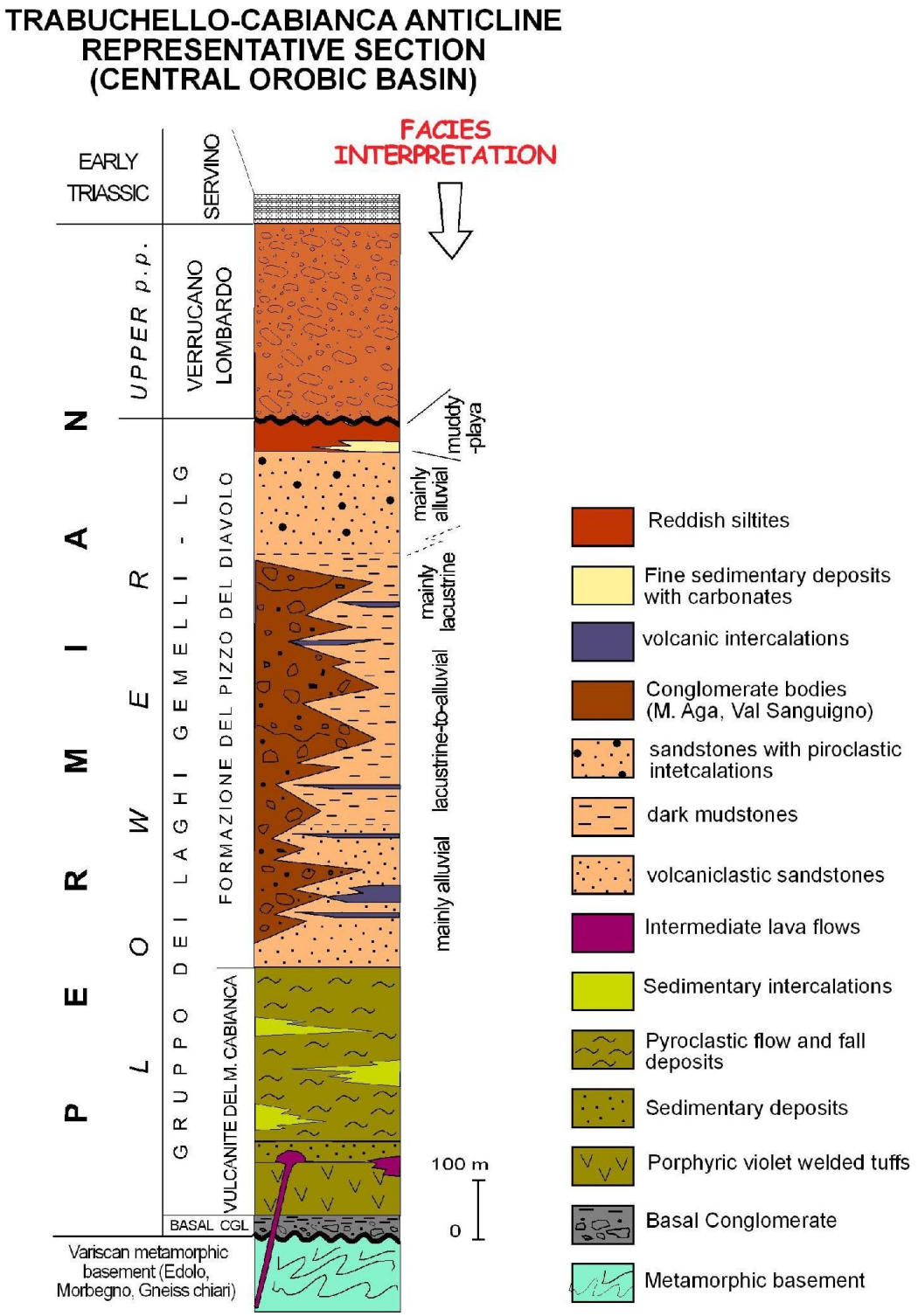


Figure 8. *Simplified stratigraphic succession of the Central Orobic Basin (Trabuchello-Cabianca Anticline): Carboniferous crystalline basement and Permian volcanic-sedimentary cover. Modified from Boriani et al. (2012).*

This event culminated with the opening of the Alpine Tethys (Zanchi et *al.*, 2019). A description of the main lithologies characterizing the Orobic Basin succession is presented below.

3.2.1 Basal Conglomerate

This unit represents the earliest sedimentary deposit and records the dismantling of the Variscan chain (the crystalline basement), as indicated by quartz pebbles and metamorphic lithic clasts, and it rests unconformably on the various units of the crystalline basement, including the Morbegno Gneiss.

With an average thickness of 30 m, the Basal Conglomerate consists of conglomerates, breccias, and pebbly sandstones, typically red or grey–green in color. These deposits are commonly poorly organized; clast sorting is generally poor as well, and clast shapes range from sub-rounded to highly angular. The unit is usually subdivided into two portions: the lower parts of the unit are more massive and coarse-grained, suggesting a deposition in proximal alluvial fan settings. In contrast, the occurrence of fining-upward cycles, channelized bodies, clast imbrication as well as pervasive bioturbation, which characterize the reddish medium to fine grained sandstones and siltstones of the middle to upper portions of the unit, indicate deposition by braided fluvial systems (see Cadel et *al.*, 1996; Boriani et *al.*, 2012).

The transition to the overlaying volcanic units is marked by an apparent paraconformity, likely corresponding to a time interval of uncertain duration during which no significant sedimentation took place. The age of this unit is thought to be constrained between Late Carboniferous and early Permian (Boriani et *al.*, 2012).

3.2.2 Cabianca Volcanite

The Cabianca Volcanite unconformably overlies the Basal Conglomerate and is particularly developed in the southern part of the Orobic Basin, in the Trabuchello Cabianca anticline. The unit consists predominantly of volcanic deposits, mainly pyroclastic flow and fall deposits, with minor sedimentary intercalations. Its thickness ranges from approximately 500 m up to 1000 m.

Several facies can be distinguished within the unit (Cadel et *al.*, 1996; Boriani et *al.*, 2012).

(1) The basal lithofacies, directly overlying the Basal Conglomerate, consists of welded tuffs and violet porphyric tuffs, intercalated by conglomerates and reddish sandstones in the lower portions, and with siltstones in the upper parts.
(2) Massive dark grey-green andesitic lava flows.
(3) Stratified sedimentary deposits, composed of medium to coarse sandstones alternated by conglomeratic or pelitic levels, and volcaniclastic layers, likely deposited in a fluvial braided system.

(4) Rhyolitic flow and fall pyroclastics, typically organized in very compact, meter-thick layers, green or violet in color.

The only available age on the Cabianca Volcanite is around 280 Ma and was obtained on zircons from an ignimbritic flow in the Val Seriana zone by Philippe et *al.* (1987).
More recent, radiometric dating using U-Pb methods ((LA)-ICP-MS) on zircons from a basal tuff indicates an age of 280 ± 2.5 Ma (late Cisuralian, Kungurian) for the base of this formation (Berra et *al.*, 2015), while ignimbritic samples from the upper part of the unit gave a very less reliable age of 270 Ma probably due to glassy inclusions, Pb loss and generally poor preservation of the crystals, (Marchetti, 2016).

3.2.3 Pizzo del Diavolo Formation

Previous studies and new interpretations

The Pizzo del Diavolo formation represents the Lower Cycle of the Permian succession, and is essentially composed of alluvial-lacustrine and terrigenous sediments, locally intercalated with evaporites, carbonates and volcanic products (e.g. tuffs, ash layers). From a stratigraphic point of view, this unit lies unconformably on top of the Cabianca Volcanites, and is overlain by the Verrucano Lombardo, which constitutes the Upper Permian Cycle. The sedimentary succession of the Pizzo del Diavolo formation has been described and subdivided in different ways over the years, with several subsequent studies progressively refining the recognition of its lithofacies. Rather than representing completely distinct sedimentary successions, these classifications can be regarded as different levels of detail applied to the same heterogeneous alluvial-lacustrine system.

Starting with the research carried out by Casati & Gnaccolini (1967), various methods have been used by researchers to describe and divide the true sedimentary succession of the Pizzo del Diavolo Formation. These classifications do not distinguish between separate successions; rather, they give different levels of detail to the same heterogeneous alluvial-lacustrine system. The focus has since changed from a general lithological subdivision to one that is increasingly grounded in depositional processes and environments (Fig. 11). Casati & Gnaccolini in 1967 laid the geological foundation for the Western Orobic Alps (Orobic Anticline), upon which the succession was subsequently studied. Their study serves as the basis for identifying the rock type variations; at that time the succession was known as the Basal Conglomerate, the “Lower Volcanic Member" (later on Cabianca Volcanite) and the "Upper sedimentary Member” of the Collio Formation (later

on Pizzo del Diavolo Fm.). These units are unconformably covered by the upper Permian alluvial sediments of the Verrucano Lombardo.

Cassinis et al. (1986) then grouped this variation into three main lithofacies groups: terrigenous, evaporitic and extrabasinal volcanogenic deposits. More specifically, these authors identified: conglomerate and sandstone facies (alluvial fan); heterolithic sand-dominated facies (sand flat); heterolithic mud-dominated facies (mud flat); mud-dominated facies (perennial lacustrine); evaporitic deposits (saline lake); volcanogenic deposits.

Ten years later Cadel et *al.* (1996), whose work is still considered one of the most important concerning the geological setting of the Central Southern Alps basins, extended this scheme by classifying the facies on the basis of their sedimentological features and depositional environment. In addition to the proximal alluvial-fan settings (basement-sourced conglomerates), these authors identified specific facies for thick-bedded fluvial sandstones, heterolytic deposits dominated by sand and mud (the first of these being the main rock type at Monte Aga and at Pizzo del Diavolo di Tenda), perennial and ephemeral lacustrine sediments, and upper-level tuffs.

Sciunnach (2001) then put forward a more compact version of the interpretation. He continued to assign the geological history to the "Upper Member of the Collio Formation" (Map units 4 to 8 of Cadel et *al.* 1996), but he reduced the sequence to three main lithofacies, extending from high- to low-energy deposits: proximal conglomerates and sandstones, medium- to coarse volcanic arenites, and fine- to medium dark-grey volcanic arenites with some pelitic layers intercalated. Cassinis (2007) made another revision of the framework, to separate formally and namely the lower Permian successions in the Orobic and Collio basins. He officially recognised the succession as a separate unit, first referred to it as the Laghi Gemelli Group.

Boriani et *al.* (2012) applied the same classification to the Note Illustrative della Carta Geologica d'Italia alla scala 1:50,000, Foglio 056 – Sondrio, as part of the CARG Project. In this instance, the lithofacies are also correlated with the other stratigraphic units and are situated within the structural setting previously proposed for the Orobic Basin (Fig. 9). Five lithofacies were identified:

- an arenaceous lithofacies (FPZa) of volcanic-rich lithic sandstones and epiclastites, locally associated with pelitic and conglomeratic intervals, interpreted as a sandy alluvial plain with large alluvial fans and ephemeral watercourses;
- This pelitic lithofacies (FPZb) is made up of laminated black siltstones and claystones alternated with sandy layers; ripple marks, mud cracks, clay chips, raindrop imprints, soft-

sediment deformation structures and tetrapod tracks show that there were repeated changes between shallow lacustrine conditions and subaerial exposure;

- a conglomeratic lithofacies (FPZc), interpreted as proximal to distal alluvial-fan deposits;
- volcanites (FPZe), which record volcanic events;
- a carbonate-evaporitic lithofacies (FPZf), consisting of dolostones and lacustrine carbonate layers, is interpreted as having been formed by ephemeral alkaline lakes which were periodically affected by evaporation.

Subsequent research placed a greater emphasis on depositional processes. Berra & Felletti (2011) and Berra et *al.* (2016) went on to improve the scheme with regard to sedimentary architecture in the area from Mt. Farno and Pizzo del Diavolo di Tenda, by distinguishing between coarse proximal alluvial-fan deposits and finer distal-fan, alluvial-plain and basin-floor facies. The finer facies comprised deposits from ephemeral flows, shallow lakes and periodically exposed floodplains, as well as volcanic-rich and oncoid-bearing sections (Berra et *al.*, 2019) that record synsedimentary volcanism and playa-lake environments. In particular: L-PDVa: prevailing bedded, laterally continuous, fine-grained sandstones and siltstones, distal alluvial fan-terminal fan (with thin pelitic layers with chicken-wire nodules intercalate); L-PDVb: prevailing massive sandstone, with cross-laminations, scoured base and basal lags of clay chips, alluvial fan; L-PDVc: massive conglomerate with volcanic clasts (Val Sanguigno Conglomerate of Cadel et *al.*, 1996), proximal alluvial fan; P-PDV: Pelitic Lithozone, consisting of siltstones, shales and microbial carbonates.

Marchetti and others (2015) supported this classification by demonstrating the relationships between three types of environments: unconfined sheet-flood processes (arenitic lithofacies); shallow ephemeral lakes which contained numerous fossil traces, plant remains and carbonate deposits (pelitic lithofacies); and distal floodplain/playa areas that developed under arid or semi-arid climatic conditions (heterolithic arenitic-pelitic lithofacies).

Figure 9. shows the correlations between each lithofacies and other stratigraphic formations, as well as the structural settings proposed for the Central Southern Alps, specifically for the Orobic Basin.

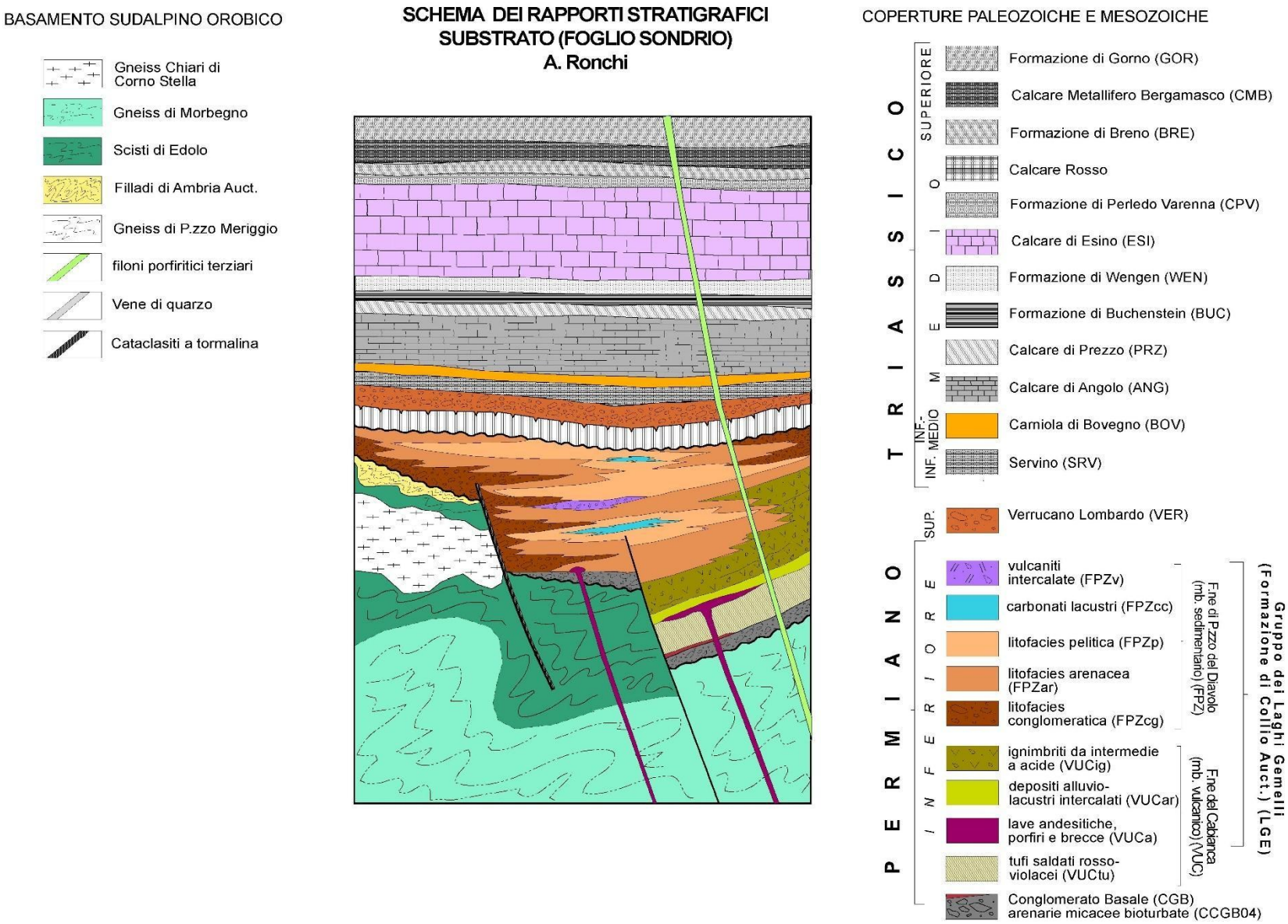


Figure 9. *Schematic representation of the stratigraphic relationships of the Orobic Basin. From Boriani et al. (2012).*

The state of the art

The most up-to-date and thorough account of the sedimentary succession cropping out upper Val d'Ambria is given by Cattaneo (2025a, master thesis). Six lithofacies were recognised in the study area on the basis of the succession's main lithological and sedimentary features, in accordance with Miall's (1996) facies-association criteria. This classification scheme forms the basis of the present thesis: unless otherwise mentioned, all the lithofacies referred to hereafter are those defined by Cattaneo (2025a) and locally revised in this study (see Section 7.1). They occur in the following order from base to top:

- Massive or weakly stratified conglomerates (**FPDa**)*: this unit comprises two sub-facies: 1) centimetric, matrix-supported quartz conglomerates rich in basement clasts and with subordinate volcanic, interbedded with dark pelitic/arenaceous layers; 2) massive, grain-supported polygenic conglomerates lacking sedimentary structures, forming extensive tabular bodies.
- Massive sandstones with quartz pebbles and flow structures (**FPDb**): this facies is characterized by metric-thick, reddish to greyish-white sandstone beds. It exhibits plane-parallel and cross-lamination, along with basal clay chips and sporadic quartz pebbles. Due to the inaccessibility of the outcrop, observations were primarily conducted from the debris fan.
- Laminated pelites alternated with sandstones (**FPDc**): composed of dark siltstones and claystones densely interbedded with fine grey sandstones. This facies preserves a wide range of sedimentary and biological structures, including ripples, rain-drop prints, algal mats (*elephant skins*), and well-preserved tetrapod footprints, as well as local seismically induced load structures.
- Lacustrine Carbonates and siltstones (**FPDd**): this lithofacies is defined by centimetric alternation of dark sandstones/siltstones and reddish carbonate layers. Carbonates also occur as spherical nodules (oncolites), suggesting deposition in a perennial lacustrine environment. Usually, this unit is limited to certain areas of the entire valley, interdigitating with other lithofacies.
- Reddish sandstones and siltstones (**FPDe**): this is the least common unit, occurring as discontinuous outcrops along the walls of Pizzo dell'Omino and as scattered debris blocks. It consists of alternating laminated and massive sandstones and pelites, locally displaying tectonic shear and clay chips.

- Volcanic sandstones with tuffs and cinerites (**FPDf**): characterized by tabular, laterally continuous beds of cineritic and pyroclastic material interbedded with fine epiclastics. Sedimentary structures (e.g., plane-parallel laminations, ripple marks) and occasional carbonate nodules indicate subaqueous reworking of these materials and syndepositional volcanic activity.

Fig.10 represents the stratigraphic succession based on the lithofacies descriptions provided by Cattaeno (2025).

* This lithofacies corresponds to the Monte Aga Conglomerate, cropping out for up to 200 meters-thick in the Orobic watershed (Cadel et *al*., 1996; Berra et *al*., 2016). This unit consists of a thick succession of crudely bedded, poorly sorted conglomerates with minor intercalations of sandstones and siltstones. The clasts (mostly metapelites, metagranitoids, mylonitic gneisses, and quartz; pebbles of volcanic origin are rare) derive mainly from erosion of the Variscan metamorphic basement (mostly Edolo micaschists and Ambria phyllite) and are generally angular (Zanoni et *al.*, 2010). The conglomerates thin out to the SE and interfinger with micaceous dark siltstones and sandstones, documenting both lateral (basinward) and vertical transition to fine-grained deposits. The contact with Variscan metamorphic basement to the north is tectonic and is interpreted as a syndepositional fault (Blom & Passchier 1997) locally reactivated during the Alpine orogenic events (Cadel et *al*., 1996).

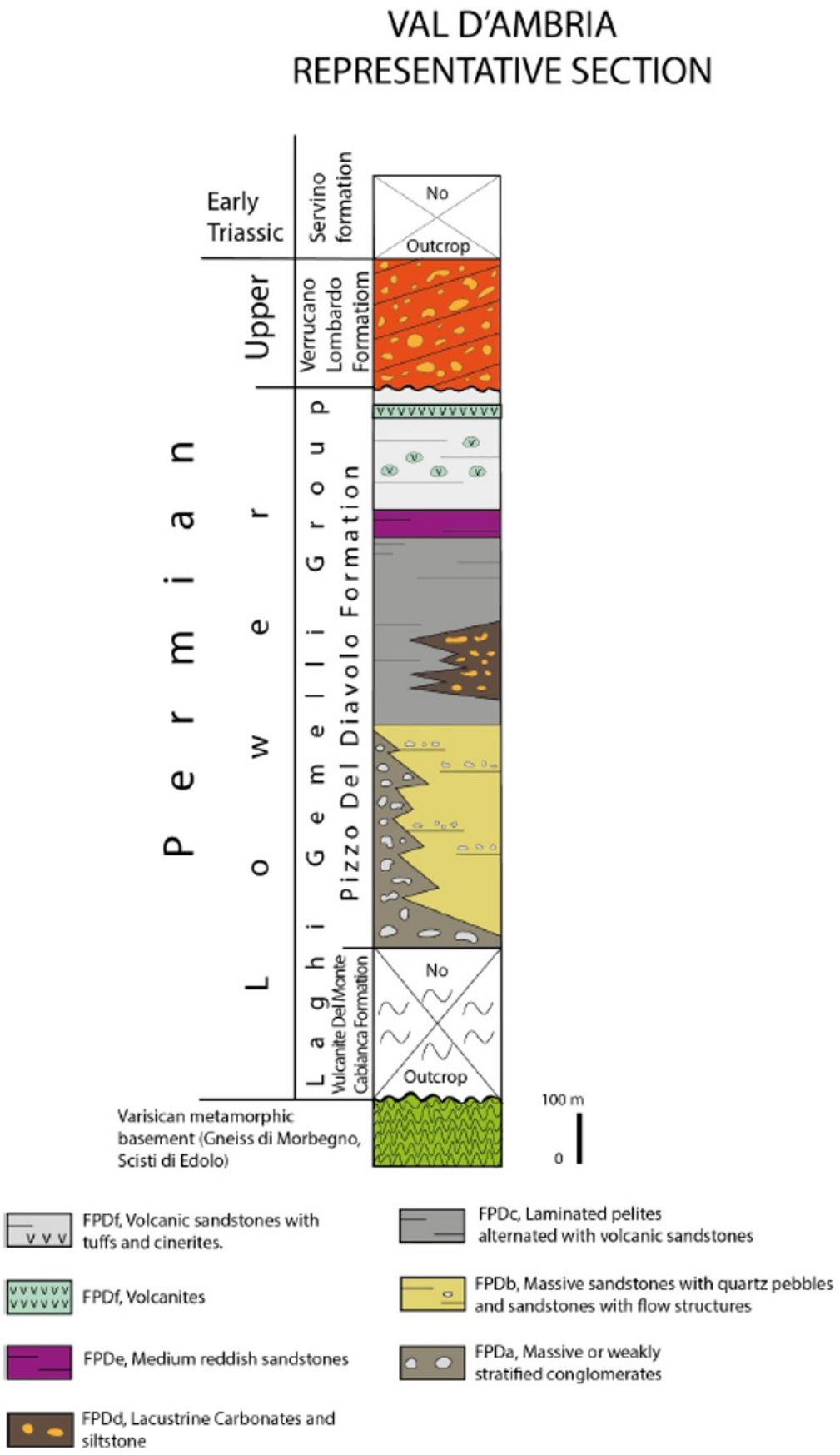


Figure 10. *Representative stratigraphic succession of the Val d'Ambria proposed by Cattaneo (2025a).*

The succession described above crops out in the area of the Omino peak (Fig. 11).

All considerations regarding the description of the Pizzo del Diavolo Formation discussed in this section are summarized in Fig. 12, which allows the highlighting of their similarities and differences.

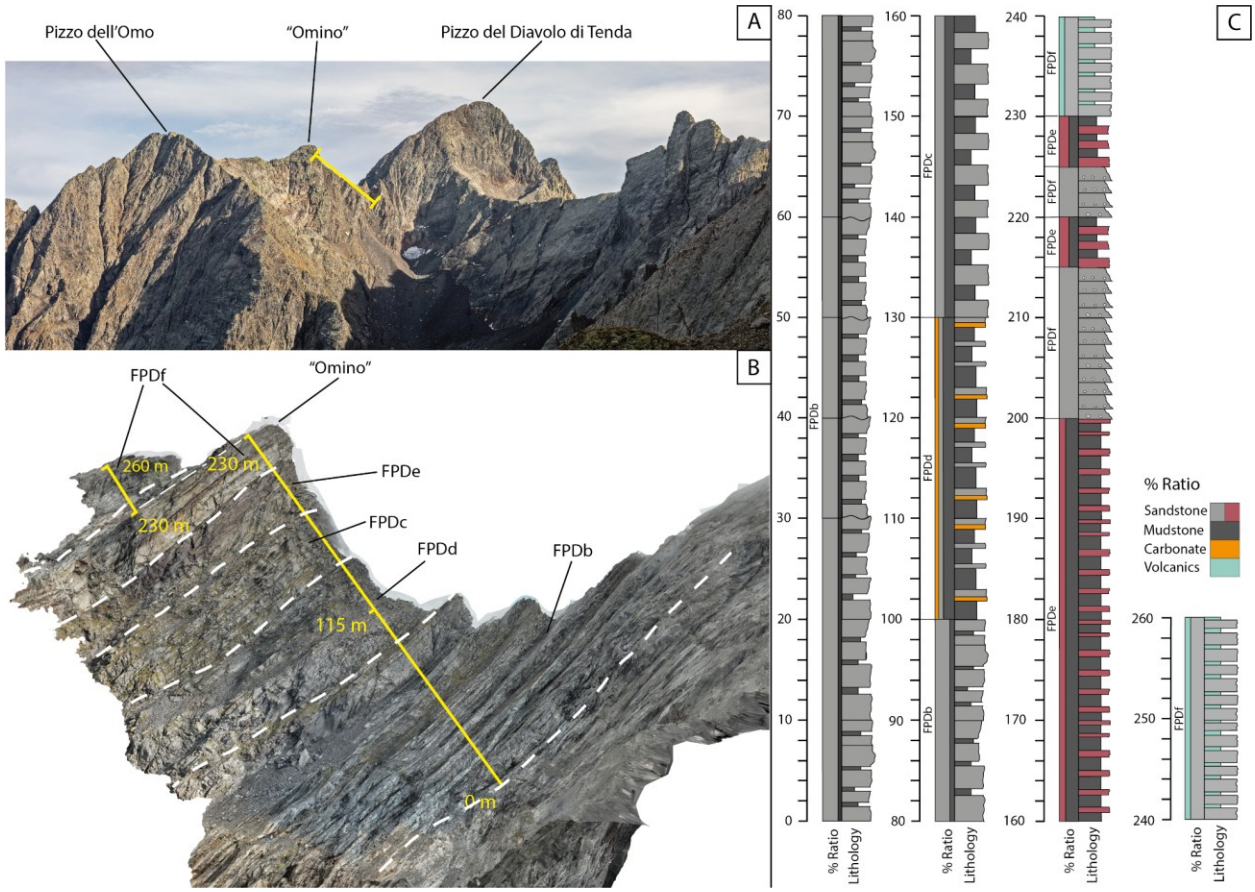


Figure 11. *Geological and stratigraphical setting of the upper Val d'Ambria headwall. A) Panoramic view showing the main peaks of the Val d'Ambria (e.g. Pizzo dell'Omo, "Omino" and Pizzo del Diavolo d Tenda) with the stratigraphic log trace (yellow line); B) 3D model providing a detailed view of the stratigraphic section with lithofacies boundaries (FPDb-FPDf); C) Stratigraphic log displaying different lithofacies, as interpreted by Cattaneo (2025a). The interpretation regarding the presence of the FPDd lithofacies has been updated. For further details, see Fig. 26 in Section 6.2.1.*

Figure 12. *Comparison between different descriptions of the lithofacies of the Pizzo del Diavolo Formation provided by various authors.*

3.2.4 Verrucano Lombardo

The Verrucano Lombardo lies unconformably on top of the Pizzo del Diavolo formation and it is composed of polygenic conglomerates consisting of subrounded, pluricentimetric clasts of quartz, purplish volcanites and, more rarely, crystalline schists, with sizes ranging between 3 cm and 4 cm. Sometimes, thin layers of reddish sandstones and dark-red lenses of siltstones can be found inside this formation, as well as channelized structures typical of *braided* alluvial systems (parallel and concave cross-laminations) in the coarser levels, while mud-cracks and bioturbations characterize its finer-grained intervals.

Generally speaking, the Verrucano Lombardo can be subdivided into two portions: the lower section is represented by conglomerates and conglomeratic sandstones, often characterized by the presence of siltstones lenses; the upper section consists of coarse-grained sandstones alternating with siltstones. These features describe the evolutionary trend of the formation, starting from an anastomosing river system, passing through a meandering system and, finally, evolving to an alluvial plain environment.

Based on its stratigraphic position (the unit lies below the Servino Formation), as well as its correlation with the Arenarie della Val Gardena – which is richer in fossils (e.g., tetrapod tracks) and into which it grades laterally east of the Val D'Adige – the Verrucano Lombardo is usually associated with the upper Permian. In the area under consideration, the Verrucano Lombardo outcrops are limited to small patches near the top of both Monte Aga and Monte Masoni (Boriani et *al.*, 2012).

3.3. The paleontological record of upper Val d'Ambria

Recently, an extremely well-preserved fossil record has been discovered from this formation in the upper Val d'Ambria, including several vertebrate (tetrapod) and invertebrate footprints, as well as plant and seed remains (e.g., conifers and horsetails?). *Amphisauropus*, *Batrachichnus*, *Limnopus*, *Dromopus*, *Erpetopus*, *Hyloidichnus*, *Varanopus*, *Tambachichnium*, *Pachypes* and *Dimetropus* represent the ichnogenera identified for the vertebrate tracks, while *Diplopodichnus* and *Diplichnites* are among the ichnotaxa recognized for the invertebrate record (see also Bonizzoni, 2024 and Cattaneo, 2025a, unpublished thesis). Not only do these discoveries appear to be consistent with the fossil record described for the entire Orobic Basin in previous studies (e.g., Dozy, 1935; Santi and Krieger 2001; Ronchi e Santi, 2003; Marchetti et al., 2015; Marchetti, 2016; Santi et *al.*, 2020; Marchetti et *al.*, 2022) – and for the other Permian basins of the Central Southern Alps – but they also testify to an extremely rich environment in terms of biodiversity.

The newly described record for the Val d'Ambria, together with the available radiometric constraints on the Cabianca Volcanites, constrains the age of the Pizzo del Diavolo formation to the late early Permian (Kungurian).

4. STRUCTURAL SETTING OF THE OROBIC BASIN

From a geological point of view, the Val d'Ambria is located inside the so-called Orobic Basin, one of the three main Permian sedimentary basins of the Southern Alpine Domain, together with the Collio Basin and the Athesian District (Fig. 13a).

This domain, currently separated from the northern Alpine domains by the Insubric Line (dextral strike-slip fault) and extending southwards beneath the Quaternary sediments of the Po Plain, represents a remnant of the Adria passive margin and it was characterized by an episode of crustal extension starting in the Early Permian, immediately after the late stages of the Variscan orogeny (Pohl et *al.*, 2018; Zanchi et *al.*, 2019; Locchi, 2023; Zanchetta et *al.*, 2022); the structures created during this specific event are now well-preserved in the geological record of the area (Berra et *al.* 2016; Zanchetta et *al.*, 2022). Among these, the so-called *Low Angle Normal Faults* (LANFs) and their related *High Angle Normal Faults* (HANFs) are of particular interest, as discussed in the following chapters. As said previously, these kinds of structures are described in the study area by Zanchi et al. (2019) and in the Orobic anticline by Locchi et *al.* (2022).

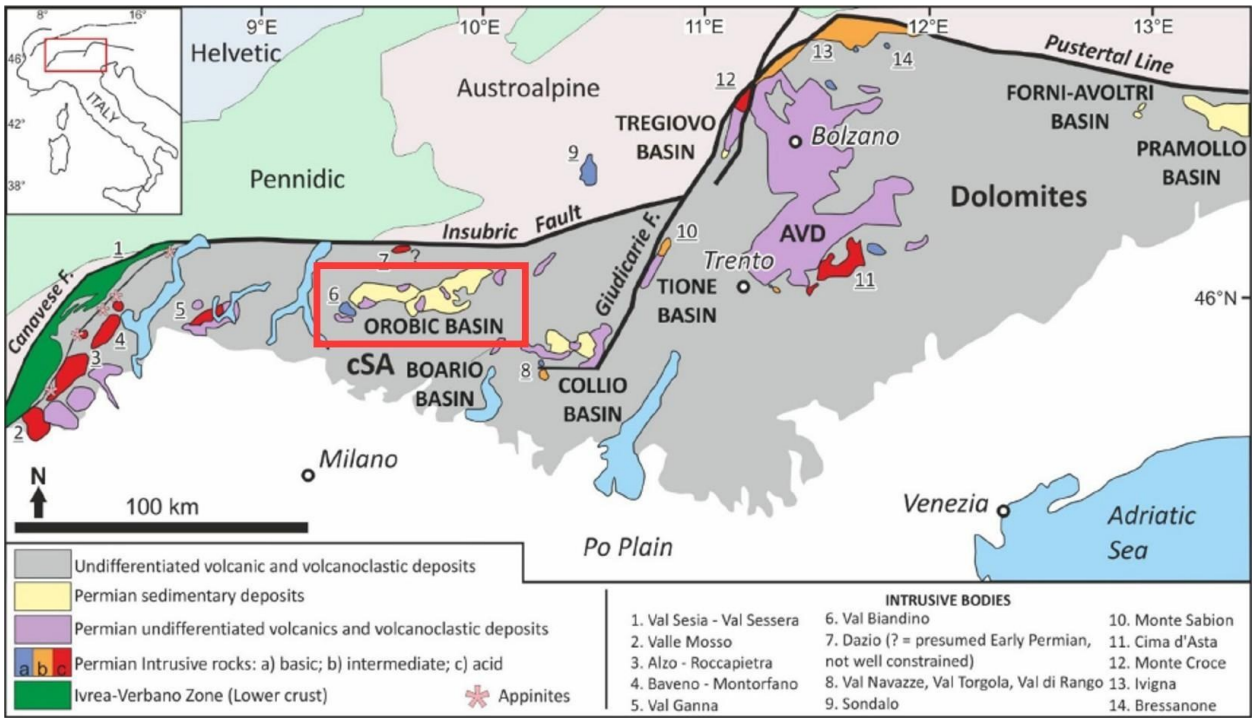


Figure 13a. *Geological setting of the Southern Alpine Domain. Red shape: area of interest, the Orobic Basin. The map represents the Permian lower crust, intrusive bodies, volcanic and sedimentary cover. Central Southern Alps (cSA); Athesian Volcanic District (AVD). Modified from Locchi et al. (2022).*

The LANFs (dip < 30°) were later reactivated, and partially inverted, during the Alpine shortening that triggered the Orobic Thrust development starting from the Late Cretaceous.
These tectonic events resulted in the present-day thick-skinned fold-and-thrust grown belt that constitutes the area of the Central Southern Alps (cSA).

The general structural setting of the cSA is characterized by several tectonic domains with an overall E-W trend. In the area located south of the Insubric Line, the Variscan basement is structured into a belt defined by two main thrusts: the Orobic Thrust to the west and the Gallinera Thrust to the east, the latter being intruded by the tonalites of the Adamello massif. Toward the south, both structures override the Orobic Anticlines, a regionally developed anticline system with a WSW-ENE axis, arranged in a dextral en echelon pattern (Fig. 13b). Westwards, the anticline belts end against the Valsassina Fault, whereas to the east (Cedolo and Val Camonica valleys) the Variscan basement of the Cedolo Anticline widely outcrops (Albini et *al.*, 1994).

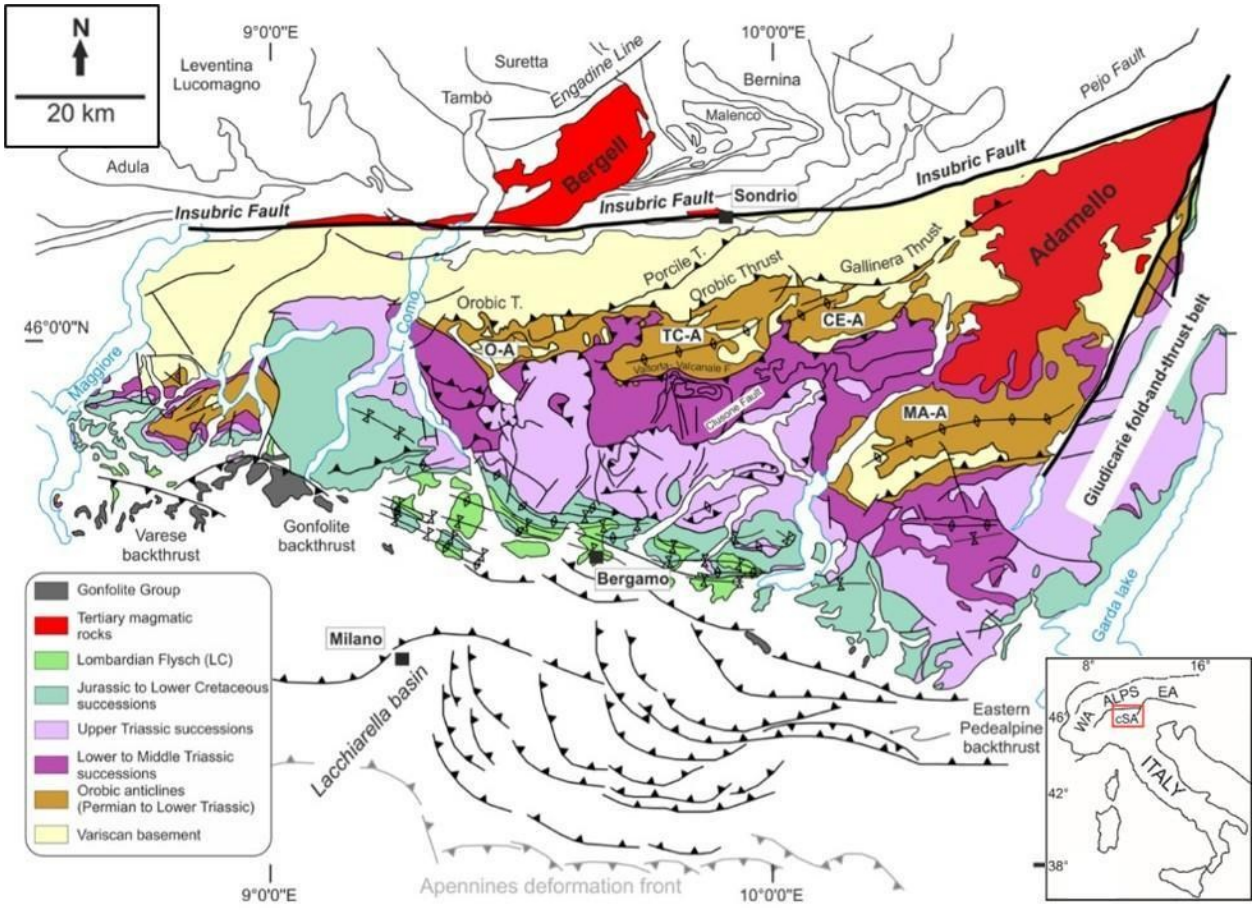


Figure 13b. *Main structures of the Central Southern Alps (cSA). Modified from Zanchetta et al. (2022).*

As above mentioned, a complex geodynamical evolution, that can be divided into three main phases, characterized the cSA: the Variscan tectonics, the extensive pre-Alpine phase and, finally, the Alpine collisional phase (Boriani et *al.*, 2012).

4.1 Tectonic evolution

4.1.1 Late-to-post Variscan tectonics

Two main deformation phases ("D_1" and "D_2" happened at amphibolite and greenschists facies) can be recognized in the evolution of the pre-Alpine basement, which consists of two mica-paragneisses and mica-schists, named "Morbegno Gneiss" and "Edolo Schists" respectively (Locchi et *al.*, 2022; Mittempergher et *al.*, 2021). Each phase is associated with distinct types of metamorphism. The first phase is related to a significant crustal thickening caused by the Variscan tectonic collision, and it is followed by prograde metamorphism; the second phase is characterized by the exhumation and, consequently, the erosion of the orogenic belt, caused by a number of regional left-lateral wrenches (Cadel et *al.*, 1996) and resulting in the so-called "Basal Conglomerate" (see the stratigraphic description below). This process is associated with retrograde metamorphism and a lithospheric thinning linked to the rifting that led to the opening of the Tethys Ocean and the development of *pull-apart* basins throughout the entire Southern Alpine Domain, starting from the Early Permian (Boriani et *al.*, 2012; Locchi et *al.*, 2022).

4.1.2 Pre-Alpine extensional phase

Three main hypotheses have been proposed to identify the mechanism responsible for the lower Permian crustal extension and lithospheric thinning, and the consequent development of the Permian sedimentary basins (such as the Collio Basin and the Orobic Basin): (1) dextral transtension and wrenching along a WSW-ENE trending megashear between Laurasia and Gondwana (Arthaud & Matte, 1977 among many others); (2) pure N-S directed extension, and (3) lithospheric extension and thinning as the initial phases of continental rifting. This last interpretation is still under debate.

Among the different geodynamic models proposed to explain the lower Permian crustal extension in the Southern Alps, the transtensional hypothesis ((1) in the above list) is the most widely accepted interpretation.

According to this model, the lower Permian basins of the Southern Alps, including the Orobic and Collio basins, have traditionally been interpreted as transtensional pull-apart basins controlled by dextral strike-slip fault systems (Cassinis & Perotti 1993; Cassinis & Perotti, 2007; Cassinis et *al.*,

2012; Edel et *al.*, 2014), generated by the activity of a dextral megashear system developed between Laurasia and Gondwana, during the Permo-Carboniferous. Cassinis & Perotti (2007) specified that this dynamic was probably controlled by a dextral shear along NNE faults in present day configuration, involving Giudicarie, Val Camonica and Canavese paleo-lines, and by extension or normal or oblique throws along ENE faults, Val Trompia, Val Sugana and Insubric Lineaments (Fig. 14). According to the study, this regime would have succeeded the Late-Variscan deformative stages and persisted up to the last Alpine Orogenic phases.

This tectonic regime, already pointed out in all western Europe by Arthaud & Matte (1977), in the last thirty years is often associated with the transition from the lower Permian Pangea B configuration (with Gondwana further located to the East) to the upper Permian Pangea A setting, characterized by a counter-clockwise rotation of Gondwana with respect to Laurasia (Muttoni et al., 1996; 2003; 2009).

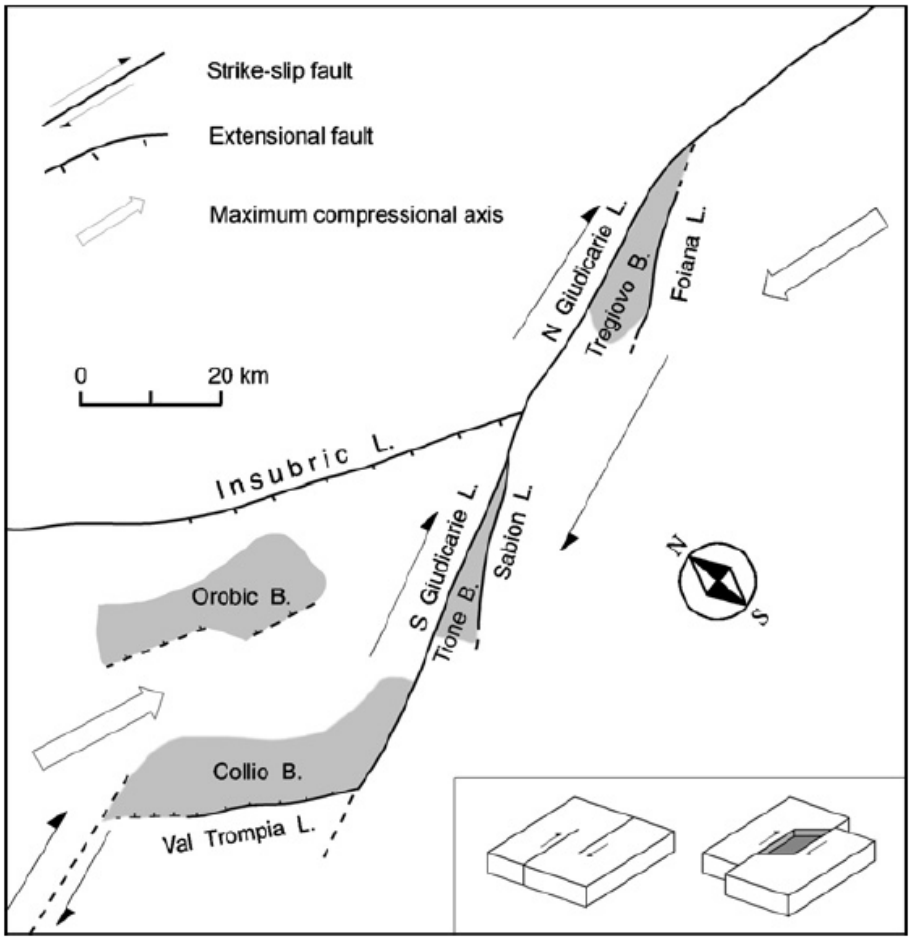


Figure 14. *Schematic interpretation of the development of the Southern Alps sedimentary basins, according to the transtensional geodynamic model. From Cassinis & Perotti (2007).*

This interpretation is also reflected in the geological synthesis provided by the Note Illustrative della *Carta Geologica d'Italia* alla scala 1:50,000, Foglio 056 – Sondrio (Boriani et *al.*, 2012), where the early Permian tectonic evolution of the Central Southern Alps is described as dominated by a transtensional regime characterized by dextral strike-slip fault systems, the formation of pull-apart basins and widespread magmatic activity associated with the collapse of the Variscan belt. The authors also introduced the hypothesis of an inversion of the tectonic regime, from a transtensional to a transpressional dynamics, occurring at the transition between the lower and the upper sedimentary cycles, marked by a visible unconformity.
The transtensional origin of these basins has also been emphasized by Berra et *al.* (2016), who reviewed the principal geodynamic models proposed for the Permian volcanic and sedimentary successions of the Southern Alps. Interestingly enough, the authors pointed out that a transtensional component characterizes the development of these basins *regardless of the preferred geodynamic interpretation*.

Recently, Elter et *al.* (2020) concluded that the so-called EVSZ – the *East Variscan Shear Zone*, one of the largest Variscan intracontinental dextral strike-slip shear zones, extending from Slovenia trough the Alps and to North Africa and active between 325 ± 1.3 Ma and 315 ± 1.3 Ma (based on U-Pb radiometric age on monazite and on zircons, respectively) – was not only the responsible for the development of the late Carboniferous-early Permian basins (as well as for the mid- to late Permian basins), but also that its transtensional regime activity continued into the Triassic, controlling the opening of the Ligurian-Piedmont Ocean (the Alpine Thetys,).
Moreover, Siravo et *al.*, 2026 reviewed the origin of Permian intra-Pangea basins from Europe and Iberia, highlighting that they have generally been interpreted as the product of transtensional tectonics. They even cited the study by Filippi et *al.* (2025), which documented rapid Early Permian crustal exhumation associated with extensional tectonics in the Western Alps (probably "an extensional component"?).

However, Froitzheim et *al.* (2008) proposed an alternative mechanism centered on pure, large-scale extension: the authors identified a low-angle extensional shear zone, the *Grassi Detachment Fault* – which separates the Variscan metamorphic basement (Morbegno Gneiss), in its foot-wall, from the overlying lower Permian volcanic and sedimentary rocks of the Collio Formation – and associated metamorphic core complex, formed on the northwestern flank of the Collio Basin; its foot-wall mylonites, formed under temperatures of at least 500°, were juxtaposed to hanging-wall erupted volcanic rocks, indicating a large amount of exhumation, similar to the situation of the core complexes of the Colorado River extensional corridor, in Western North America.

Therefore, the authors concluded that the Collio Basin, in this case, was “a rapidly extended rifting”.

Thermo-mechanical modelling performed by Spalla et *al.* (2014) suggested that active lithospheric extension, followed by asthenospheric upwelling and crustal thinning is required to reproduce the observed metamorphic, igneous, structural and age data of the Permian-Triassic geological evolution of the Southern Alps. This idea is supported by the identification of mafic intrusive complexes (290-215 Ma) within the Southalpine and Austroalpine domains, which the authors interpreted as evidence of an asymmetric lithospheric stretching preceding the opening of the Alpine Tethys.

The idea of a pure extensional mechanism has recently been re-proposed by Zanchi et *al.*, 2019 and Locchi et *al.* (2022). According to these authors, the development of the Permian basins of the Southern Alps was driven by a predominantly N–S-directed crustal extension, which ultimately resulted in significant lithospheric thinning during the Early Permian. In this framework, the Orobic Basin is interpreted as an asymmetric extensional basin, whose evolution was controlled by the interaction between major *Low-Angle Normal Faults* (LANFs) and their related *High-Angle Normal Faults* (HANFs). Among these, the Aga-Vedello Fault and the Masoni Fault represent two of the major structures (LANFs) identified by the two studies. Notably, the Aga-Vedello Fault extends into the northern sector of the Val d’Ambria – the primary focus of this study.
The extensional nature of this tectonic regime is further supported by the distribution of synsedimentary structures that can be identified within the *Laghi Gemelli Group*. Among these, growth strata, synsedimentary faults, progressive unconformities and widespread soft-sediment deformation indicate that tectonic activity occurred contemporaneously with sedimentation (see also Berra & Felletti, 2011).
From a kinematic point of view, Zanchi et *al.* (2019) and Locchi et *al.* (2022) proposed that the early Permian stress field was characterized by a subvertical maximum principal stress (σ_1) and a subhorizontal minimum principal stress (σ_3), oriented approximately N–S. This configuration is typical of Andersonian normal faulting.
Under these conditions, the extension was accommodated by large detachment faults rooted within the upper crust, while steeper synthetic and antithetic normal faults developed in their hanging-walls, progressively segmenting the basin into smaller sectors.
The same authors pointed out that strike-slip tectonics can be responsible for a later partial tectonic inversion of the basins, as evidenced by the angular unconformity separating the lower Permian

succession (i.e. Pizzo del Diavolo Formation, for the Orobic Basin) from the overlying upper Permian Verrucano Lombardo.

The Permian extensional phase was also responsible for HT metamorphism processes and a widespread magmatic activity lasted about 20 Ma (ranging from 290 to 270 Ma, as suggested by Schaltegger & Brack, 2007), occurred at different crustal levels (e.g. Ivrea-Verbano body and Laghi Granites), which resulted in the emplacement of gabbro to gabbro-diorites bodies at the lower crust-mantle transition, acid intrusive complexes at intermediate levels and, finally, volcanic products above the upper Carboniferous-Lower Permian Variscan unconformity (Berra et *al.*, 2011; Locchi et *al*., 2022).

4.1.3 Alpine Orogeny

The Alpine orogeny is traditionally subdivided into three main compressive phases. The first one, the Eo-Alpine phase (Early-to-Late Cretaceous, according to Manatschal et *al.*, 2022), developed following the closure of the Alpine Tethys (also known as the Ligurian-Piedmont Ocean), occurred in two stages: D_{3a} and D_{3b} deformation events (following Zanchetta et *al.*, 2015), involving and partially inverting the previous (normal) faults inherited from Permian and Triassic extension.
D_{3a} is related to the emplacement of the overall E-W trending *Gallinera-Porcile-Orobic thrust system* (GPO, also known as the Orobic Thrusts), which occurred in a transitional ductile-brittle regime, and related south-verging folds in basement and cover units (*Orobic Anticlines*?). A penetrative S3 disjunctive cleavage recorded within the cover rocks is often associated with this deformation event (Mittempergher et *al.*, 2021). The Orobic Thrusts form the roof of the present-day structural architecture of the cSA, involving the metasedimentary succession of the South Alpine Basement, which consists of phyllites, micaschists and paragneiss, intruded by Late Variscan tonalites and diorites. The development of the eastern thrust, the Gallinera Thrust, is thought to mark a change of the regional strike of the Orobic Thrusts, from E-W to NW-SE, presumably due to the inheritance of the paleofaults that opened the Collio Basin (Fantoni et *al.*, 2004). The ages of the Orobic Thrust activity is constrained by radiometric age of the andesitic dykes that cross-cut the Permian succession, and range from 63 Ma to 54-36 Ma (Fantoni et *al.*, 2004), 80 Ma to 68 Ma (Zanchetta et *al.*, 2011), while the oldest U-Pb radioisotopic ages, derived from the shear veins in San Pellegrino and Sorisole areas presented in Rocca (2025) range from 98.2 ± 9.9 Ma to 82 ± 11 Ma.
The Orobic Anticlines consist of a regional complex of anticlines characterized by a dextral *en-échelon* arrangement related to the original shape of Collio Basin (Fantoni et *al.*, 2004).

D_{3b} event is linked to the development of fault-bend folds during out-of-sequence thrusting at deeper structural levels, and the southward propagation of the Orobic Anticlines. Based on the analysis of the Apatite Fission Tracks, it is suggested that these anticlines formed at depths greater than the Partial Annealing Zone before the Eocene, as mentioned in Zanchetta et *al.*, 2015.
After a relative quiescence in deformational activity, collisional processes involving the European and African continental margins led to the Meso-Alpine phase (c.a. 84 Ma, according to Manatschal et *al.*, 2022), resulting in particularly complex deformation. These are well expressed in the Southern Alps, where structures with Dinaric vergence are observed. A subsequent tectonic quiescence allowed the emplacement of dykes and magmatic bodies (e.g. the Masino-Bregaglia pluton and, in part, the Adamello pluton) within already partially deformed successions (Mengoli, 1993; Mittempergher et *al.*, 2021).
The final phase, the Neo-Alpine orogenic phase (c.a. 35 Ma, Late Eocene, according to Manatschal et *al.*, 2022) – associated with the D_4 deformation event –, led to the general uplift of the chain, further deformation of the Meso-Alpine thrusts, and the development of compressional structures referred to as the "Milano Belt", extending over a wide area currently buried beneath the Plio-Quaternary deposits of the Po Plain (Mengoli, 1993; Zanchetta et *al.*, 2015).

Within this framework, along the Orobic and Porcile thrusts, structural analyses and fault-rock dating indicate a polyphase history: after their initial development in the Late Cretaceous, these structures were reactivated between the Late Paleocene and the Middle Eocene and, finally, accommodated a late strike-slip to dextral transpressive reactivation, tentatively linked to the Insubric Line activity (D'Adda & Zanchetta, 2015). This latest phase, dated to the late Oligocene–Miocene (Schmid et *al.*, 1989), crosscuts the previous structures.

5. MATERIALS AND METHODS

The research presented in this thesis was carried out using an integrated methodological approach combining traditional geological field observations, specifically regarding the description and identification of the lithofacies (Cattaneo, 2025a), with Unmanned Aerial Vehicle (UAV) Digital Photogrammetry (UAVDP) and Digital Outcrop Modelling (DOM).
My personal contribution regards the analysis and interpretations of the DOMs, operations conducted using *CloudCompare* and *Stereonet* softwares.

5.1 Cartographic analysis

To support the interpretation of the data extracted from the three-dimensional model of the study area, several geological and structural maps were referenced or directly used to gather data and generate comparison diagrams. These sources included Cadel et *al.* (1996); Sondrio sheet 056 CARG (Boriani et *al.*, 2012; Servizio Geologico d'Italia, 2012); Carta geologica della provincia di Bergamo alla scala 50.000 (Forcella and Jadoul, 2000); Mappa geologica del fiume Brembo di Carona (Mengoli, 1993); Geological map of the Val d'Ambria area (Cattaneo, 2025b). Specifically, the maps by Cadel et *al.* (1996), Boriani et *al.* (2012) and Cattaneo (2025b) were imported into QGIS (v. 3.44.14) and georeferenced using the native georeferencer tool by matching features and toponyms with satellite imagery. Fault lineaments were subsequently digitized using the *Add Line Feature* tool, and rose diagrams of their orientations were generated by using the *Line Direction Histogram* plugin.

5.2 UAV survey

The UAV surveys were performed in July and September 2025, using a DJI Mavic 3E equipped with an integrated 20-Megapixel camera (CCD sensor 1 inch size) and an on-board RTK GNSS system (*Real Time Kinematic Global Navigation Satellite System*) (Fig. 15).
Nine flights were conducted, acquiring a total of 2669 RGB photographs.
During the acquisitions, image overlap was kept above 80% to guarantee adequate image matching during photogrammetric processing, while flying altitude was set between 67.9 m and 386 m above ground level. Ground resolution ranges from 2.34 cm/pix to 13.5 cm/pix.



Figure 15. *DJI Mavic 3E used for the acquisition of the images in Val d'Ambria.*

Photogrammetric processing and 3D reconstruction were carried out using *Agisoft Metashape* software (v. 2.2.1). Image processing was conducted at full image resolution to generate high-resolution Digital Outcrop Models (DOMs).
The workflow used to generate the DOMs is discussed in the next paragraph.

5.3 Digital Outcrop Models (DOMs) development and analysis

Three-dimentional Digital Outcrop Models (DOMs) were created using *Agisoft Metashape* software (v. 2.2.1). Following UAV photogrammetric acquisition, the first step of the workflow consisted of image alignment. During this automated process, tie points were identified across overlapping photos, which maintained a minimum overlap of 80%. These tie points were selected by matching distinctive visual features shared by multiple images.

After images alignment, a sparse point cloud was generated and subsequently used to produce its related dense point cloud, consisting of a three-dimensional distribution of points extracted from the overlapping photographs and displayed within an XYZ coordinate system. This model provided the first digital approximation of the real outcrop (Fig. 16).

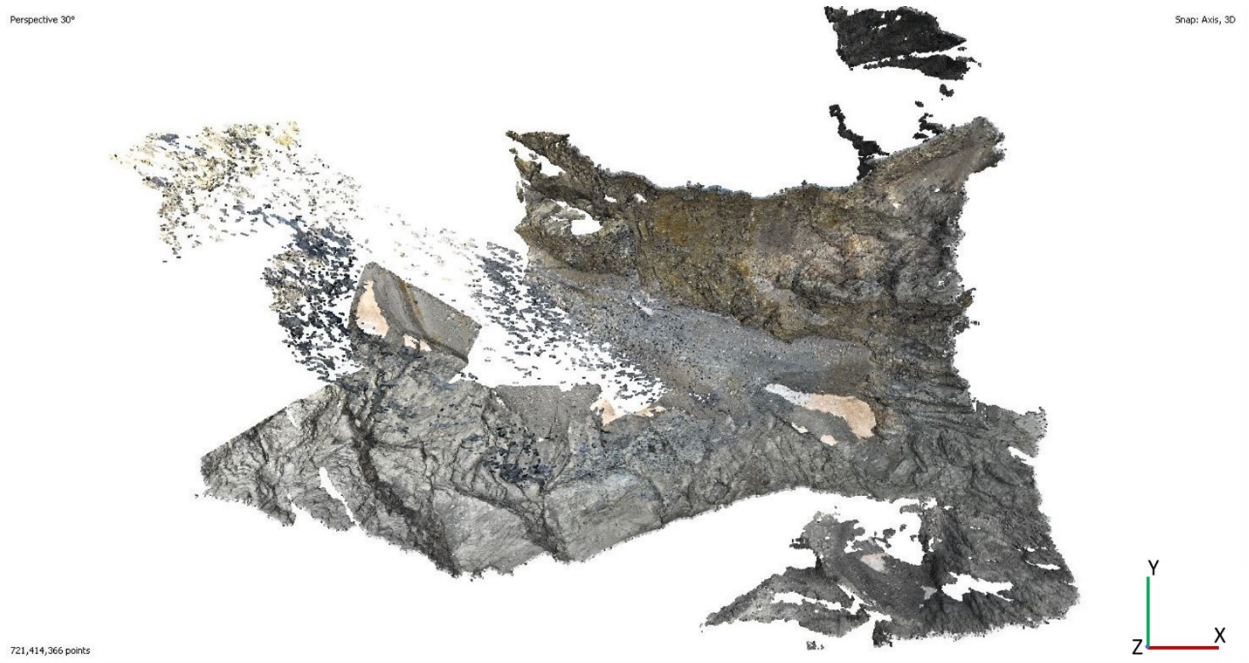


Figure 16. *Example of dense point cloud generated from UAV data, a portion of the 3D model (Y-axis pointing North). Agisoft Metashape (v. 2.2.1).*

The dense point cloud was then used to generate the so-called "mesh", a continuous 3D surface consisting in a network of triangular-shapes connecting each point of the cloud (Fig. 17).

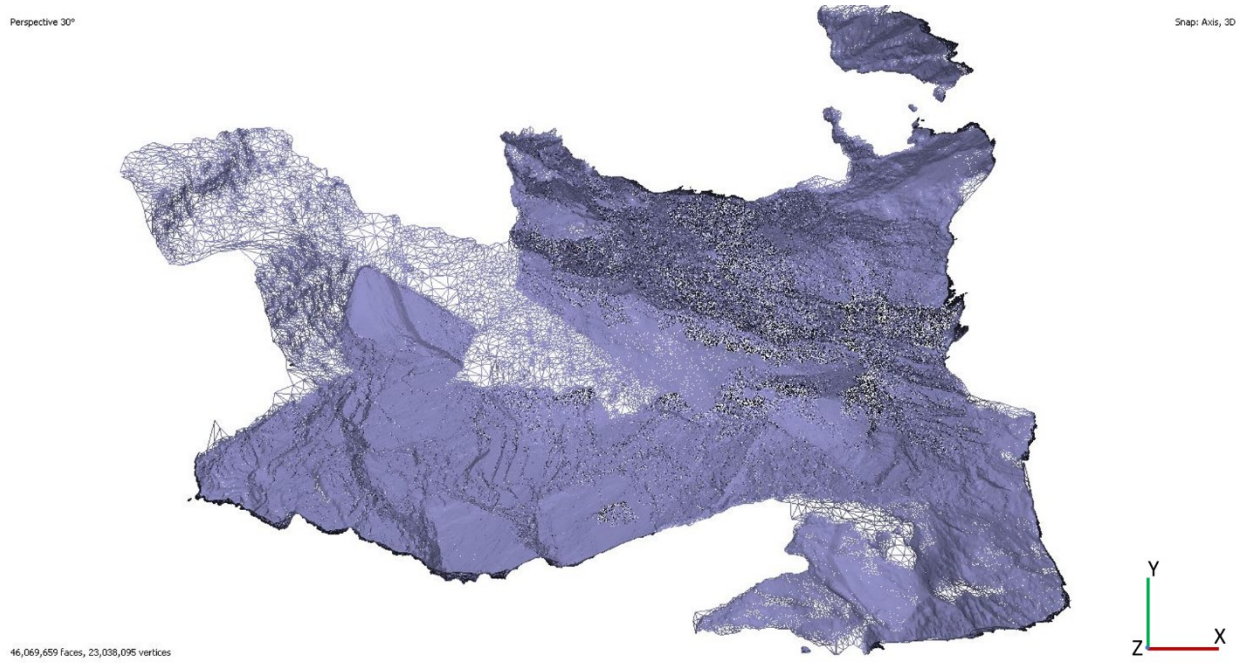


Figure 17. *Digital mesh obtained from the previous dense point cloud displayed in Fig. 16 (Y-axis pointing North). Agisoft Metashape (v. 2.2.1).*

Finally, a realistic texture extracted from the acquired photographs was projected onto the mesh, faithfully reproducing the original outcrop and yielding the DOM (Fig. 18).



Figure 18. *Realistic texture applied to the digital mesh shown in Fig. 17 (Y-axis pointing North). Agisoft Metashape (v. 2.2.1).*

This procedure was applied to generate multiple DOMs each representing distinct sections of the same broad area.

The final step consisted of manually aligning and merging the individual DOMs to construct the complete 3D model (point cloud) of the study area (Fig. 19).

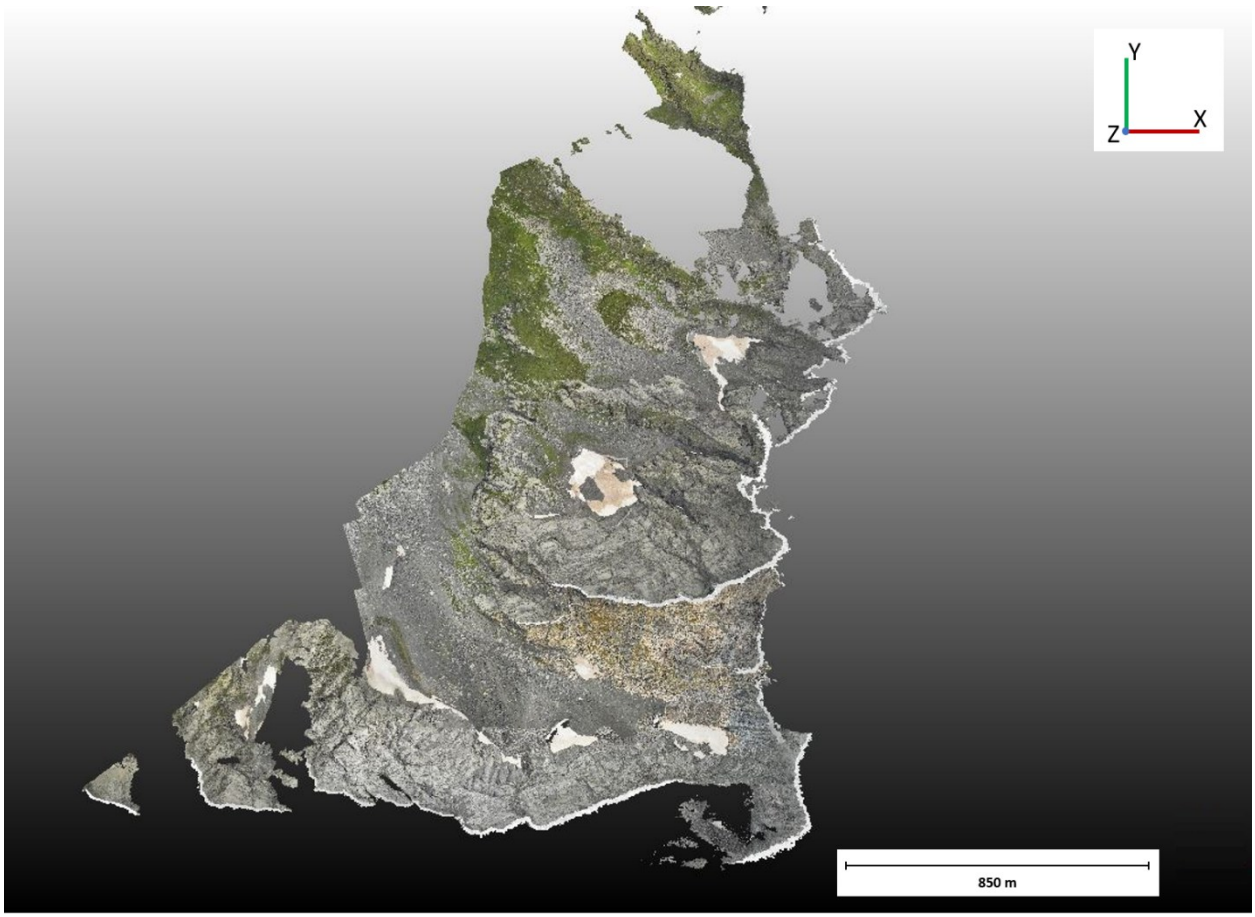


Figure 19. *Complete 3D point cloud of the uppermost area of Val d'Ambria (Y-axis pointing North). Scale bar: 850 m. CloudCompare (v. 2.12.1).*

This operation was completed by importing the individual models into *CloudCompare* software (v. 2.12.1).

Best-fit planes were constructed for the surfaces depicted in each sector. Most of the measurements were acquired mainly using a manual sampling technique, the *Trace Polyline* tool, while other minor data were collected using the computer-aided mapping tool, the *Trace Tool* of the *Compass* plugin, both displayed in *CloudCompare*. Stereoplots were ultimately generated by importing the data into *Stereonet* software (v. 11).

6. RESULTS

6.1 Critical interpretation of previous maps

The following is a brief description of the area of the upper Val Brembana tectonic configuration, which can be useful for comparing its main structural arrangements with the assets identified in Val d'Ambria.
The descriptions provided by the Note Illustrative della *Carta Geologica d'Italia* alla scala 1:50,000, Foglio 056 – Sondrio (Boriani et *al.*, 2012) divide the upper Val Brembana into two main sectors: the southern portion and the central area. The last sector discussed in the paper, the northern area, bounded between Monte Aga, Pizzo del Diavolo di Tenda and Monte Masoni, is described in the following chapters, representing the study area of this thesis and being its direct adjacent zone.

6.1.1 Southern sector of the upper Val Brembana

It corresponds to the area surrounding Monte Cabianca, south of Linea del Monte Sardegnana-Lago Fregabolgia-Lago Rotondo. This sector is characterized by an extensive monocline dipping 40° towards SSW. Several sub-vertical to steeply SW-dipping reverse faults, trending NW-SE to NNW-SSE, intersect the monocline and are associated with late Alpine dynamics. Minor sub-vertical reverse faults, likely with a strike-slip component, trending NW-SE to WNW-ESE (e.g., west of the line connecting Passo di Portula-Rifugio Calvi), alongside WNW-trending folds, are also present (Fig. 20).

Overall, almost the entire Southern sector is characterized by a homogeneous stratigraphic sequence, with the exception of the area west of Monte Val Rossa. Here, detachment surfaces induce structural repetitions within the pelitic lithofacies of the Laghi Gemelli Group (LG) and at the base of the Verrucano Lombardo (Boriani et *al.*, 2012).

6.1.2 Central sector of the upper Val Brembana

This sector is represented by the so-called Costa della Mersa, an E-W elongated area stretching for 500-1000 m in width and bounded by two major, steeply dipping E-W trending tectonic lineaments. The southern lineament corresponds to the Lago Fregabolgia fault, whereas the

northern one is defined by the Pizzo Poris-Lago del Prato fault, with the former having been reactivated as a reverse fault during the Alpine compression.

Due to the exclusive presence of the terrigenous lithofacies of the Laghi Gemelli Group, the major deformations characterizing the area are essentially associated with a ductile regime, featuring large- to small-scale, E-W oriented, sub-horizontal folds. It is worth noting the presence of an extensive syncline whose north-dipping limb is significantly more developed than the south-dipping one, which is truncated by the Lago Fregabolgia fault.

Two main *master joint* sets are also present in the area: the first, characterized by vertical planes trending NW-SE, crosscuts the E-W trending Alpine structures; the second set consists of sub-vertical planes dipping steeply towards the north, with an average E-W trend (Albini et *al.*, 1994; Boriani et *al.*, 2012).

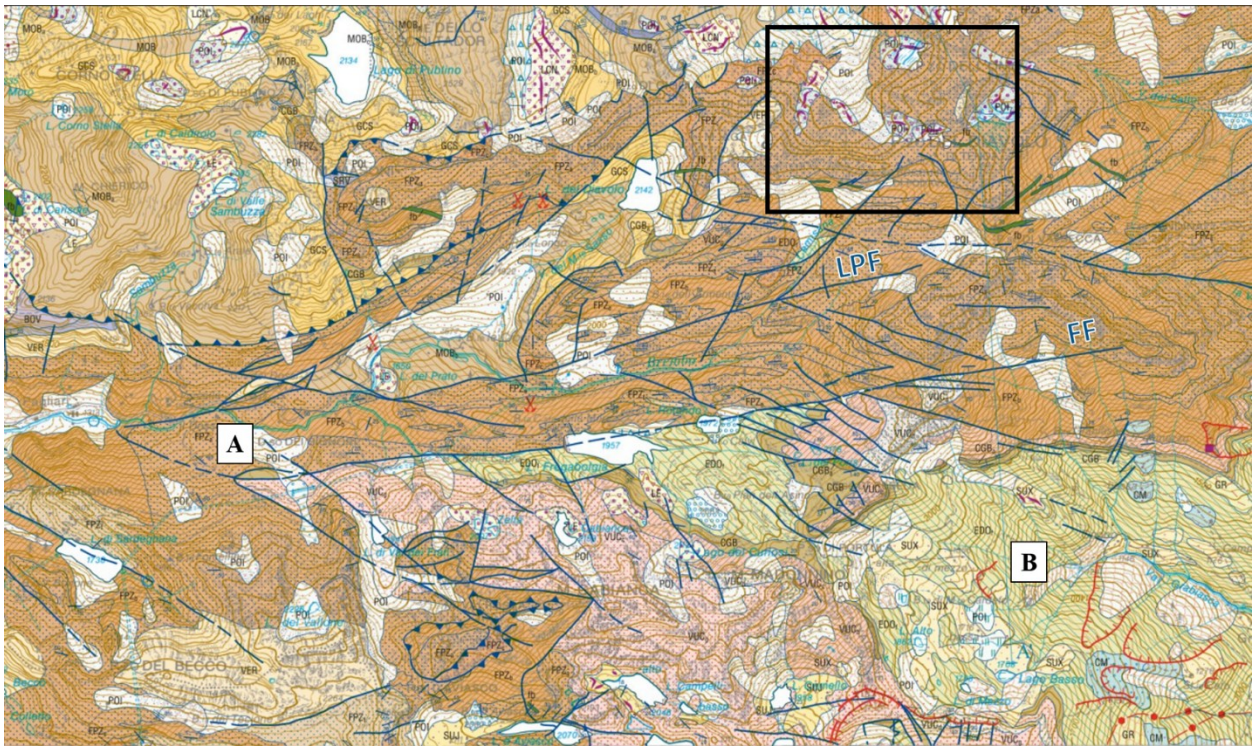


Figure 20. *Geological and structural map of the Upper Val Brembana. A) Central sector; B) Southern sector. FF: Fregabolgia Fault; LPF: Lago del Prato Fault. Black shape: study area. Modified from Servizio Geologico d'Italia (2012) – Carta Geologica d'Italia alla scala 1:50,000 – F. 056 Sondrio.*

Furthermore, the 1:25,000 geological and structural map representing the area between the upper Val Brembana and the southern sectors of Val Venina, Val d'Ambria and Valle di Scais (Cadel et *al.*, 1996) and the 1:50,000 proposed by Forcella e Jadoul (2000), provide a more detailed representation of the two sets of faults (NW-SE and ENE-WSW), characterizing both sectors of the upper Val Brembana (Fig. 21a; Fig. 21b).

Two other main sets of high-angle faults have also been identified in adjacent areas. The first set, trending NNE-SSW to ENE-WSW, includes Passo di Pila, Pizzo Cavrel and the Baite del Barbellino faults (located east of the upper Val Brembana). The second set, oriented NW-SE (e.g., Malgina Fault), characterized by a trend of dykes that dissect the area, is probably one of the most representative of the Orobic Alps (particularly north of the Valtorta-Valcanale Fault, in the Val Seriana area). Based on geometrical ground, morphological features and scattered displacement determinations, these two sets are thought to represent a conjugate system characterized by a direct maximum horizontal compression trending NNW-SSE, in a pure shear deformation field (Albini et *al.*, 1994). These sets are associated with the Alpine deformations.

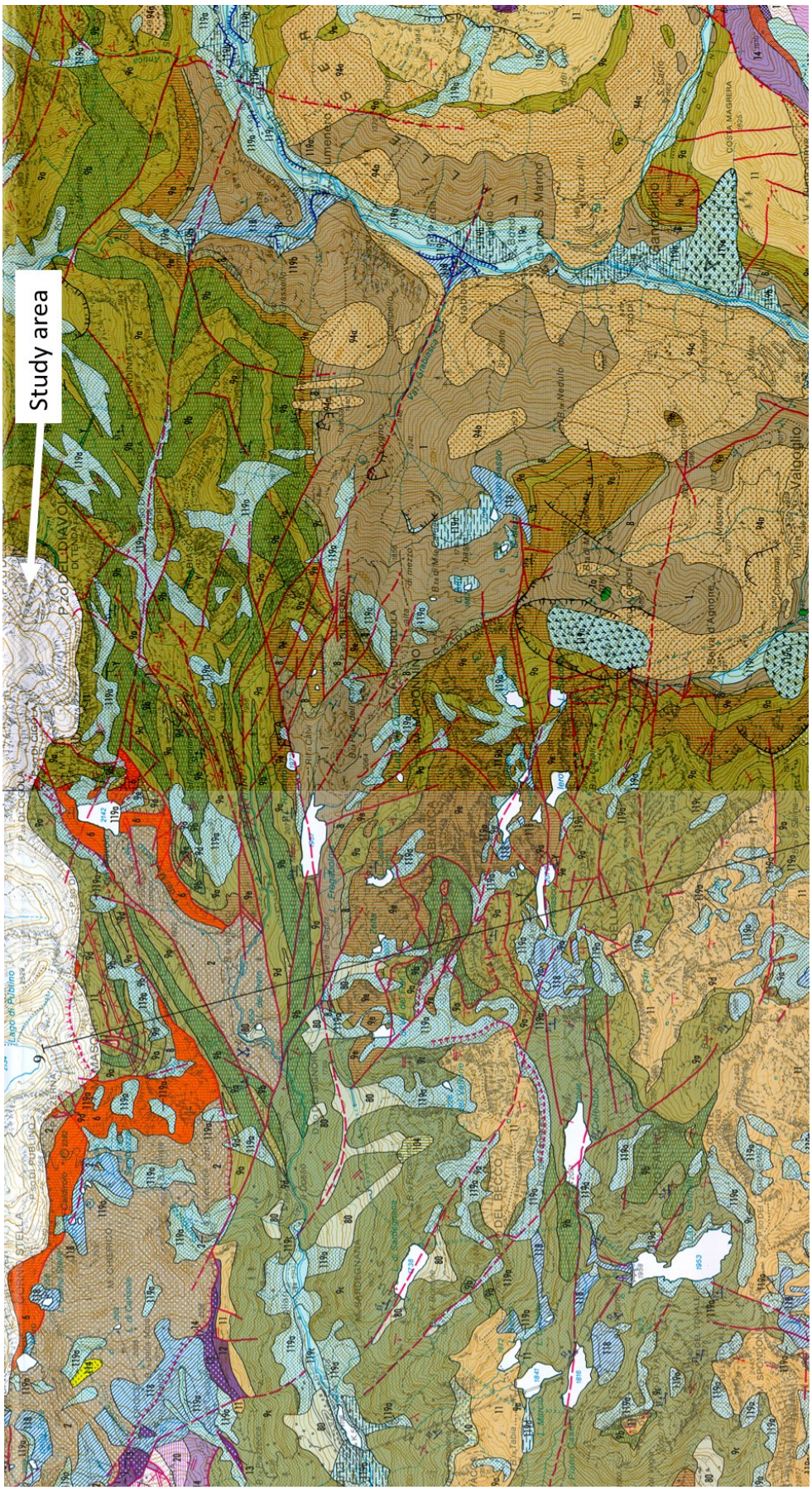


Figure 21a. *Geological and structural map of Val Brembana, modified from Forcella e Jadoul (2000) – scale: 1:50,000. The yellow square highlights the area between the two sectors of the upper Val Brembana and the study area (white box). Continuous and dashed red lines represent continuous and inferred (alpine?) faults, respectively.*

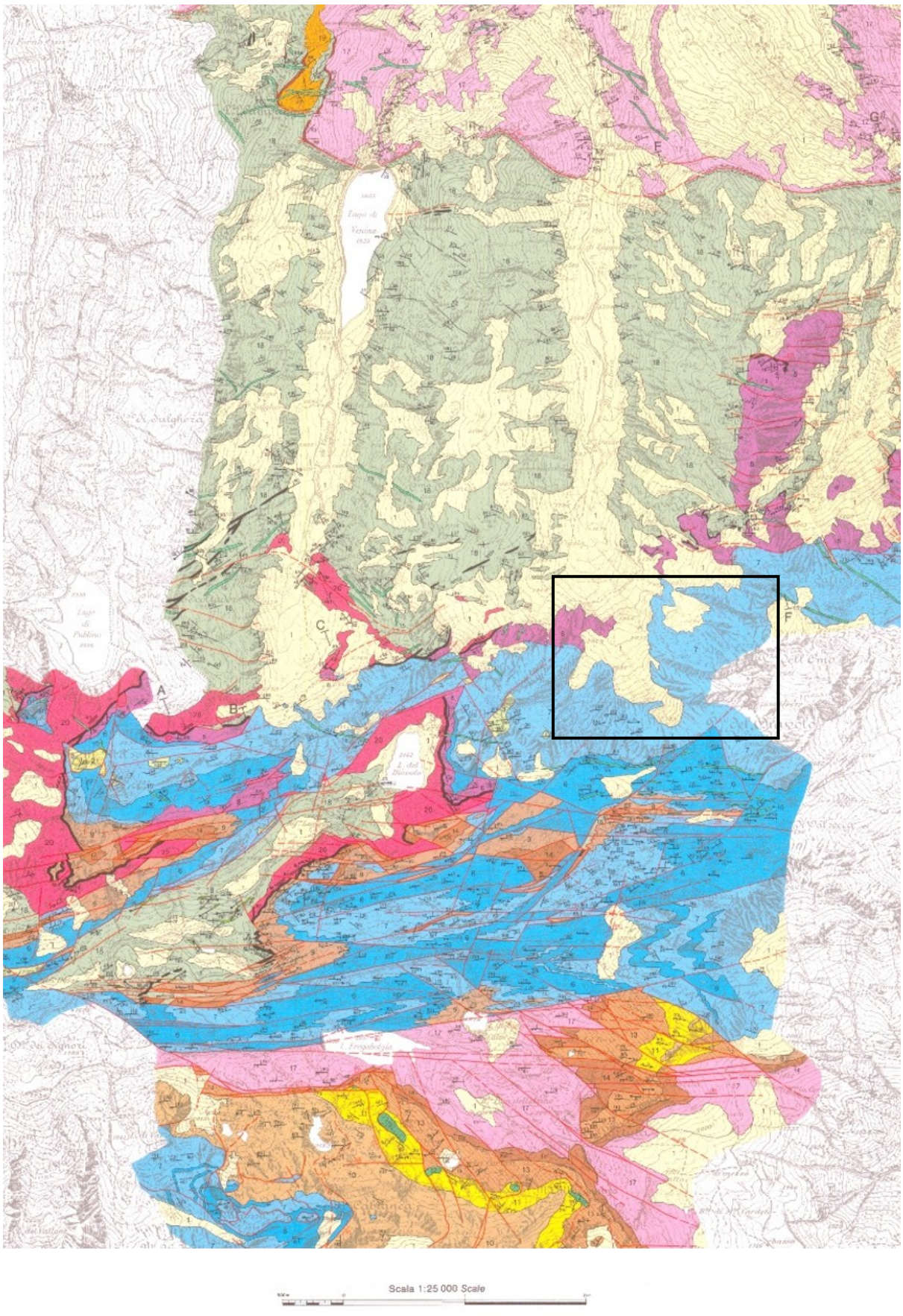


Figure 21b. *Geological and structural map of the area between upper Val d'Ambria (black square) and upper Val Brembana (detail, scale 1:25,000). Red lines represent the two (alpine?) fault sets, trending NW-SE and ENE-WSW. Modified from Cadel et al. (1996).*

6.1.3 Fault trace analysis

As mentioned in section 5.1, fault lineaments were digitized and rose diagrams were generated from several geological maps. The results are presented below in Fig. 22a and 22b. Fig. 23 shows the same workflow applied to the tectonic scheme and the main regional faults characterizing the entire central Southern Alps area, reported by Boriani et *al.* (2012).

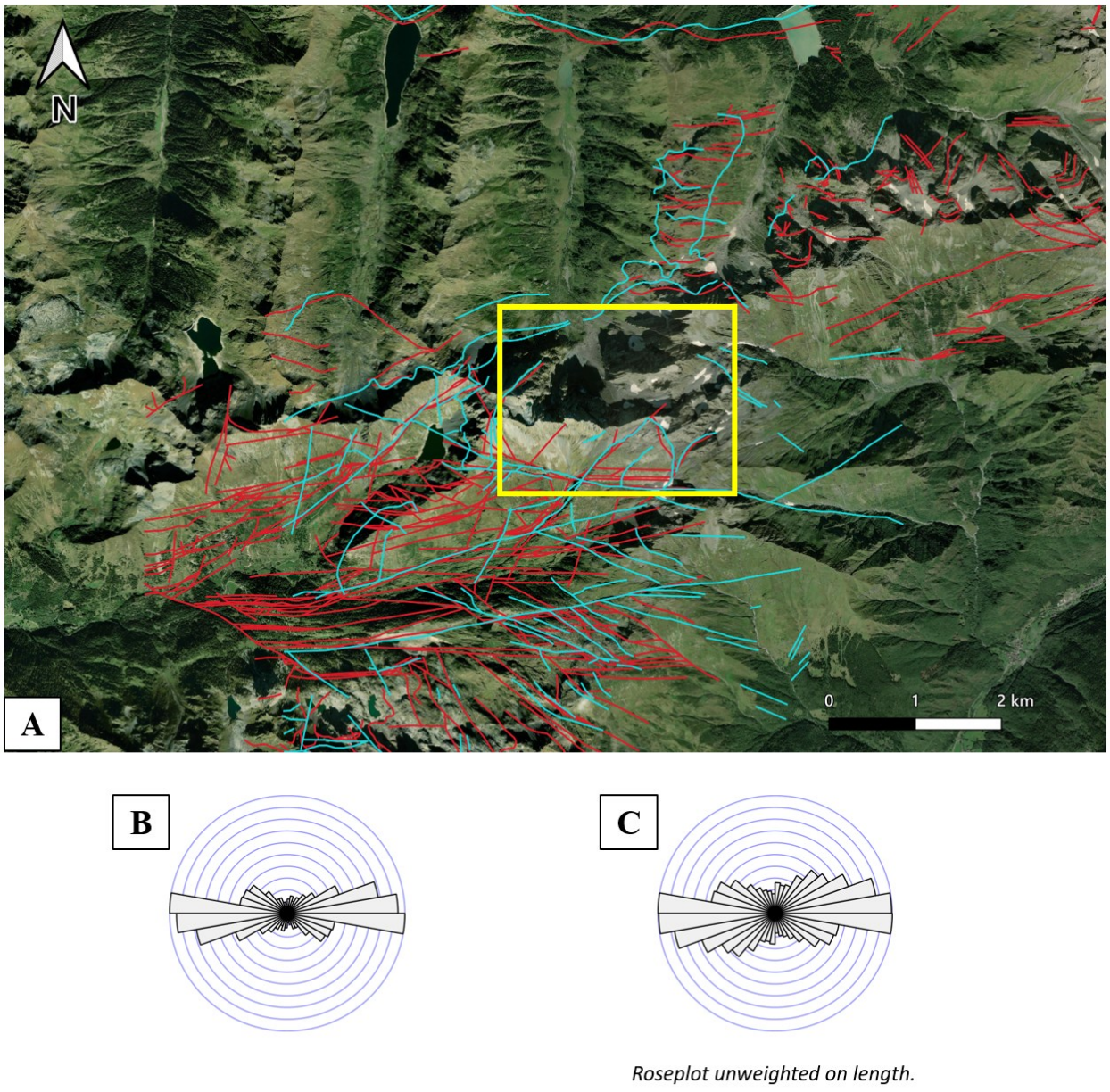
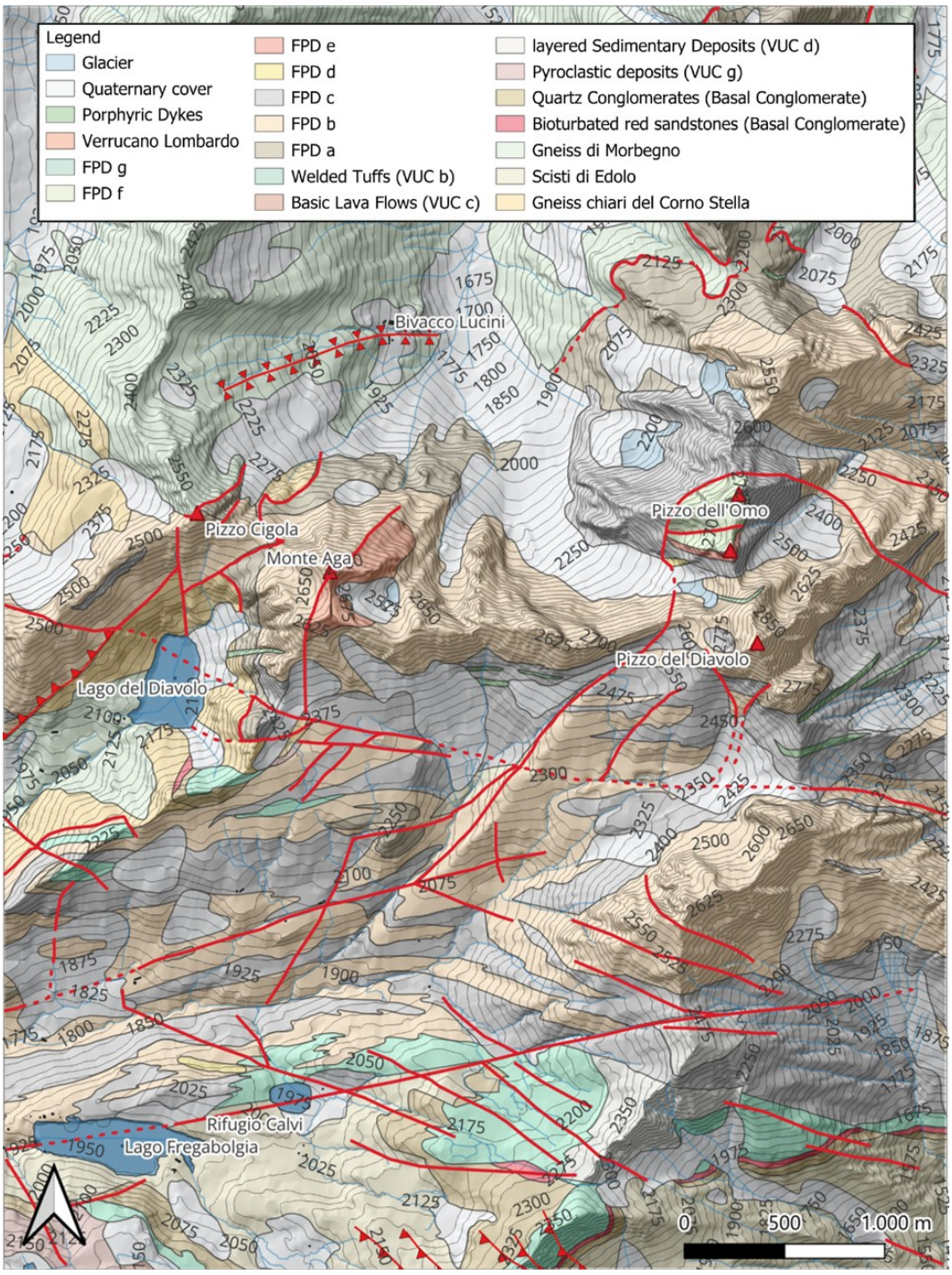
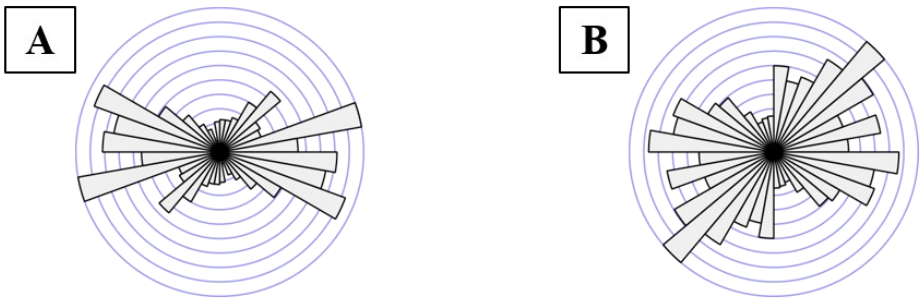


Figure 22a. *Comparison between mapped fault lineaments and local 3D model data. (A) Map showing the lineaments (n = 773) extracted from Cadel et al. (1996) (red lines), Boriani et al. (2012) and Zanchi et al. (2019) (light-blue lines). (B) Rose diagram of the fault lineaments shown in (A) and the corresponding unweighted on length diagram (C). Yellow box: study area. QGIS (v. 3.44.14; v. 4.2.2).*





Roseplot unweighted on length.

Figure 22b. *Geological and structural map of the Val d'Ambria modified from Cattaneo (2025b). Red lines: faults (A). Associated rose diagram (B) and corresponding unweighted on length (C) based on 93 fault lineaments.*

While minor sets trending NW-SE, NE-SW and nearly N-S are identified in the study area as shown in the map modified after Cattaneo (2025b) (Fig. 22b), a clear dominant E-W orientation is highlighted both in Fig. 22a and in the regional setting of Fig. 23.

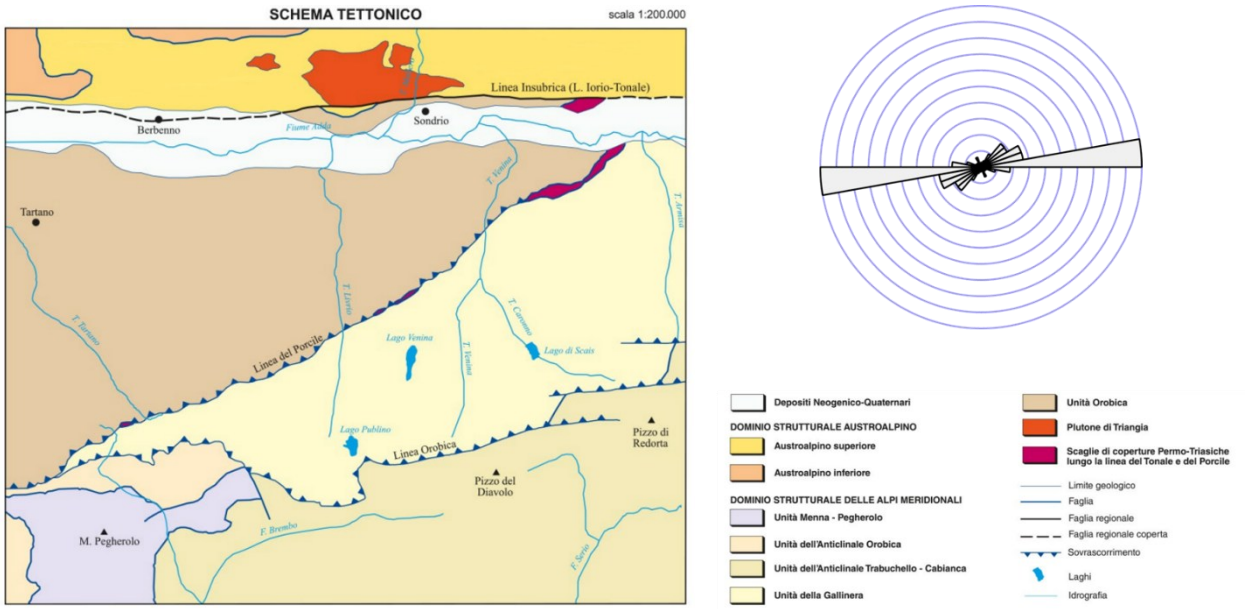


Figure 23. *Tectonic scheme showing regional faults (i.e., Insubric Line, Porcile Line and Orobic Thrust, from north to south) and related 2D rose diagram displaying a clear E-W fault lineaments trend, and minor sets (n = 9). Modified from Boriani et al. (2012). Rose diagram generated using QGIS (v. 3.44.14).*

6.2 DOM analysis

The area depicted in the final Digital Outcrop Model (DOM) represents the upper part of the Val d'Ambria, bounded between Monte Aga, Pizzo dell'Omo, "Omino" and Pizzo del Diavolo di Tenda, from West to East, (Fig. 24).

Several representative sectors of the complete DOM of the area have been selected for detailed structural and stratigraphic analyses: Sector A, Sector B and Sector C. What follows is the discussion of those operations, complete with locations, stereoplots (representing all the measurements of both bedding and fault surfaces) and various considerations.

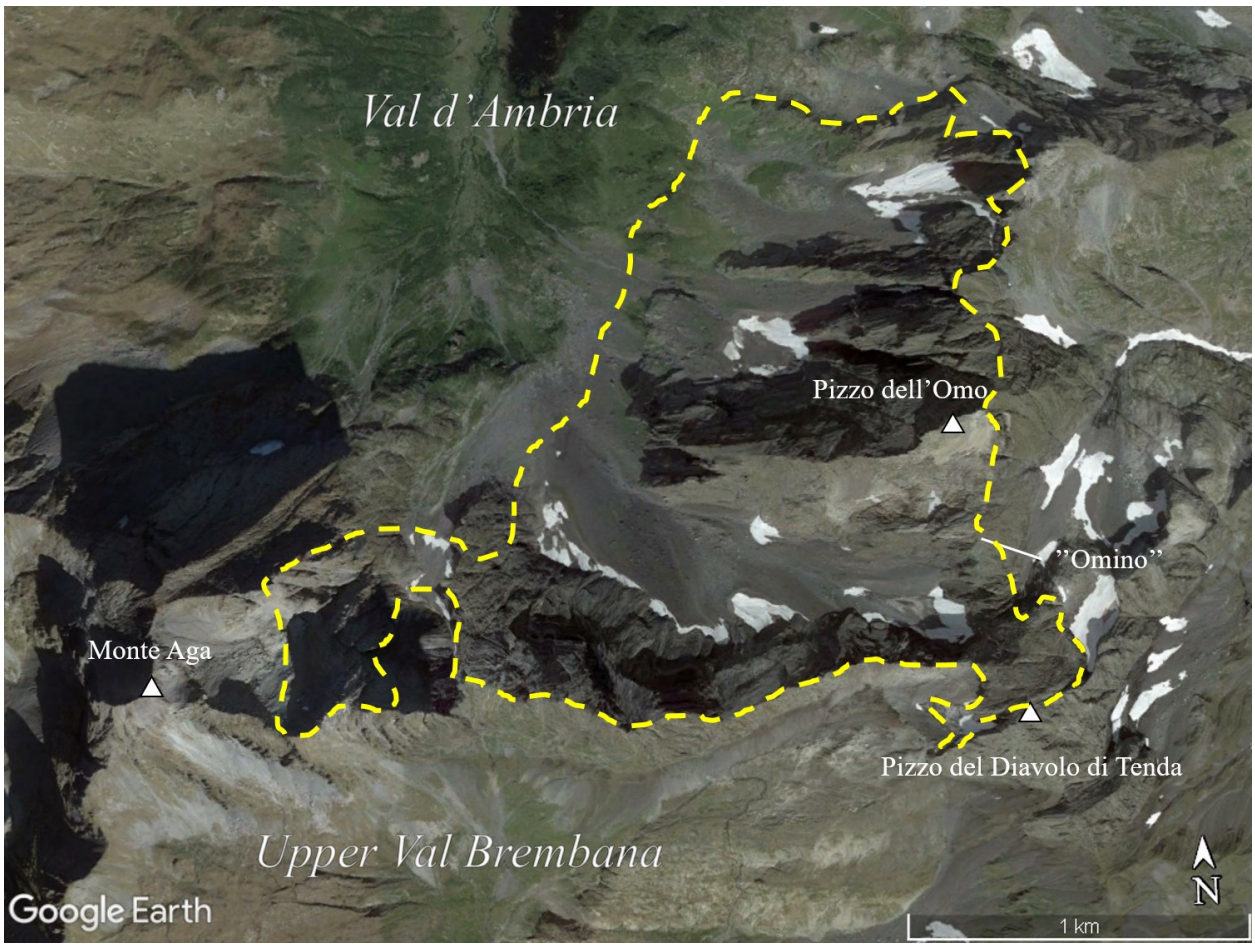


Figure 24. *Approximation of the area represented by the full Digital Outcrop Model (DOM) – yellow shape. Google Earth (2017), modified.*

6.2.1 Sector A

Sector A is located in the uppermost part of the valley and includes the "Omino" peak (Fig. 25). Given the high level of preservation of the outcrop despite its exposure, a sedimentological analysis was carried out by Cattaneo (2025a) and six different lithofacies were described, including massive to weakly stratified sandstones and conglomerates, representing the coarser alluvial component (FPDa); massive sandstones (FPDb); laminated pelites and sandstones, recording finer-grained depositional conditions (FPDc); and reddish siltstones, which represent another fine-grained component of the succession (FPDe). These siliciclastic facies are locally associated with lacustrine carbonates and siltstones (FPDd), highlighting the development of shallow lacustrine conditions within the predominantly continental depositional system. Volcanic and andesitic products additionally record the persistence of volcanic activity during sedimentation (FPDf).

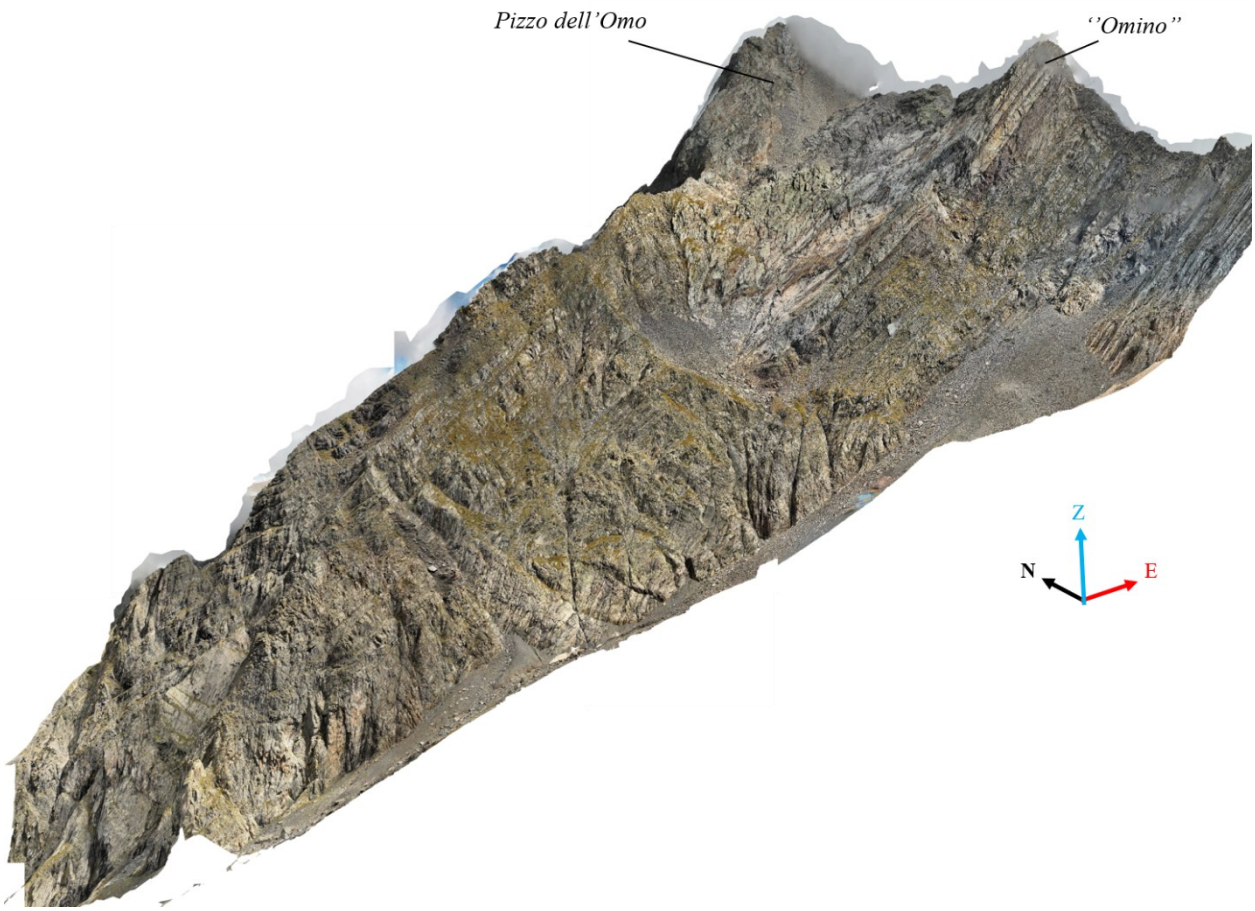


Figure 25. *Horizontal view of Sector A. Orthophoto extracted from 3D model. Agisoft MetaShape (v. 2.2.1).*

The subdivision in lithofacies of Sector A is illustrated in Fig. 26.
It is important to note that no evidence of the Verrucano Lombardo was identified in the 3D model analyses.

From a structural point of view, the area included in Sector A is characterized by a highly complex fault system (Fig. 27). One of the most interesting features is represented by the presence of multiple faults exhibiting an apparent normal stratigraphic displacement. In Figure 27, continuous light-blue lines represent the aforementioned structures – faults exhibiting evidence of an apparent normal sense of movement based on their stratigraphic offsets – while dashed light-blue lines correspond to their inferred or hypothesized extensions. One of these main structures marks the contact between the entire succession of lithofacies and the FPDc unit, which appears to predominantly characterize the section of the model (marked as 1 and 2 in Figure 27). A second fault system is represented by continuous red lines and their associated dashed segments.

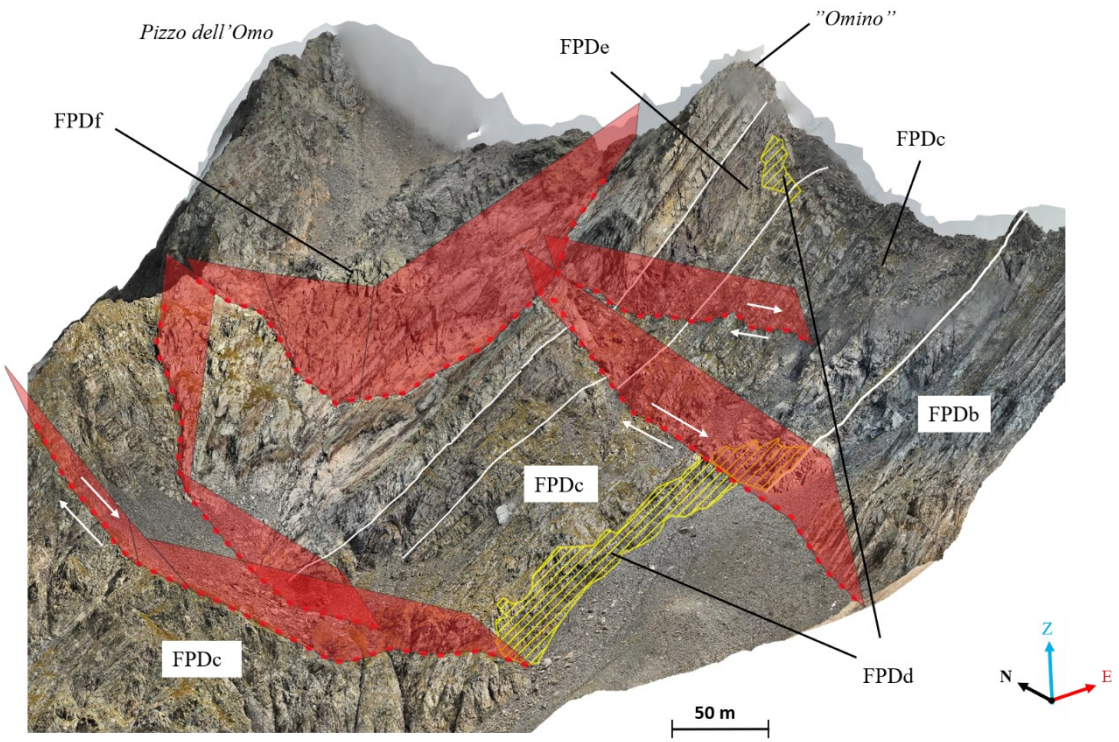


Figure. 26. *Interpretation of upper Sector A, SSE of Val d'Ambria. White: lithofacies contacts; yellow hatched: FPDd (carbonates) interdigitating other units; red dashed: main faults and approximate planes showing apparent stratigraphic displacement. Scale bar: 50 m. Map: QGIS (v3.44.1).*

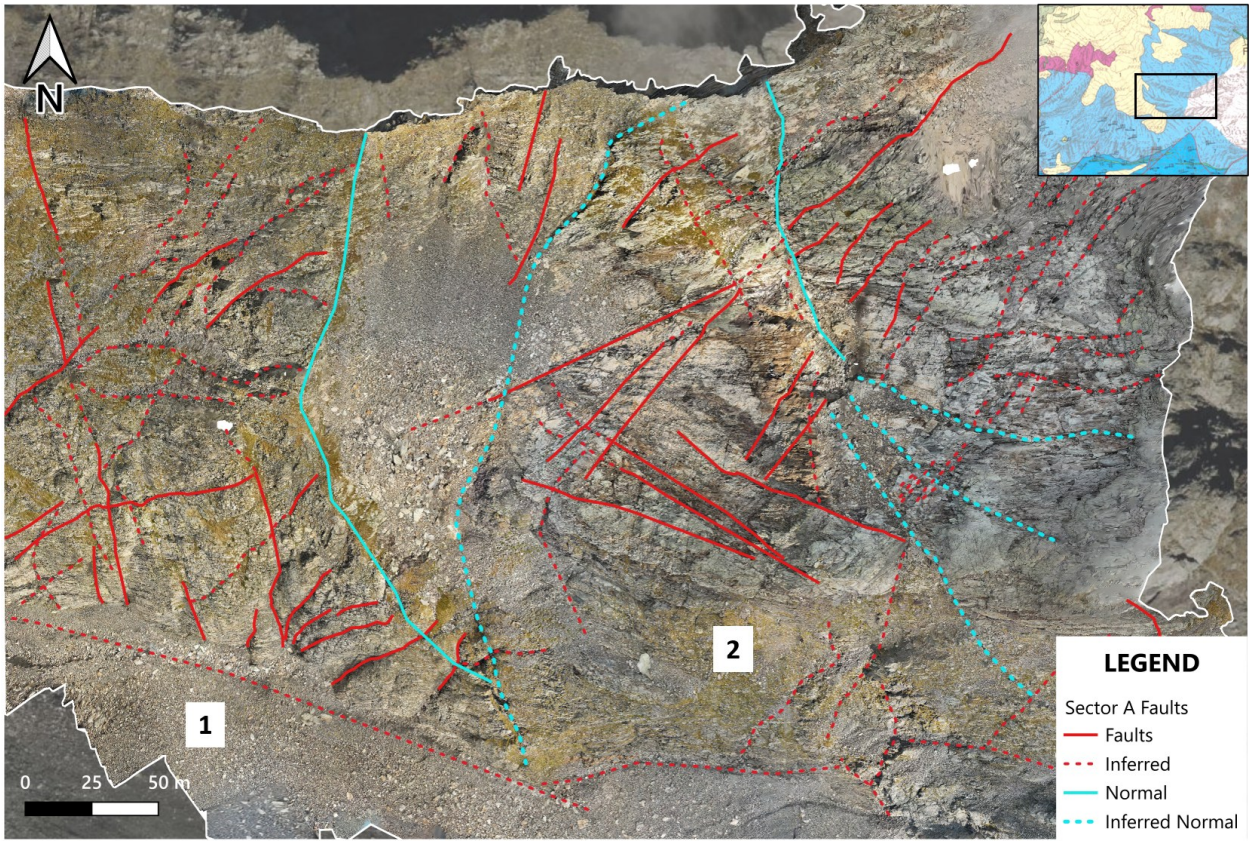


Figure. 27. *Nadir view of upper Sector A showing the main fault system. Light blue: apparent and inferred (dashed) normal faults. Red: faults and inferred extensions (dashed). (1) and (2): sections with different stratigraphy separated by an apparent N–SSE normal fault. Map: QGIS (v4.2.2); inset: modified from Cadel et al. (1996).*

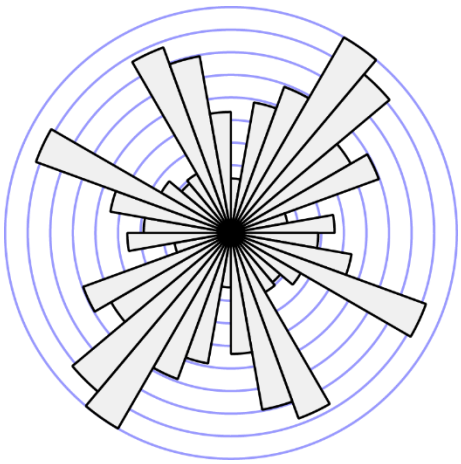


Figure 28. *Orientation analysis of the structural features characterizing Sector A (2D rose diagram, n = 175). Generated from the lineaments in Fig. 27 using QGIS (v. 3.44.1).*

To quantitatively evaluate the surface directional distribution of these lineaments, a 2D orientation analysis was performed. The resulting rose diagram (Fig. 28) reveals a clear preferred directional trend, with a primary NE-SW striking set accompanied by secondary NNW-SSE and WNW-ESE trending sets. Minor N-S and E-W sets are also identified.

Furthermore, the general orientation of all these structures has been summarized and analyzed using stereographic projections (Fig. 29). Based on 119 surfaces generated directly on the 3D model in *CloudCompare*, three main sets of faults are displayed in the stereoplot (*A1*, *A2* and *A3*), the main one (*A1*) being associated with the orange and red areas of the stereographic projection of the poles and displayed as a bold line in Fig. 29-B.

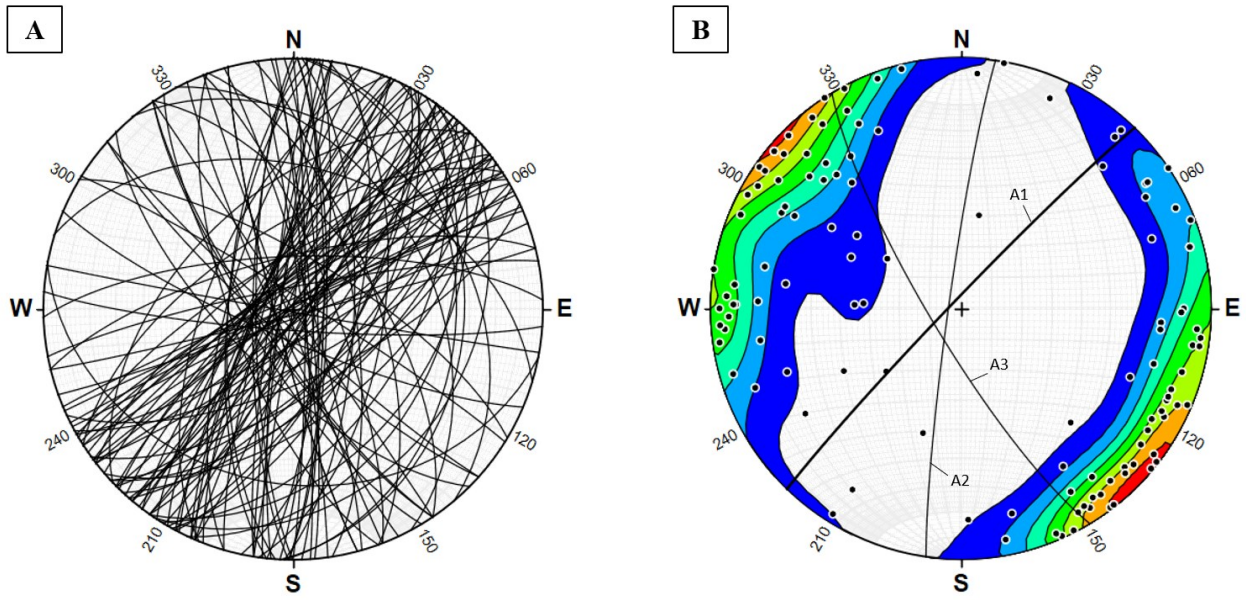


Figure 29. *Stereographic projections (equal area, lower hemisphere) of the structural features of sector A. A) Stereoplot representing 119 measurements (fault planes) characterizing the sector; B) main fault sets (A1, A2 and A3) associated with their related poles. Bold line highlights the primary set (A1). A2 is associated with the green areas along the W-E axis, while A3 corresponds to the blue lobe located in the northeastern quadrant of the diagram. Both images have been generated using Stereonet software (v. 11).*

Table 1 presents the orientations of each set.

The average strike of the principal set is NE-SW and statistically it represents the highest number of fault planes of Sector A; *A2* trends NNE-SSW, while NW-SE is the average strike of the *A3* set. The association between these two sets with red structures of Fig. 28 can easily be assumed based on their respective strikes.

Table 1.

Mean orientation of the main sets of faults identified in Sector A.

Fault sets	Dip Direction (°)	Dip (°)
A1	314.0	87.0
A2	278.0	86.0
A3	239.0	80.0

Interestingly, the acute angle calculated between *A1* and *A3* is 74.7°. It is possible that the two sets could represent a pair of conjugate faults.

Furthermore, the western section of the model, marked as “1” in Fig. 28, exhibits a particularly interesting structural arrangement. This zone, possibly characterized by the FPDc lithofacies, is heavily influenced by specific faults that appear to be organized into a distinctive "horsetail" pattern, fanning out as they near the western boundary of the study area, possibly indicating the

termination of a major structure. This localized structural arrangement is shown separately in Fig. 30.

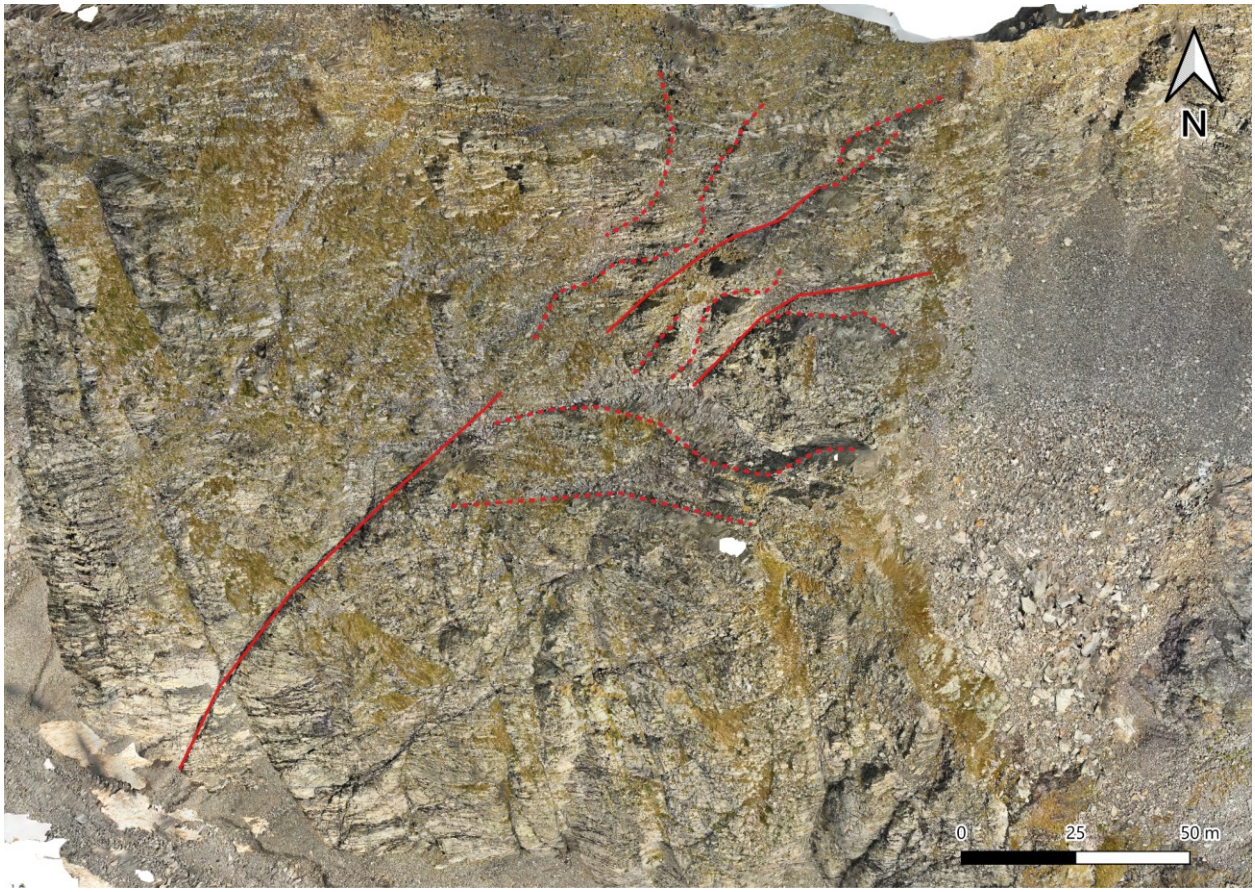


Figure 30. *Possible horsetail splay structure highlighted in Sector A and affecting the stratigraphic succession (FPDc lithofacies) – nadir view. Orthophoto exported from Agisoft Metashape (v. 2.2.1). Map generated using QGIS (v. 4.2.2).*

6.2.2 Sector B

Sector B is located in the northern area of the three-dimensional model, immediately North of Sector A (Fig. 31).

The mountain walls exposed in this sector appear to be essentially characterized by a single lithofacies, possibly attributed to the FPDc lithofacies. This interpretation is based on the location of the sector and on the presence of bedding surfaces, which seem to correspond to the stratification surfaces visible in Sector A (Fig. 26 and Fig. 30) and that defines the aforementioned exposed rock face.

The sector is characterized by several major sub-vertical fault lineaments, some of which may represent the extension of structures previously identified in Sector A (Fig. 31). It is possible that these lineaments locally offset the exposed mountain walls and define distinct morphological features within the outcrop.

A primary NW-SE preferred directional trend can easily be recognized from the 2D rose diagram, alongside a secondary NNW-SSE strike (Fig. 32).

The stereographic projections of the fault planes (n = 28) identified in Sector B, together with their associated poles density contours and mean orientation, are presented in Fig. 33.

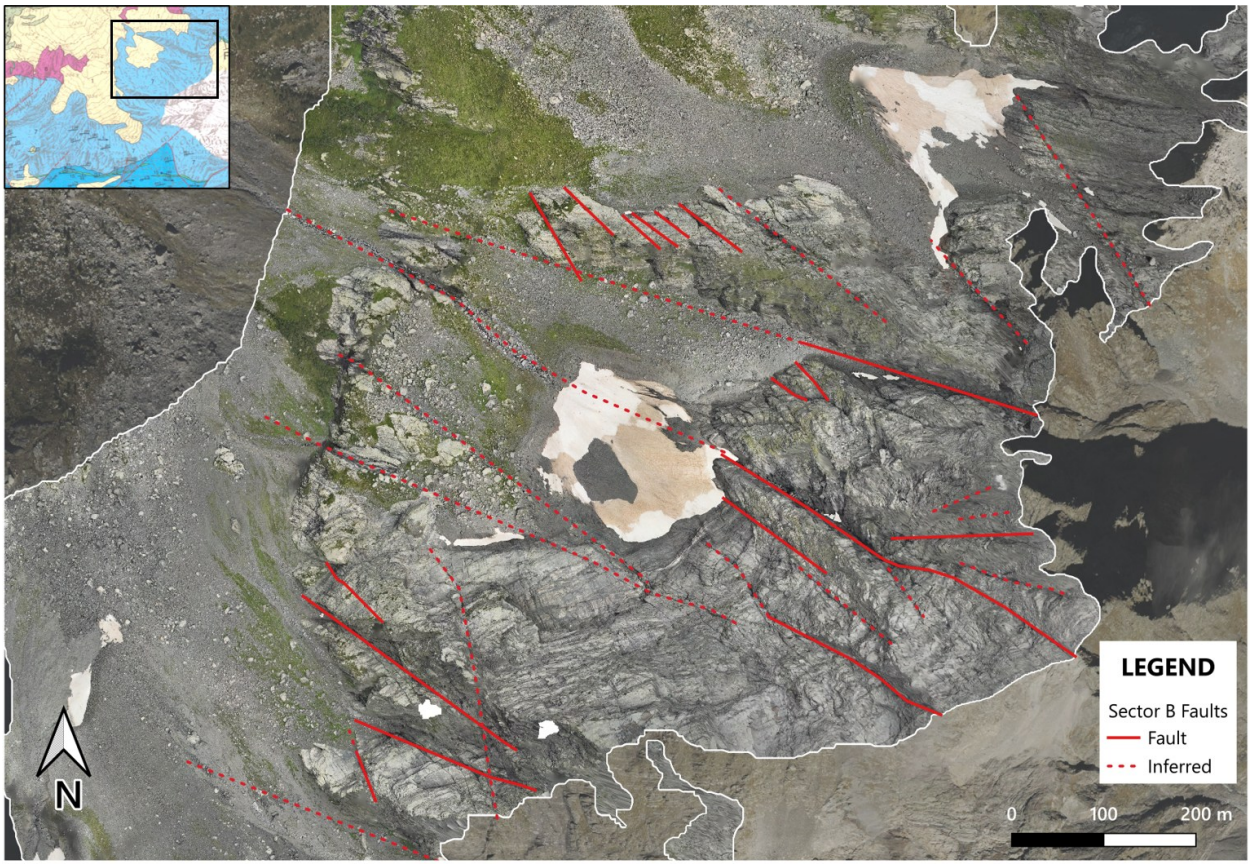


Figure 31. *Nadir view of Sector B and interpretation of the main fault system. White contour line highlights the 3D model representing the sector. Continuous red lines: faults; dashed red lines: inferred extensions of faults. Orthomosaic map exported from Agisoft MetaShape (v. 2.2.1). Map generated using QGIS (v4.2.2). The locator map (top left) is modified from Cadel et al. (1996).*

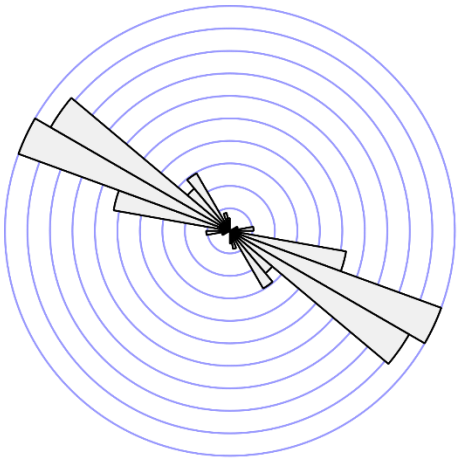


Figure 32. *Orientation analysis of the lineaments of Sector B (2D rose diagram, n = 33). Generated from the faults shown in Fig. 31 using QGIS (v. 3.44.1).*

The analysis of the measurements shown in the stereoplot suggests the presence of two fault sets, *B1* and *B2*. Both sets are characterized by a NW-SE trend (Fig. 33-B) and form an acute angle of 38.5°. This structural pattern appears to be coherent with the overall configuration of the fault system interpreted in Fig. 31.

Information regarding the mean attitude of these sets is reported in Table 2 below.

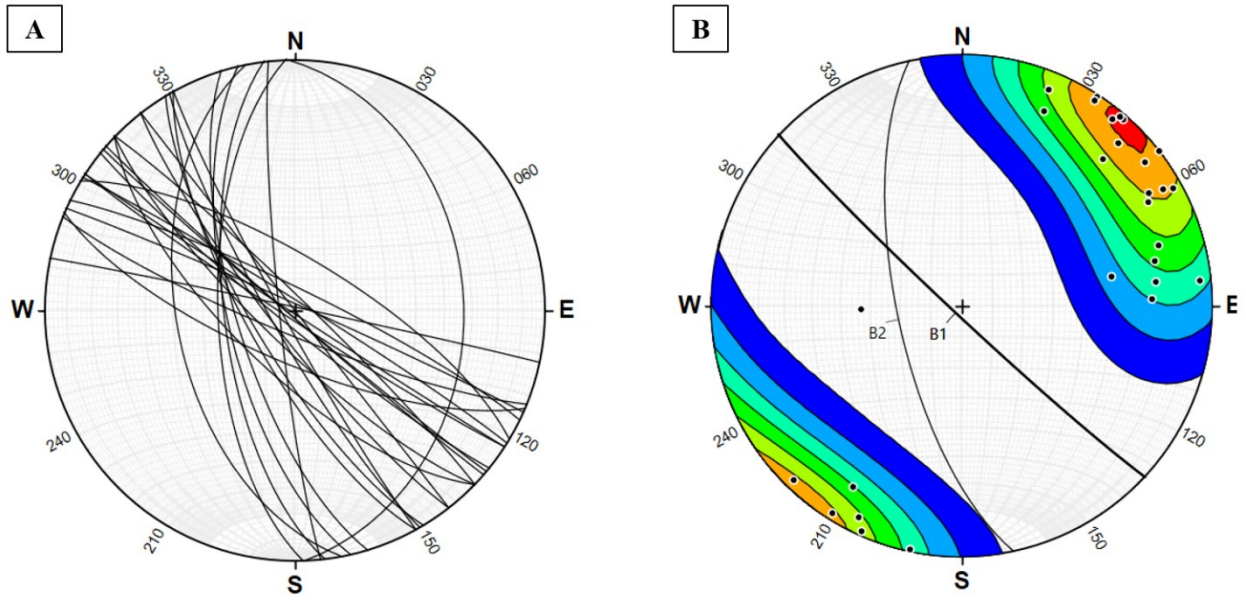


Figure 33. *Stereoplot (equal area, lower hemisphere) representing 28 measurements (fault planes) of Sector A. A) Projection of the 28 fault planes; B) Pole density contour plot and associated fault sets: B1(main set, bold line) and B2 (secondary set). Both images were generated using Stereonet software (v. 11).*

Table 2.

Mean orientation of the main sets of faults identified in Sector B.

Fault sets	**Dip Direction (°)**	**Dip (°)**
B1	223.0	87.0
B2	258.0	69.0

6.2.3 Sector C

The location of Sector C is set in the Southwestern area of the model, east of Monte Aga (Fig. 34). Although the model in this area exhibits lower point density and localized data gaps, some considerations can still be assumed, both from a stratigraphical and structural point of view. Given the orientation of the sector, the exposed rock walls are likely represented by bedding surfaces. The predominant lithofacies of the area appears to be FPDb, as interpreted by Cattaneo (2025a), (Fig. 26).

A clearly distinguished network of two main sets of lineaments (*joints?*) can be identified from the 3D model (Fig. 34), predominantly developed along NE-SW and NW-SE trends. Fig. 35 shows the 2D roseplots associated with this structural system. A minor NNE-SSW direction is also identified.

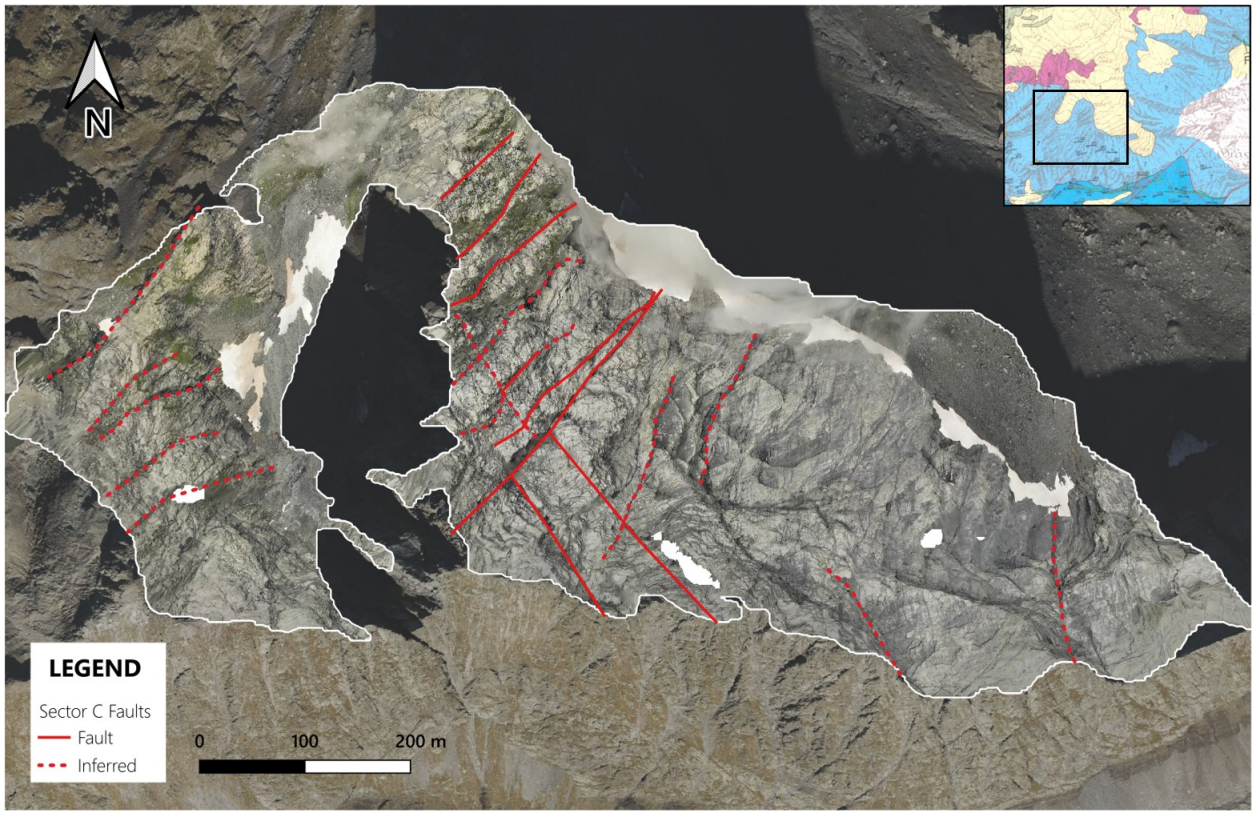


Figure 34. *Structural interpretation of the fault system of Sector C – nadir view. The 3D model is highlighted by the white contour line. Continuous red lines: faults; dashed red lines: inferred lineaments. Map generated using QGIS (v4.2.2). The locator map (top right) is modified from Cadel et al. (1996).*

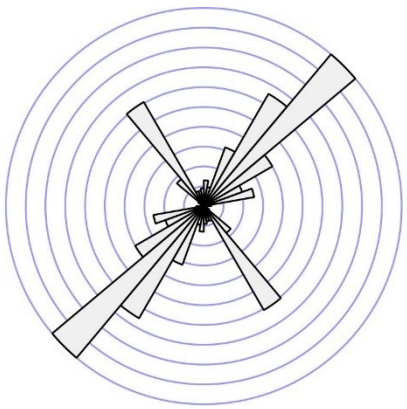


Figure 35. *Orientation analysis of the structural lineaments characterizing Sector C (2D rose diagram, n = 22). Generated from the mapped lineaments in Fig. 34 using QGIS (v. 3.44.1).*

A similar structural pattern can be highlighted by the stereographic projection shown in Fig. 36, which displays two fault sets, *C1* and *C2*, representing the primary set in the sector. Consistently, *C1* trends NE-SW, whereas *C2* trends NW-SE. The two sets intersect at an acute angle of 57.5°. The attitudes of both fault sets are reported in Table 3.

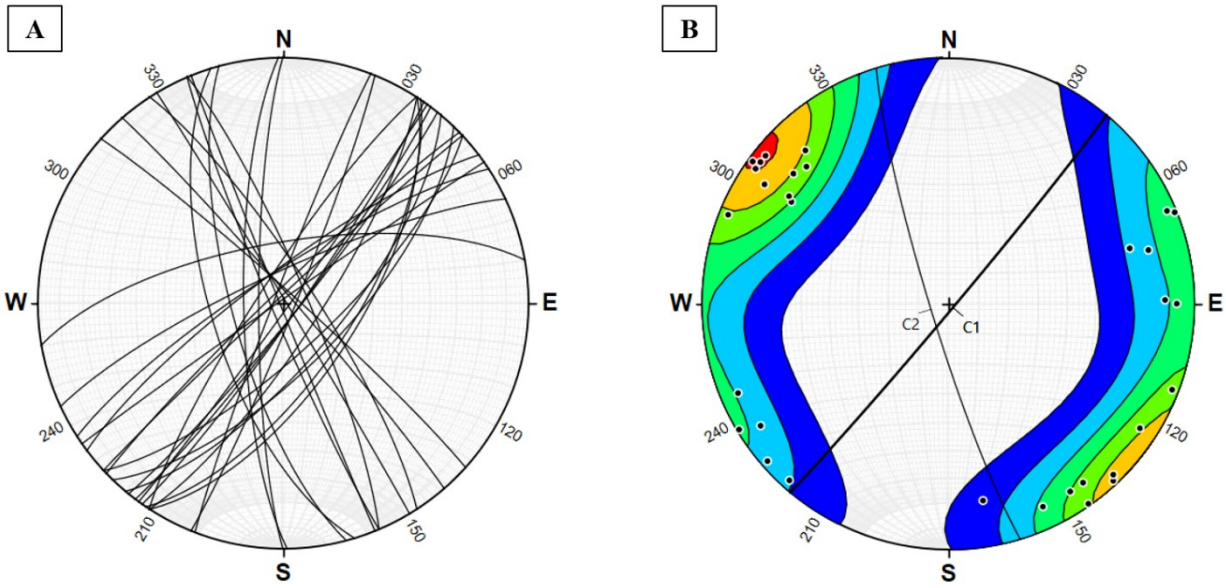


Figure 36. *Stereographic projection (equal area, lower hemisphere) in Sector C structural features (n = 31). A) Great circles representing the fault surfaces; B) Pole distribution and density contour lines of the measured planes and main fault sets, C1 (major set, associated to the orange areas, bold line) and C2 (minor set, related to the light-green lobe situated in the north-eastern part of the stereoplot). Stereonet software (v. 11).*

Table 3.

Mean orientation of the main sets of faults identified in Sector C.

Fault sets	Dip Direction (°)	Dip (°)
C1	130.0	88.0
C2	253.0	84.0

7. DISCUSSION

From a structural perspective, a total of 178 fault-surface measurements were collected across the entire 3D model of the upper Val d'Ambria using *CloudCompare*. This dataset encompasses all the three sectors analyzed in the previous chapters (Fig. 37).

Fig. 38 shows a comparison between the average orientations of each sector (Fig. 38-A) and the three main sets of sub-vertical faults recognized from the entire dataset of the 3D model, which appear to characterize the entire study area: *K1*, *K2*, *K3* (Fig. 38-B).

Specifically, *K1* displays a mean NE-SW trend, *K2* highlights a system trending N-S, while *K3*, on the other hand, exhibits an average orientation of NW-SE.

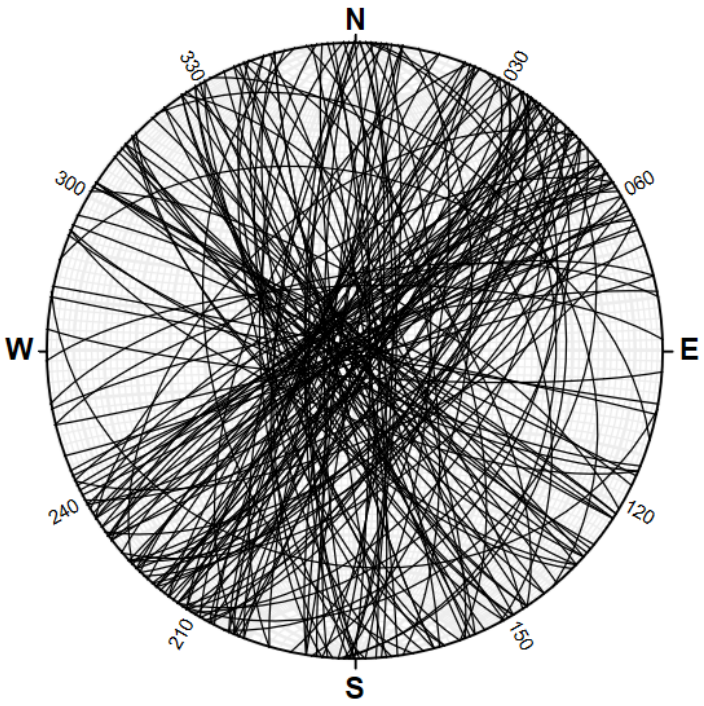


Figure 37. *Stereographic projection (equal area, lower hemisphere) of the 178 surface measurements extracted from the 3D model of Val d'Ambria using CloudCompare. The image has been generated using Stereonet (v. 11).*

These structural characteristics were also independently recognized within each of the three sectors of the model (Fig. 29; Fig. 33; Fig. 36).

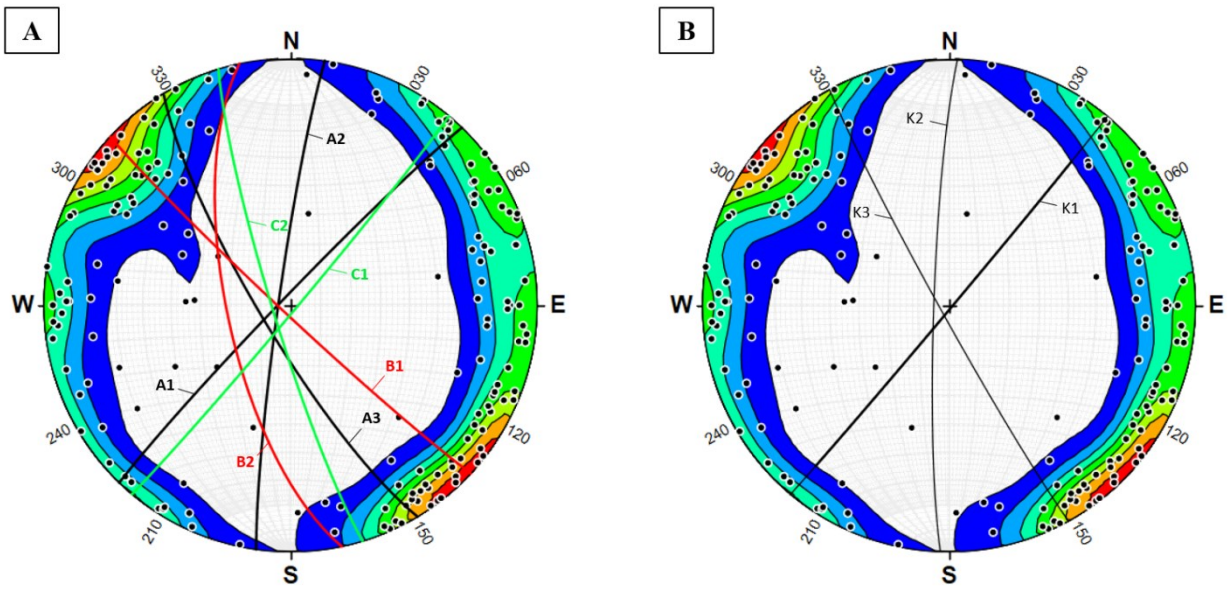


Figure 38. *Comparison between the stereographic projections (equal area, lower hemisphere) of fault surface dataset (n = 178). A) Density contouring plot of poles to planes and main sets for each Sector (A1-A3; B1-B2; C1-C2); B) Main sets (K1, K2, K3) extracted from the density distribution. Stereonet (v. 11),*

Specific details regarding the mean attitude of each fault set are summarized in Table 4 below.

Table 4.

Mean orientation of the main fault sets characterizing the upper Val d'Ambria.

Fault sets	**Dip Direction (°)**	**Dip (°)**
K1	130.0	89.0
K2	272.0	85.0
K3	241.0	87.0

K2 can presumably be associated with the apparent normal faults displayed in Sector A, Fig. 17**.** Due to its N-S trend, *K2* could be interpreted as the set of structures that crosscut the pre-existing features, developed during the late Alpine phase as described by Boriani et *al.* (2012). However, it should be noted that the normal displacement related to these lineaments is not entirely recognized in Val d'Ambria purely from the 3D model observations, nor is it possible to identify a clear cross-cut relationship between these faults and the others.

Although kinematic indicators such as *slickenlines* cannot be directly resolved from the 3D point cloud nor have they been highlighted during the past field trips, preliminary kinematic considerations can be inferred from geometric and statistical data.

Considering the overall orientations and dips of the mapped surfaces, it is possible to assume that the majority of the identified structures, represented by the *K1* and *K3* sets, can be attributed to the same tectonic regime that affected the adjacent upper Val Brembana, particularly its southern sector (Fig. 20; Fig. 21a-b).

To further evaluate how the local structural setting of the upper Val d'Ambria integrates into the broader regional tectonic framework, fault orientations were extracted from several geological maps (Cadel et *al.*, 1996 and *Carta Geologica d'Italia* alla scala 1:50,000 - Foglio 056: Sondrio, Boriani et al., 2012; Zanchi et al., 2019 and Cattaneo, 2025b), plotted on rose diagrams and compared with the 3D model dataset (Fig. 39).

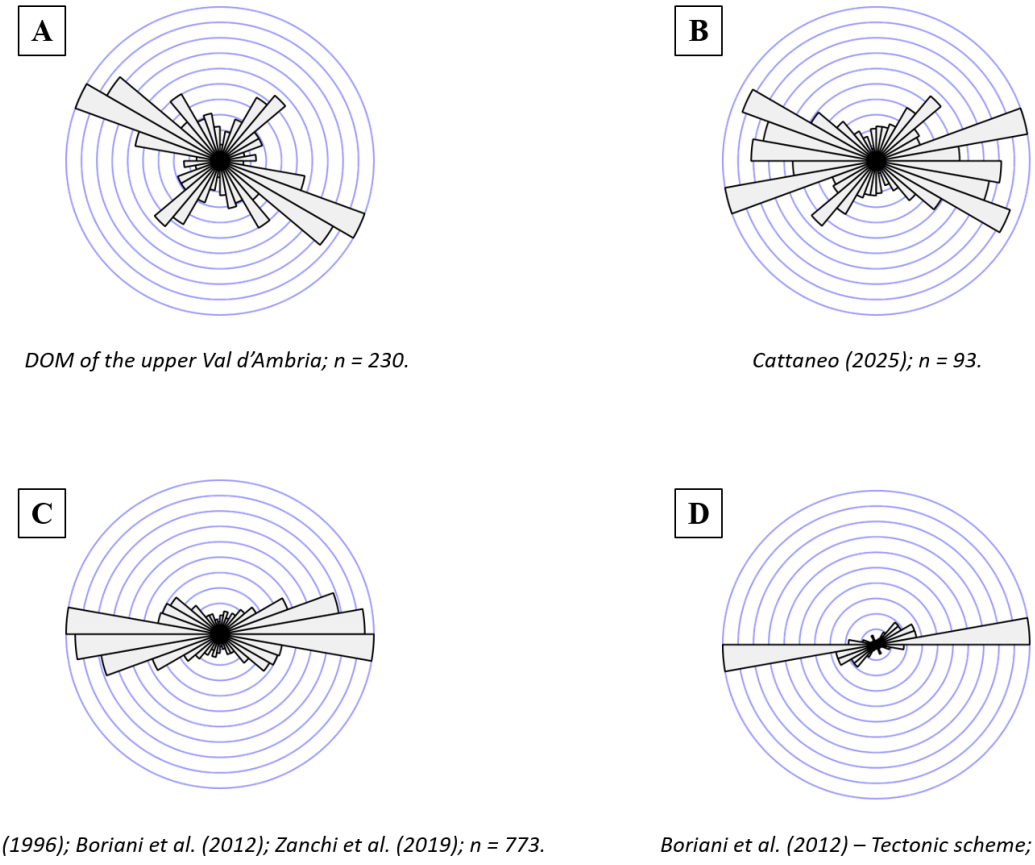


Figure 39. *Comparison between different rose diagrams. A) Rose diagram generated from the lineaments of the DOM of the upper Val d'Ambria (n = 230). B) Diagram from Cattaneo (2025b) (n = 93). C) Lineaments from Cadel et al. (1996), Boriani et al. (2012) and Zanchi et al. (2019) (n = 773). D) Rose diagram associated with the (regional) tectonic scheme of the geological map of CARG Project – Boriani et al. (2012) (n = 9). QGIS (v. 3.44.14).*

As shown in Fig. 39, the fault system of the study region is dominated by a clear E-W trend – likely associated with the Alpine compressional regime characterized by a N-S (to NNW-SSE?)

maximum principal stress (σ_1) (possibly related to the Eo-Alpine shortening phase mentioned in D'Adda & Zanchetta, 2015) – accompanied by secondary ENE-WSW and WNW-ESE sets. This regional trend is consistently observed in the adjacent areas (Fig. 39-C) as well as in the main lineaments reported in the tectonic scheme of the Foglio 056 - Sondrio, *Carta Geologica d'Italia* alla scala 1:50,000 (e.g., Insubric Line, Porcile Line, and Orobic Thrust) (Fig. 39-D).

Comparing this regional trend with the dataset obtained from the study area (Fig. 39-A and Fig. 39-B), the dominant sets in Val d'Ambria (*K1*: NE-SW and *K3*: NW-SE), interpreted as a possible local conjugate system, appear to correspond to the minor orientations of the regional framework. Additionally, these results suggest that the high-resolution 3D point cloud of the Val d'Ambria detects secondary, possibly conjugate structures (*K1* and *K3*) and the subsequent cross-cutting *K2* set, which developed between the main regional fault zones, while the large-scale maps (Cadel et *al.*, 1996; CARG; Zanchi et *al.*, 2019) primarily capture the first-order E-W regional system.
Furthermore, the analysis of the potential conjugate *K1-K3* system, with an acute angle of 69.1°, suggests a stress regime characterized by an almost horizontal maximum principal stress axis (σ_1), trending approximately N-S to NNE-SSW, according to the Coulomb criterion, which is consistent with strike-slip kinematics (Fig. 40). This orientation can be compared with the findings of Albini et *al.* (1994) regarding the two main structural sets described within the adjacent upper Val Brembana (a NNE–SSW to ENE–WSW set and a NW–SE set, yielding a regional NNW-SSE maximum compression; see also Section 6.1.2). The inferred N-S orientation is also compatible with the N-S to NW-SE Eo-Alpine shortening obtained by D'Adda & Zanchetta (2015) through fault-slip inversion along the Orobic and Porcile thrusts. It must be stressed once again, however, that the stress configuration proposed here derives from geometrical considerations only, whereas those authors rely on kinematic data.

Therefore, it can only be hypothesized that the *K1* and *K3* system developed during one of these Alpine deformation phases (i.e., Eo-Alpine shortening, according to D'Adda & Zanchetta, 2015, or late-Alpine brittle events described by Albini et *al.*, 1994), as a direct temporal correlation cannot be established.

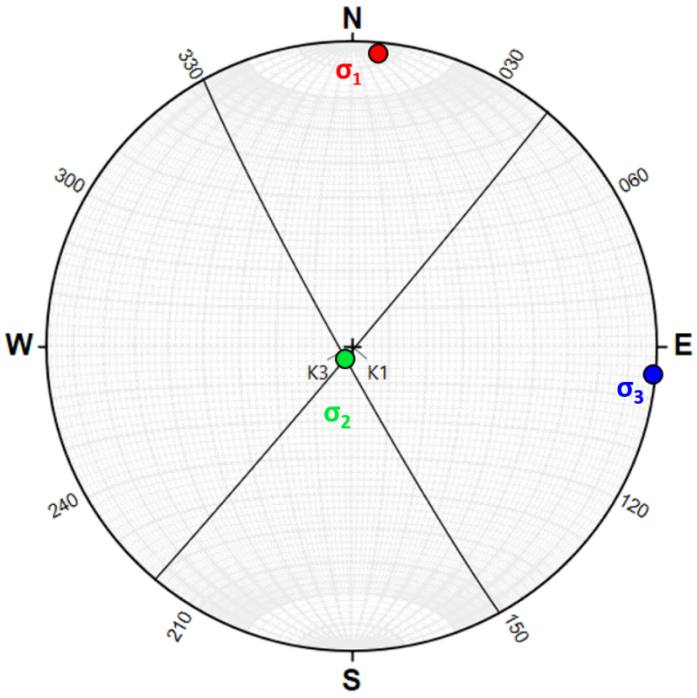


Figure 40. *Principal stress axes (σ_1, σ_2, σ_3) associated with the possible conjugate fault system (K1 and K3 sets). Red dot represents the maximum stress direction (σ_1); green dot is associated with σ_2, while σ_3 is indicated by the blue dot. Stereonet (v. 11).*

Under this configuration, *K1* would correspond to a set of sinistral faults, whereas *K3* would be characterized by a dextral kinematics. However, peculiar structures, such as the previously described horsetail splay (highlighted in Sector A) and other fault surfaces visible across the model, suggest different dynamics. Although these lineaments can possibly be attributed to the *K1* set, which is characterized by a NE-SW strike, they do not appear to be consistent with a left-lateral strike-slip kinematic. In the case of the horsetail splay, the attitude of the fault surfaces reveals a system of sub-vertical planes (dip ranges between 71° and 90°) that are possibly consistent with a right-lateral movement. A similar situation may also occur for *K3*, particularly visible in Sector B. Structures with orientations comparable to *K1* and *K3* and apparent offsets compatible with different kinematics also seem to be mapped by other authors on their geological and structural maps (e.g., Cadel et *al.*, 1996) in adjacent areas (e.g., Bocchetta di Cantonasc, near Cima Soliva, and the area between Cima di Bani and Valgoglio, in Val Seriana) (Fig. 41).

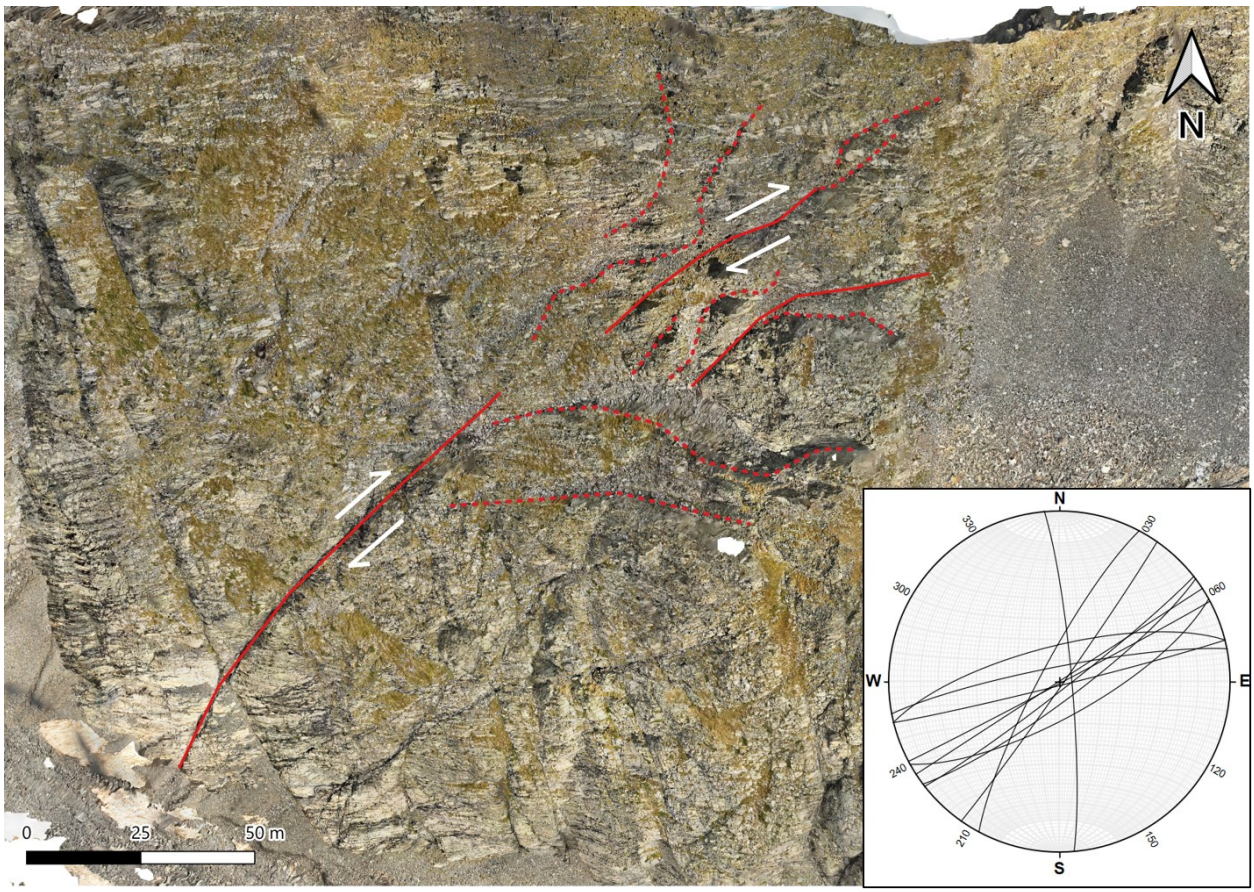


Figure 41. *Nadir view of the horsetail splay structure (highlighted by continuous and dashed red lines) and associated stereographic projection (n = 11). The sense of movement is inferred from the splay geometry and is not based on kinematic indicators. Map generated using QGIS (v. 4.2.2); Stereonet (v. 11).*

Such structures could represent reactivations of pre-existing planes during a late-stage strike-slip phase. Along the Orobic and Porcile thrusts, a late phase involving both dextral and sinistral faults have been tentatively linked to the dextral transpression of the Insubric Line (D'Adda & Zanchetta, 2015); this is dated to the late Oligocene-Miocene by Schmid et *al.* (1989). However, a dextral movement on a plane with the attitude of the horsetail splay system would require a σ_1 oriented approximately ENE-WSW, which is not predicted by the stress field proposed in this work nor by the directions reported by D'Adda & Zanchetta (2015). This could imply local stress perturbations or the rotation of the stress field.

If these considerations are correct, the *K1-K3* structures, including those with apparent opposite kinematics, and the K2 set can be attributed to different Alpine deformation dynamics.

From a stratigraphical point of view, 139 bedding surfaces (S_0) were extracted from the point cloud. Thanks to their high level of preservation, these planes were easily recognized within the FPDb and FPDc lithofacies, particularly in the area of Sector A. Due to their spatial orientation, these bedding surfaces form the rock walls of Sector B, as previously mentioned in Section 6.2.

An attitude measurement was taken directly from one of these planes during the 2024 field trip: 340N50 (expressed in dip direction/dip).

The mean attitude of the two sets identified from the dataset are 336N57 (*St1*) and 349N73 (*St2*) (Fig. 42), where *St1* is recognized as the main stratigraphic set. The stereoplot shows a pole density concentration located almost entirely in the south-eastern quadrant of the diagram.

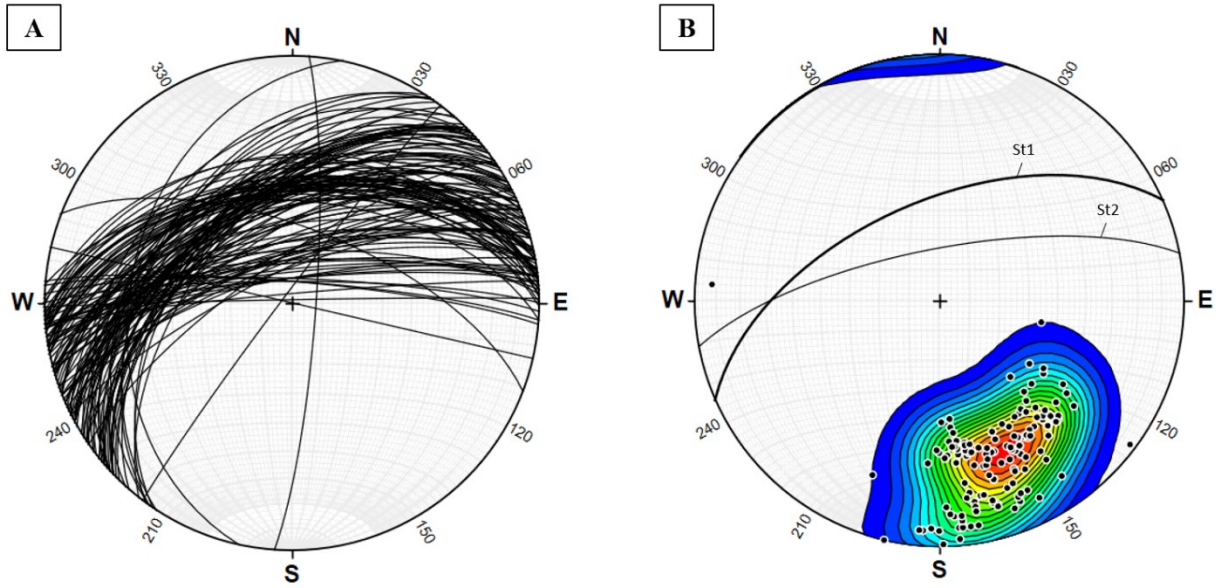


Figure 42. *Stereographic projection (equal area, lower hemisphere) of the stratigraphical surface dataset (n = 139); A) Great circles of the measured bedding planes; B) pole density contours and associated average sets, St1 and St2. Stereonet (v. 11).*

Comparing the stereographic projection of the bedding surfaces in Val d'Ambria with data reported by Mengoli (1993) (Fig. 43) and Zanchi et *al.* (2019) highlights potential similarities with their respective study areas, both localized in adjacent zones: north of the Lago del Prato-Pizzo Poris Fault and along the western slope of Monte Aga (along the Aga Growth Fault; Fig. 44 – red circles).

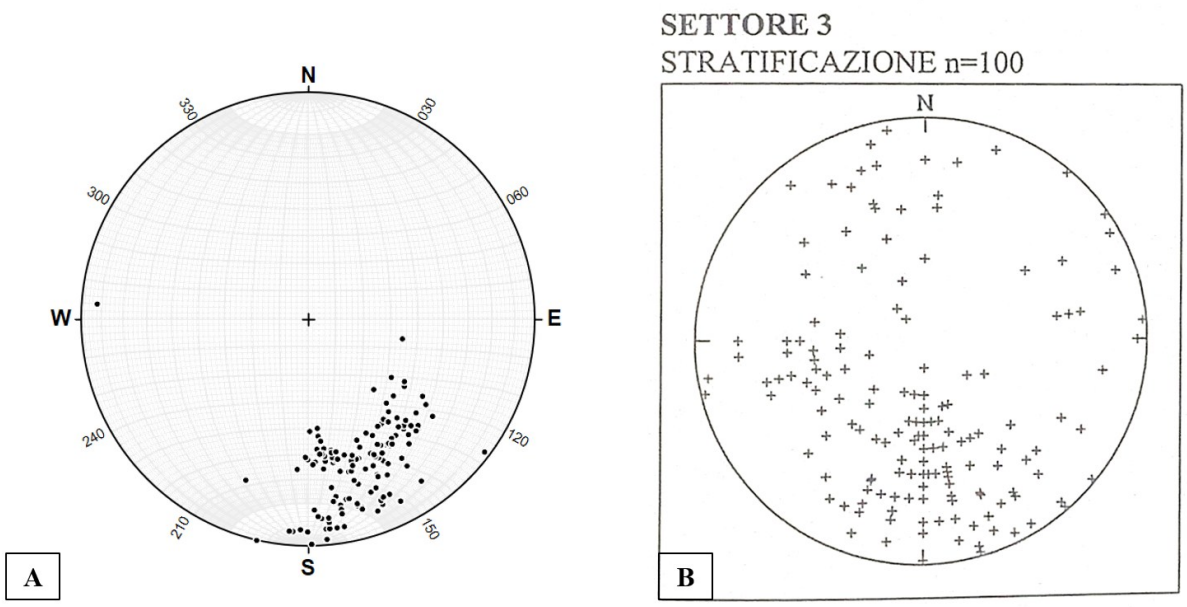


Figure 43. *Comparison between the pole distribution associated with the 139 bedding surfaces of Val d'Ambria. A) and the distribution of the 100 poles reported by Mengoli (1993) B). Plotted using Stereonet (v. 11).*

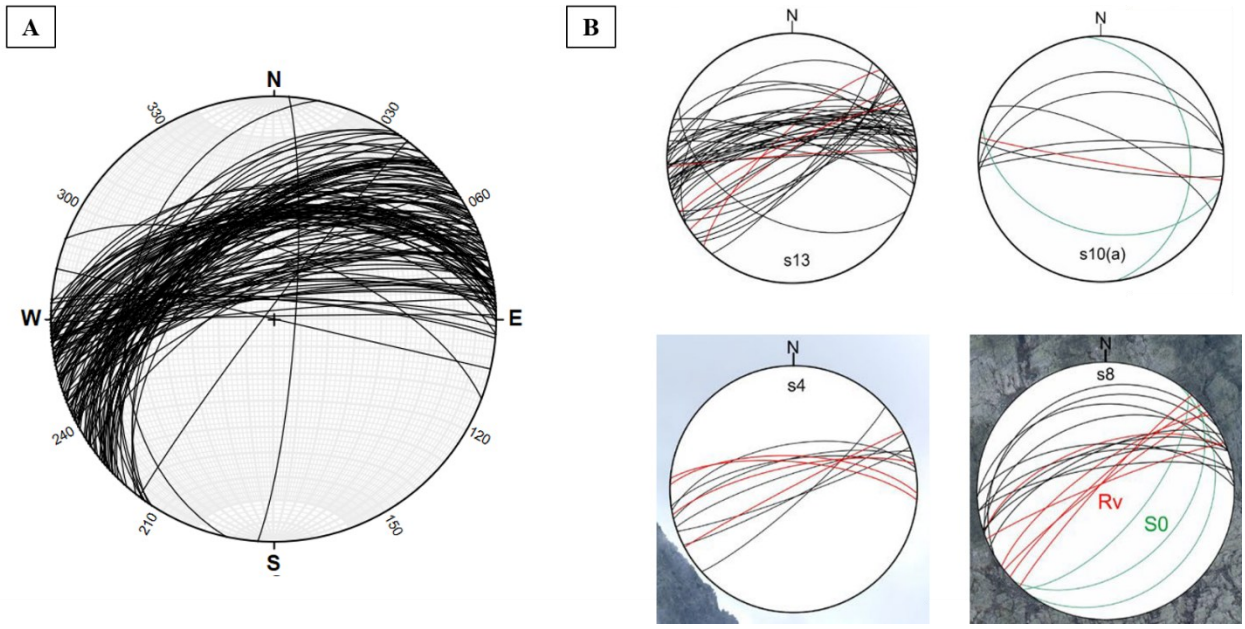


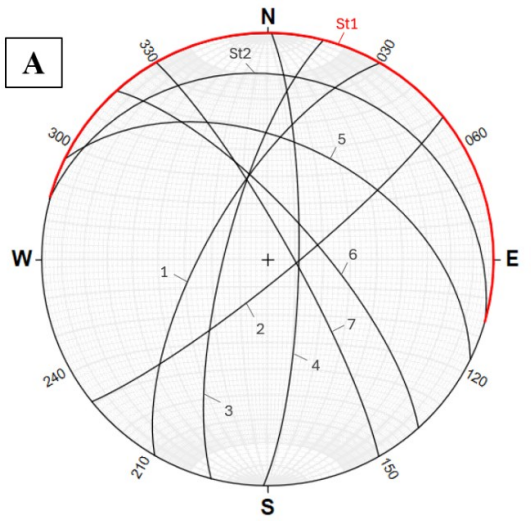
Figure 44. *Comparison between the bedding surface dataset (n = 139) of Val d'Ambria (A) with the related stereographic projections (red lines) of the western slope of Monte Aga (B) – modified from Zanchi et al. (2019).*

In particular, Mengoli (1993) confirms that in the Monte Aga and Pizzo del Diavolo di Tenda area the bedding surfaces are characterized by a predominantly northward-dipping attitude, with a pole density maximum concentrated in the S–SE sector of the stereonet, although this dataset shows a broader distribution than the one observed in the Val d'Ambria. Meanwhile, Zanchi et *al.* (2019) demonstrated that the current orientation of both bedding planes (red lines) and synsedimentary

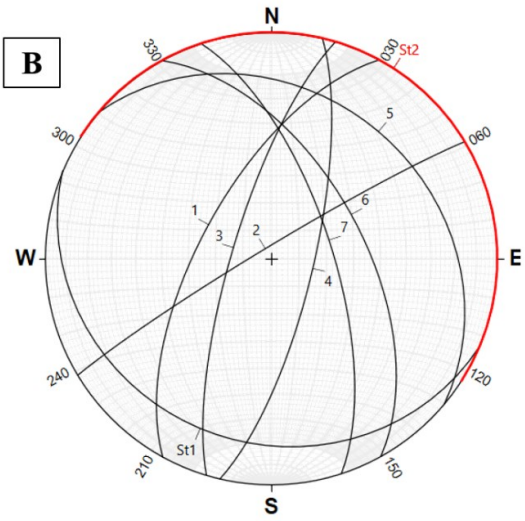
normal faults in the Monte Aga area (black circles in Fig. 44) results from significant post-depositional tilting, which increased the average dip of the structural surfaces.
The mean bedding orientations obtained in this study (336N57 and 349N73) appear to align consistently with this deformation pattern. This continuity suggests that the strata in Val d'Ambria experienced the same post-depositional tilting history associated with the structural evolution of the sectors described by those authors.

In order to verify the kinematic nature and timing of the apparent normal faults of Sector A (displayed as light-blue lines in Fig. 27), a structural restoration (tilt correction) was also performed using Stereonet (v. 11). The dataset - comprising the attitudes of the main fault segments (1-4) and the two mean sets of the bedding surfaces (*St1* and *St2*) - was rotated twice around the respective strike axes of each stratigraphic set to restore them to a horizontal configuration. Following the restorations, certain fault segments dip with an angle of about 60° (labeled "1" in Fig. 45-A and Fig. 45-C; "1", "6" and "7" in Fig. 45-B and Fig. 45-C). While these geometries align with Anderson's classical model for normal faulting, and could attribute those structural features to a possible (Permian?) extensive regime, the lack of kinematic indicators (e.g., *slickenlines*) is still remarkable.
Another interesting feature concerns the thickness of the lithofacies surrounding the segments named "1" and "2" in Fig. 45-C. As previously mentioned in section 6.2.1, the area is divided into two portions characterized by two distinct lithologies: FPDc, in the northwestern area, with an estimated thickness of ~260 m, and the entire stratigraphic succession described by Cattaneo (2025a) near the "Omino", where the FPDc lithofacies has a thickness of ~115 m. This could be indicative of a possible Permian synsedimentary dynamic. However, the present-day fault plane dips towards the southeast, pointing toward the complete lithofacies succession where the FPDc has a lower thickness. Assuming that this lineament is indeed an extensional Permian fault, this would mean that the fault plane experienced a rotation following the tilting that affected the strata. The hanging-wall would have then been displaced by a dextral strike-slip movement (Fig. 26).
This being said, it is not entirely possible to confirm the age and the kinematics of these faults.

Furthermore, for the same reasons, it is not possible to identify with certainty any structures within the study area that could support or refute either of the two hypotheses in the debate regarding the geodynamic regime – transtensional or purely extensive, as proposed by many authors (Froitzheim et *al.*, 2008; Zanchi et *al.*, 2019; Locchi et *al.*, 2022) - that led to the opening of the Orobic Basin, as well as the other Permian sedimentary basins.



Dip Az	Dip	Label
299,9	67,9	1
141,0	82,4	2
284,4	74,6	3
091,0	78,7	4
026,2	46,7	5
048,1	73,0	6
060,5	81,6	7
016,0	00,0	St1
015,4	19,8	St2



Dip Az	Dip	Label
298,6	64,3	1
328,9	85,9	2
286,6	75,9	3
103,1	74,6	4
040,1	27,4	5
061,0	56,8	6
071,9	68,1	7
202,8	19,8	St1
032,7	00,0	St2

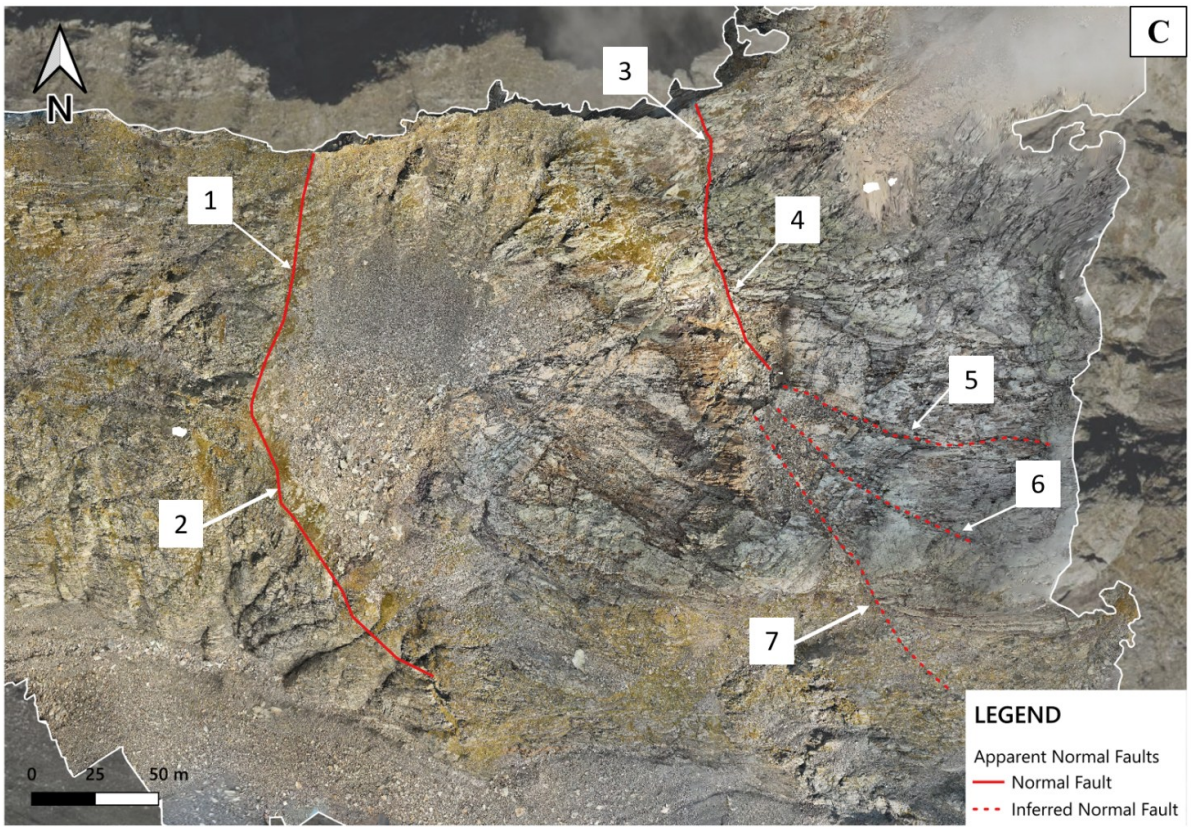
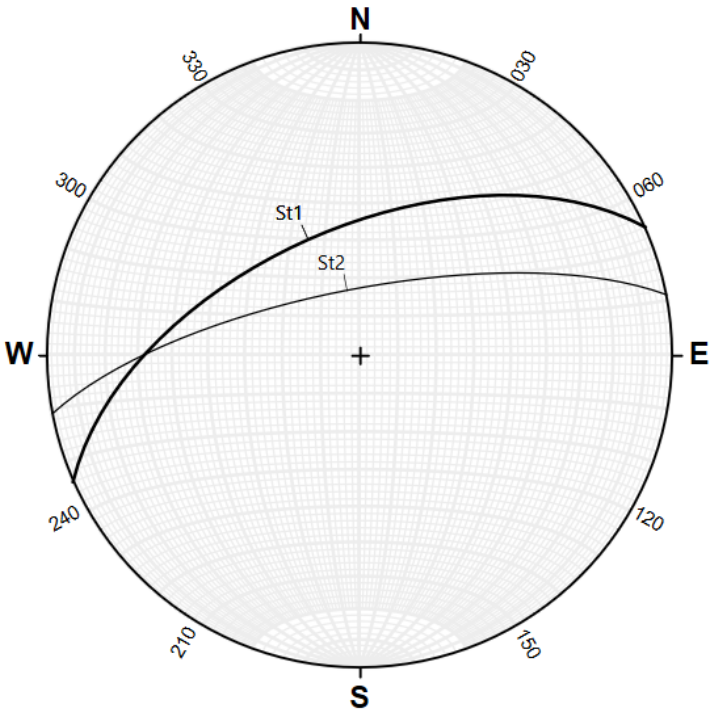


Figure 45. *Stereographic projection showing the structural restoration of the two mean bedding sets, St1 (A) and St2 (B), complete with details regarding the attitudes and segments of the possible normal faults. C) Structural map of Sector A showing the apparent normal faults labelled with the same numerical reference as the stereoplots. QGIS (v4.2.2); Stereonet (v. 11).*

8.1 Advantages of using DOMs

Another interesting aspect concerns the dip of the sedimentary layers.
The dip appears to range from an average of 57° to 73° when moving from south to north, as highlighted by the stereographic projections (Fig. 46). Specifically, based on field observations and standard panoramic photographs, the succession forming the cliff faces in the southern Val d'Ambria area (bounded by Monte Aga and Pizzo del Diavolo di Tenda) appears less steeply inclined compared to the succession further north-northeast, near Pizzo del Salto (Fig. 47). This initial observation suggested the potential presence of a medium- to large-scale fold, with an axis ENE-WSW trending. Similar structures were also reported by Boriani et *al.* (2012), who described *an intense folding within the late-Paleozoic terrigenous units (medium- to large-scale ENE-WSW trending folds), particularly visible around the Brembo River, towards the head of the upper Val Brembana-Val Camisana* (Foglio 056, Sondrio - CARG Project), attributing them to the Alpine compressive deformation phase.

However, by extracting the best-fit 3D planes corresponding to the bedding surfaces of the Pizzo del Diavolo Formation directly within *CloudCompare*, and freely rotating the high-resolution model (Fig. 48), this folding hypothesis was critically re-evaluated. Indeed, the 3D analysis revealed that the bedding surfaces across both sectors appear to be sub-parallel to each other. Furthermore, planes associated with both stratigraphic sets (Fig. 42-B and Fig. 46) belong to both the northern and the southern areas.



Bedding surfaces sets	Dip Direction (°)	Dip (°)
St1	336.0	57.0
St2	349.0	73.0

Figure 46. *Stereographic projection displaying the two main sets (St1, bold line, and St2) associated with the bedding surfaces generated in CloudCompare (v. 2.12.1) and related attitude details. Stereonet (v. 11).*

This indicates that the apparent variation in dip observed in panoramic views is merely an optical distortion caused by the orientation of the cliff faces relative to the line of sight, whereas the apparent horizontal strata (white lines in Fig. 47) are likely fracture surfaces.

Possibly, this case demonstrates how DOM-based 3D surface analyses could prevent false structural interpretations, particularly in areas that are physically inaccessible or logistically challenging for direct field observations and mapping.

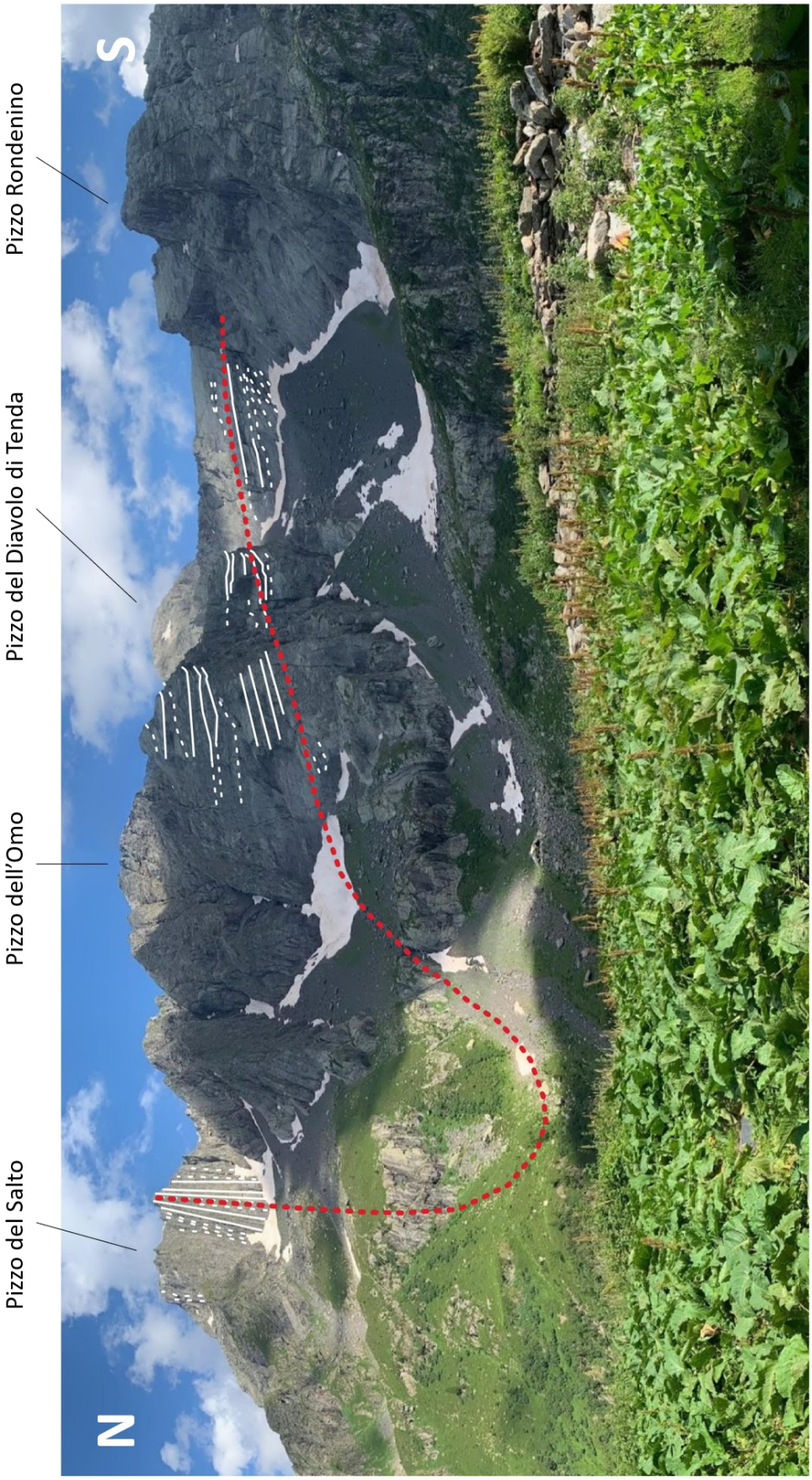


Figure 47. *Panoramic view of the rock faces of the upper Val d'Ambria, along the North-South axis. White continuous and dashed lines: sedimentary strata recognized in FPDb and FPDc lithofacies; red dashed line: inferred geometry of the hypothesized fold, based on field observations and strata attitudes. View from Bivacco Gianmario Lucini.*

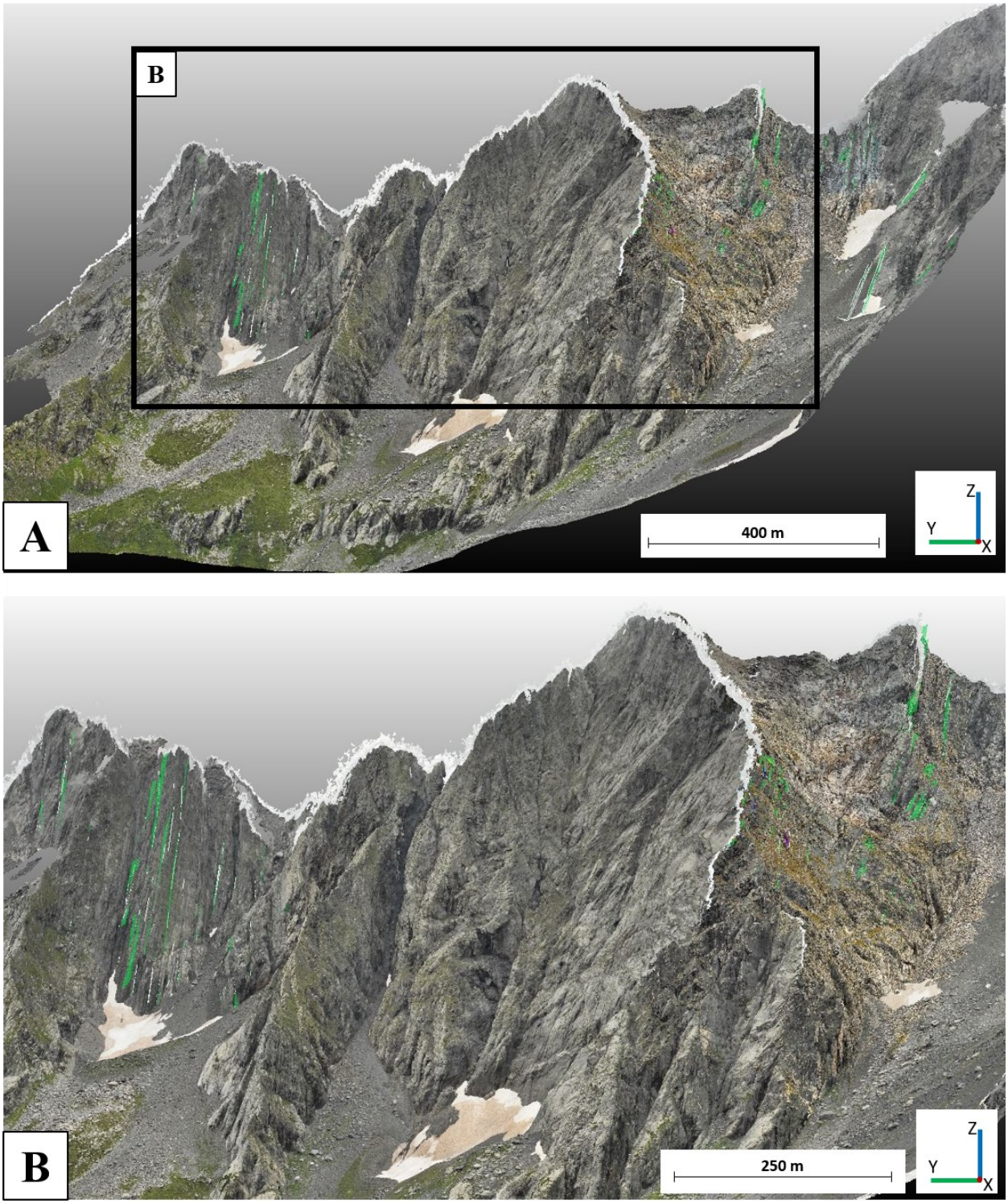


Figure 48. *Rotated 3D model of Val d'Ambria in CloudCompare (v. 2.12.1). A) 3D model and bedding surfaces displayed maintaining the same orientation (green planes); scale bar 400 m. B) Detail of image (A) - black shape. (Y-axis pointing North; X-axis pointing East – directed into the page); scale bar 250 m.*

Ultimately, all these considerations have been summarized in the proposed geological and structural map of the study area, presented in Fig. 49 and provided as an attached map.

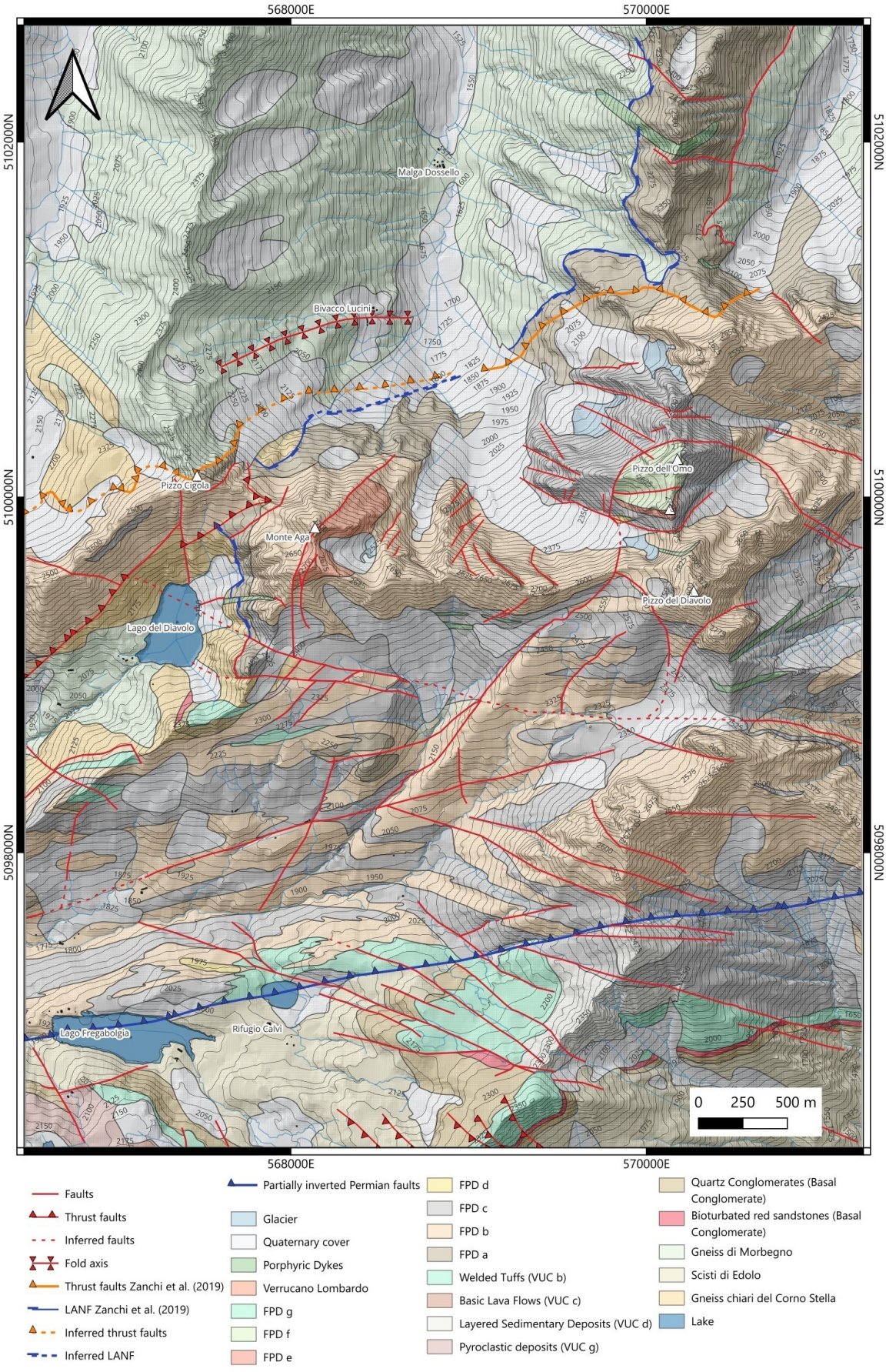


Figure 49. *Structural and geological map proposed for the area of the Val d'Ambria, complete with the new fault lineaments identified in this study. Modified after Zanchi et al. (2019) and Cattaneo (2025b). QGIS (v. 4.2.2).*

8. CONCLUSIONS

This Master's thesis provided a detailed structural and stratigraphic analysis of the upper Val d'Ambria, situated within the central sector of the Orobic Basin, by integrating geological observations, UAV photogrammetry and interpretations of the three-dimensional Digital Outcrop Models (DOMs). The aim of this work was to improve the reconstruction of the structural framework of this relatively inaccessible area and to distinguish, where possible, the structures related to the different tectonic stages that affected the Orobic Basin.
The results are the following:

A total of 178 fault surfaces and 139 bedding surfaces were generated and measured across the 3D model using *CloudCompare* software. Three main sub-vertical structural sets, referred to as *K1*, *K2* and *K3* were identified within the fault planes dataset. *K1* shows a mean NE-SW trend, *K2* a N-S trend, and *K3* a NW-SE trend. These structural orientations are consistently recognized in all the three sectors investigated, in which the entire model was subdivided, indicating that they represent a widespread structural pattern. Furthermore, these sets were compared with the regional fault framework extrapolated through a critical review and data extraction from existing published geological maps covering the study area and surrounding sectors (Mengoli, 1993; Cadel et *al.*, 1996; Forcella and Jadoul, 2000; Boriani et *al.*, 2012; Cattaneo, 2025b), providing a solid regional basis for interpreting the dataset extracted from the digital point cloud.

The comparison between the local structural dataset and the regional fault framework suggests that the *K1* and *K3* sets may represent secondary structures developed between the major regional fault zones. These two sets could also represent a conjugate system, whose sub-vertical N-S σ_1 is compatible with the Alpine deformation which also affected the adjacent upper Val Brembana (Albini et *al.*, 1994) and with the N-S to NW-SE Eo-Alpine shortening proposed by D'Adda & Zanchetta (2015). However, since this stress field derives from geometrical considerations only, a direct temporal correlation cannot be established. Moreover, some structures, such as the horsetail splay in Sector A, plot within K1 but show an apparent opposite (dextral) kinematics in plan view, suggesting that *K1*, and possibly *K3*, may represent composite populations including later reactivations during the late-stage strike-slip deformation tentatively linked to the Insubric Line (Schmid et al., 1989; D'Adda & Zanchetta, 2015). The N-S-trending *K2* set, instead, appears to be in line with surfaces that crosscut the other structures and may represent a younger structural feature.

The analysis of the bedding surfaces provides further evidence for the structural continuity between Val d'Ambria and the neighbouring areas of Monte Aga and Pizzo del Diavolo di Tenda. The two main bedding sets identified in the DOM have mean attitudes of 336N57 and 349N73, respectively - expressed in "Dip Direction-Dip". Their overall northward dip is consistent with structural orientations documented in adjacent sectors of the Orobic Basin and supports the interpretation of a common post-depositional tilting history.

The structural restoration of the hypothesized Permian fault surfaces, identified in Sector A, also showed that some segments of the apparent normal faults acquire geometries compatible with normal faulting after correction for the present-day bedding attitude, as predicted by Anderson's faulting model. However, due to the lack of kinematic indicators, such as *slickenlines*, it is not possible to assure that these structures are indeed associated with the Permian period and a definitive normal-faulting sense cannot be established solely from the available data extracted from the digital model.

An important outcome of this work concerns the geometry of the sedimentary succession of the upper Val d'Ambria (along its N-S axis). Panoramic and field observations initially suggested the presence of a possible large-scale fold, based on an apparent variation in bedding dip between the southern and northern portions of the study area. However, three-dimensional analysis of the bedding surfaces showed that the strata remain broadly sub-parallel across the investigated area. The apparent variation in dip can therefore be explained, at least in part, by the orientation of the cliff faces relative to the observer's viewpoint. This result highlights the potential of DOM-based analysis to reduce possible ambiguities and prevent potentially misleading structural interpretations, especially in areas where direct field measurements are very difficult.

Overall, the results indicate that the structural architecture of the upper Val d'Ambria records the emplacement of structures inherited from the Permian structuration and possibly developed during different stages of the Alpine extensional and compressional deformation. The observed fault systems can be integrated within the broader Alpine structural framework, while some geometries may preserve evidence of earlier transtensional (extensional?) deformation associated with the Permian basin evolution. The proposed geological and structural map summarizes these observations, which provides a more detailed structural representation of the study area, and can be used as a starting point for further investigations.

9. REFERENCES

Albini, S., Battaglia, D., Bellini, G., Bigoni, C., Carminati, E., Ceriani, S., ... & Spalla, M. I. (1994). Alpine deformations and pre-Alpine remnants in the north-eastern Orobic Alps, Southalpine Belt. *Quad. Geodin. Alp. Quat*, *2*, 25-39.

Arthaud, F., & Matte, P. (1977). Late Paleozoic strike-slip faulting in southern Europe and northern Africa: Result of a right-lateral shear zone between the Appalachians and the Urals. *Geological society of America bulletin*, *88*(9), 1305-1320.

Berra, F., & Felletti, F. (2011). Syndepositional tectonics recorded by soft-sediment deformation and liquefaction structures (continental Lower Permian sediments, Southern Alps, Northern Italy): stratigraphic significance. *Sedimentary Geology*, 235(3-4), 249-263.

Berra, F., Tiepolo, M., Caironi, V., & Siletto, G. B. (2015). U–Pb zircon geochronology of volcanic deposits from the Permian basin of the Orobic Alps (Southern Alps, Lombardy): chronostratigraphic and geological implications. *Geological Magazine*, *152*(3), 429-443.

Berra, F., Felletti, F., & Tessarollo, A. (2016). Stratigraphic architecture of a transtensional continental basin in low-latitude semiarid conditions: the Permian succession of the central Orobic Basin (Southern Alps, Italy). *Journal of Sedimentary Research*, *86*(4), 408-429.

Berra, F., Felletti, F., & Tessarollo, A. (2019). Oncoids and groundwater calcrete in a continental siliciclastic succession in a fault-controlled basin (Early Permian, Northern Italy). *Facies*, *65*(4), 38.

Blom, J. C., & Passchier, C. W. (1997). Structures along the Orobic thrust, Central Orobic Alps, Italy. *Geologische Rundschau*, *86*(3), 627-636.

Bonizzoni S. (2024). Il Permiano della Val d'Ambria: nuovi dati stratigrafici e paleontologici, Università di Pavia, Corso di Laurea in Scienze Geologiche, tesi di laurea ined., 51 pp.

Boriani, A., Bini, A., Beretta, G. P., Bergomi, M. A., Berra, F., Cariboni, M., Ferrario, A., Ferliga, C., Mazzoccola, D., Migliacci Bellate, R., Ronchi, A., Rossi, R., Rossi, S., Papani, L., Sciesa, E., Tognini, P. (2012). Note Illustrative della Carta Geologica d'Italia alla scala 1: 50.000. Foglio 056-Sondrio.

Cadel, G., Cosi, M., Pennacchioni, G., & Spalla, M. I. (1996). A new map of the Permo-Carboniferous cover and Variscan metamorphic basement in the Central Orobic Alps, Southern Alps-Italy: Structural and stratigraphical data. *Memorie di Scienze Geologiche, 48*, 1-53.

Casati, P., & Gnaccolini, M. (1967). Geologia delle Alpi Orobie occidentali. *Riv. Ital. Paleont. Stratigr.,* 73: 25-162.

Cassinis, G., 2007. Formazione di Collio. I Quaderni, serie III, del SGI. Volume 7 – Carta Geologica d'Italia 1:50.000 - Catalogo delle Formazioni Fascicolo VII – Unità tradizionali, 2, pp. 42–51.

Cassinis, G., & Perotti, C. R. (2007). A stratigraphic and tectonic review of the Italian Southern Alpine Permian. *Palaeoworld*, *16*(1-3), 140-172.

Cassinis, G., Dal Piaz, G. V., Eusebio, A., Gosso, G., Martinotti, G., Massari, F., ... & Zerbato, M. (1986). Report on a structural and sedimentological analysis in the Uranium province of the Orobic Alps, Italy. *Uranium*, *2*(3), 241-260.

Cassinis, G., Perotti, C. R., & Ronchi, A. (2012). Permian continental basins in the Southern Alps (Italy) and peri-mediterranean correlations. *International Journal of Earth Sciences: Geologische Rundschau*, *101*(1), 129.

Cattaneo M. (2025a). Stratigraphy, facies analysis and ichnology of the Pizzo del Diavolo Formation, Orobic Basin (Val d'Ambria, SO), Università degli Studi di Pavia, Corso di Laurea in Geoscienze per lo Sviluppo Sostenibile, tesi di laurea ined., 96 pp.

D'Adda, P., & Zanchetta, S. (2015). Geological-structural map of the Orobic and Porcile thrust junction, central Southern Alps (N Italy). *Journal of Maps*, *11*(1), 25-38.

De Sitter, L. U., & de Sitter-Koomans, C. (1949). The Geology of the Bergamasc Alps Lombardia Italy. *Leidse Geologische Mededelingen*, *14*(2), 1-257.

Dozy, J. J. (1935). Einige Tierfährten aus dem unteren Perm der Bergamasker Alpen. *Paläontologische Zeitschrift*, *17*(1), 45-55.

Edel, J. B., Casini, L., Oggiano, G., Rossi, P., & Schulmann, K. (2014). Early Permian 90° clockwise rotation of the Maures–Estérel–Corsica–Sardinia block confirmed by new palaeomagnetic data and followed by a Triassic 60° clockwise rotation.

Fantoni, R., Bersezio, R., & Forcella, F. (2004). Alpine structure and deformation chronology at the Southern Alps-Po Plain border in Lombardy. *Bollettino della Società geologica italiana*, *123*(3), 463-476.

Filippi, M., Farina, F., Ovtcharova, M., Caso, F., Roda, M., Piloni, C. B., & Zucali, M. (2025). High-precision zircon geochronology constrains early Permian exhumation of the deep Adriatic crust in the western Italian Alps. *Earth and Planetary Science Letters*, *671*, 119689.

Froitzheim, N., Derks, J. F., Walter, J. M., & Sciunnach, D. (2008). Evolution of an Early Permian extensional detachment fault from synintrusive, mylonitic flow to brittle faulting (Grassi Detachment Fault, Orobic Anticline, southern Alps, Italy).

Locchi, S. (2023). The post-Variscan evolution of the central Southern Alps: Insights from synchronous fault activity, hydrothermalism and magmatism in the Orobic and Collio basins. Unpublished PhD Thesis, Università di Milano Bicocca, 187 pp.

Locchi, S., Zanchetta, S., & Zanchi, A. (2022). Evidence of Early Permian extension during the post-Variscan evolution of the central Southern Alps (N Italy). *International Journal of Earth Sciences*, *111*(6), 1717-1738.

Manatschal, G., Chenin, P., Haupert, I., Masini, E., Frasca, G., & Decarlis, A. (2022). The importance of rift inheritance in understanding the early collisional evolution of the Western Alps. *Geosciences*, *12*(12), 434.

Marchetti, L. (2016). New occurrences of tetrapod ichnotaxa from the Permian Orobic Basin (Northern Italy) and critical discussion of the age of the ichnoassociation. *Papers in Palaeontology*, *2*(3), 363-386.

Marchetti, L., Ronchi, A., Santi, G., & Voigt, S. (2015). The Gerola Valley site (Orobic Basin, Northern Italy): a key for understanding late early Permian tetrapod ichnofaunas. *Palaeogeography, Palaeoclimatology, Palaeoecology*, *439*, 97-116.

Marchetti, L., Tessarollo, A., Felletti, F., Ronchi, A., 2017. Tetrapod footprint paleoecology: behavior, taphonomy and ichnofauna disentangled. A case study from the Lower Permian of the Southern Alps (Italy). Palaios 32, 506-527.

Marchetti, L., Forte, G., Kustatscher, E., DiMichele, W. A., Lucas, S. G., Roghi, G., ... & Ronchi, A. (2022). The Artinskian Warming Event: an Euramerican change in climate and the terrestrial biota during the early Permian. *Earth-Science Reviews*, *226*, 103922.

Menegoni, N., Cipriani, A., Scarani, R., Stori, L., Citton, P., Romano, M., ... & Ronchi, A. (2024). The Cala Viola-Torre del Porticciolo coastal area: a key tectono-stratigraphic site to unravel the polyphase tectonics in NW Sardinia. *Italian Journal of Geosciences*, *143*(1), 75-104.

Mengoli M. (1993). Geologia, assetto strutturale e deformazioni recenti del bacino del fiume Brembo di Carona (Bergamo), Università degli Studi di Milano, Corso di Laurea in Scienze Geologiche, Università di Milano, tesi di laurea.

Mittempergher, S., Zanchi, A., Zanchetta, S., Fumagalli, M., Gukov, K., & Bistacchi, A. (2021). Fault reactivation and propagation in the northern Adamello pluton: The structure and kinematics of a kilometre-scale seismogenic source. *Tectonophysics*, *806*, 228790.

Muttoni, G., Kent, D. V., & Channell, J. E. (1996). Evolution of Pangea: paleomagnetic constraints from the Southern Alps, Italy. *Earth and Planetary Science Letters*, *140*(1-4), 97-112.

Muttoni, G., Kent, D. V., Garzanti, E., Brack, P., Abrahamsen, N., & Gaetani, M. (2003). Early permian pangea 'B' to late permian pangea 'A'. *Earth and Planetary Science Letters*, *215*(3-4), 379-394.

Muttoni, G., Gaetani, M., Kent, D. V., Sciunnach, D., Angiolini, L., Berra, F., ... & Zanchi, A. (2009). Opening of the Neo-Tethys Ocean and the Pangea B to Pangea A transformation during the Permian. *GeoArabia*, *14*(4), 17-48.

Philippe, S., Lang-Villemaire, C., Lancelot, J., Girod, M., & Mercadier, H. (1987). Données minéralogiques et isotopiques sur deux gîtes hydrothermaux uranifères du bassin volcano-sédimentaire permien de Collio Orobico (Alpes Bergamasques): mise en évidence d'une phase de remobilisation crétacée. *Bulletin de Minéralogie*, *110*(2), 283-303.

Pohl, F., Froitzheim, N., Obermüller, G., Tomaschek, F., Schröder, O., Nagel, T. J., ... & Heuser, A. (2018). Kinematics and age of syn-intrusive detachment faulting in the Southern Alps: Evidence for Early Permian crustal extension and implications for the Pangea A versus B Controversy. *Tectonics*, *37*(10), 3668-3689.

Rocca, M. (2025). Tectonic Evolution of the central Southern Alps from Jurassic to Neogene: insights from Structural, Geochemical and Thermometric Analyses of Fracture-related Carbonates - PhD thesis.

Santi, G., Marchetti, L., Schirolli, P., Ronchi, A., 2020. The Cisuralian tetrapod ichnoassociation from Italy: from historical findings to a standard reference status. In: Romano M., Citton P.

(Eds.), Tetrapod ichnology in Italy: the state of the art. J. Mediterranean Earth Sci 12, 39–59–59.

Schaltegger, U., & Brack, P. (2007). Crustal-scale magmatic systems during intracontinental strike-slip tectonics: U, Pb and Hf isotopic constraints from Permian magmatic rocks of the Southern Alps. *International Journal of Earth Sciences*, *96*(6), 1131-1151.

Schmid, S. M., Aebli, H. R., Heller, F., & Zingg, A. (1989). The role of the Periadriatic Line in the tectonic evolution of the Alps. *Geological Society, London, Special Publications*, *45*(1), 153-171.

Sciunnach, D. (2001). The Lower Permian in the Orobic Anticline (Southern Alps, Lombardy): a review based on new stratigraphic and petrographic data. *Rivista Italiana di Paleontologia e Stratigrafia*, *107*(1).

Secchi, F., Casini, L., Cifelli, F., Naitza, S., Carta, E., & Oggiano, G. (2022). Syntectonic magmatism and reactivation of collisional structures during late-Variscan shearing (SW Sardinia, Italy). *International Journal of Earth Sciences*, *111*(5), 1469-1490.

Siravo, G., Speranza, F., Oggiano, G., & Spagnuolo, L. (2026). Post-Eocene 90° CCW Rotation of Sardinia-South Corsica: Paleomagnetic Evidence From Permian-Cretaceous Sediments of Nurra (NW Sardinia). *Tectonics*, *45*(5), e2026TC009397.

Spalla, M. I., Zanoni, D., Marotta, A. M., Rebay, G., Roda, M., Zucali, M., & Gosso, G. (2014). The transition from Variscan collision to continental break-up in the Alps: insights from the comparison between natural data and numerical model predictions.

Zanchetta, S., D'Adda, P., Zanchi, A., Barberini, V., & Villa, I. M. (2011). Cretaceous-Eocene compression in the central Southern Alps (N Italy) inferred from 40Ar/39Ar dating of pseudotachylytes along regional thrust faults. *Journal of Geodynamics*, *51*(4), 245-263.

Zanchetta, S., Malusà, M. G., & Zanchi, A. (2015). Precollisional development and Cenozoic evolution of the Southalpine retrobelt (European Alps). *Lithosphere*, *7*(6), 662-681.

Zanchetta, S., Locchi, S., Carminati, G., Mancuso, M., Montemagni, C., & Zanchi, A. (2022). Metasomatism by boron-rich fluids along Permian low-angle normal faults (Central Southern Alps, N Italy). *Minerals*, *12*(4), 404.

Zanchi, A., Zanchetta, S., Berio, L., Berra, F., & Felletti, F. (2019). Low-angle normal faults record Early Permian extensional tectonics in the Orobic Basin (Southern Alps, N Italy). *Italian Journal of Geosciences*, *138*(2), 184-201.

Zanoni, D., Spalla, M. I., & Gosso, G. (2010). Vestiges of lost tectonic units in conglomerate pebbles? A test in Permian sequences of the Southalpine Orobic Alps. *Geological Magazine*, *147*(1), 98-122.

GEOLOGICAL MAPS

Cadel, G., Cosi, M., Pennacchioni, G., & Spalla, M. I. (1996). *Carta geologico-strutturale delle Alpi Orobiche Centrali (tra le Valli Armisa e Venina e l'Alta Val Seriana)*, *scala 1:25.000. Memorie di Scienze Geologiche* - Padova.

Cattaneo, M. (2025b). Geological map 1:50,000 of the Val d'Ambria area. Unpublished material.

Forcella, F., Jadoul, F., BINI, A., & FERLIGA, C. (2000). Carta geologica della Provincia di Bergamo alla scala 1: 50.000 con relativa nota illustrativa. 3 fogli geologici e vol. di 300 pp. *Assessorato all'Ambiente della Provincia di Bergamo, Bergamo*.

Mengoli, M. (1993). Carta Geologica del Bacino del Brembo di Carona (Alpi Orobiche Centrali – BG), scala 1:10.000.

Montrasio, A., Bigioggero, B., Brigo, L., Casati, P., Cremaschi, M., Ferrario, A., Gaetani, M., Gelati, R., Gregnanin, A., Jadoul, F., Orombelli, G., Rossi, P.M., Zuffardi, P. (1990). *Carta Geologica della Lombardia, scala 1:250.000* – Regione Lombardia & Università degli Studi di Milano.

SERVIZIO GEOLOGICO D'ITALIA (2012) - *Carta Geologica d'Italia alla scala 1:50.000, F. 056 Sondrio*. ISPRA, Roma. DOI: 10.15161/oar.it/211475

SITOGRAPHY

https://www.cartografia.servizirl.it/viewer40/map/2D?config=config_dbtbase.json

SOFTWARES

Agisoft. (2023). *Agisoft Metashape* (Version 2.2.1) [Computer software]. Agisoft LLC. https://www.agisoft.com/

Allmendinger, R. W. (2020). *Stereonet* (Version 11.0) [Computer software]. Cornell University. https://www.rickallmendinger.net/stereonet

Girardeau-Montaut, D. (2024). *CloudCompare* (Version 2.12.1) [Computer software]. CloudCompare Project. https://www.cloudcompare.org/

QGIS Development Team. (2025). *QGIS Geographic Information System* (v. 3.44.14 / v. 4.2.2) [Computer software]. QGIS Association. https://www.qgis.org

RINGRAZIAMENTI

Innanzitutto, desidero esprimere la mia più profonda gratitudine al mio relatore, prof. Ausonio Ronchi, per l'opportunità concessami, la disponibilità e i preziosi consigli che mi ha offerto lungo tutto il percorso di stesura di questo lavoro.
Un sentito ringraziamento va anche ai miei correlatori, prof. Niccolò Menegoni e dott. Rudy Scarani, per il costante supporto (non solo tecnico e scientifico), e per avermi aiutato a superare i momenti di dubbio con grande professionalità.

Un ringraziamento speciale va al dott. Cristiano Dal Sasso (curatore della Sezione di Paleontologia dei Vertebrati del Museo di Storia Naturale di Milano), al dott. Lorenzo Marchetti (icnologo) e a Elio Della Ferrera (fotografo naturalista): il loro entusiasmo è stato fondamentale per la valorizzazione del sito della Val d'Ambria e per la nascita del progetto di ricerca. Esprimo la mia sincera gratitudine anche al dott. Massimo Merati (Direttore del Parco delle Orobie Valtellinesi), insieme a Simone Luca Marchesini, sindaco di Piateda, per la loro grande ospitalità e disponibilità, e a Stefano Rossi (Soprintendenza Belle Arti e Paesaggio per le province di Como, Lecco, Monza-Brianza, Pavia, Sondrio e Varese) per aver concesso i permessi necessari allo svolgimento di questa ricerca.

Ringrazio, inoltre, i dottori Matteo Foletti e Giuliana Testa per il fondamentale aiuto durante le fasi di interpretazione dei dati in laboratorio, e il dott. Marco Cattaneo, compagno d'avventura durante il progetto della mia tesi triennale.

Il ringraziamento più grande va alla mia famiglia per il continuo sostegno e per i sacrifici fatti durante tutti questi anni di università. Spero un giorno di poter ricambiare, in qualche modo.
Questo traguardo è anche vostro.

Infine, ringrazio di cuore anche i miei amici di sempre e i compagni di università, i migliori che potessi desiderare.